

**HIGH TEMPERATURE OXIDATION AND NITRIDING
KINETICS OF ZIRCONIUM**

**HIGH TEMPERATURE OXIDATION AND NITRIDING
KINETICS OF ZIRCONIUM**

By

CASIMIR JOSEPH ROSA, M.Eng. (Met.)

**A Thesis
Submitted to the Faculty of Graduate Studies
in Partial Fulfilment of the Requirements
for the Degree
Doctor of Philosophy**

McMaster University

June, 1965.

DOCTOR OF PHILOSOPHY (1965)
(Metallurgy)

McMASTER UNIVERSITY
Hamilton, Ontario

TITLE: High Temperature Oxidation and Nitriding Kinetics of Zirconium.

AUTHOR: Casimir Joseph Rosa, B.Eng. (Met.), University of Cracow, Poland

M.Eng. (Met.), University of Cracow, Academy
for Mining and Metallurgy,
Poland.

SUPERVISOR: Professor W. W. Smeltzer

NUMBER OF PAGES: xii plus 157

SCOPE AND CONTENTS:

An investigation is reported on the oxidation properties of alpha-zirconium at 850°C and beta-zirconium at 950°C in oxygen for periods extending to 400 hr. and 100 hr., respectively. Nitriding kinetics of zirconium in the range of 750° to 1000°C up to 200 hr. were investigated. The kinetics were determined by volumetric and gravimetric techniques and may be represented by a parabolic relationship after a period of more rapid oxidation. The uptakes of oxygen or nitrogen were consistent with the mathematical evaluations based on multi-phase diffusion models. Two diffusion models were advanced; one based upon differential and the other upon integral solutions of diffusion equations. It was possible to separate quantitatively the oxygen or nitrogen partitions in the scale, alpha and beta phases of zirconium.

The diffusivity of nitrogen in alpha-zirconium was determined by using transverse microhardness measurements. The diffusivity is: $D = 0.15 \exp(-54100/RT)$ cm/sec² for the temperature range of 750°- 1000°C.

The influence of oxygen-nitrogen atmospheres on the scaling rate of alpha-zirconium at 850°C was investigated. Small additions of either gas to the other increased the scaling rate. A definite breakaway point was observed in the scaling kinetics and the time interval to the transition point varied with the relative amounts of nitrogen to oxygen.

Scaling rates of zirconium at 850° and 950°C in the oxygen-water vapor atmospheres initially obeyed to a good approximation a parabolic relationship which was followed by a much faster scaling rate.

ACKNOWLEDGEMENTS

The author wishes to express his gratitude to his supervisor, Dr. W. W. Smeltzer for his guidance and contribution to the theoretical part; to Dr. G. R. Wallwork from the University of New South Wales, Australia, for encouragement and practical advice on experimental procedures, and Dr. C. Calvo for his advice on identification methods by X-rays. Dr. R. Thomas of A.E.C.L., Chalk River, kindly supplied the zirconium metal.

TABLE OF CONTENTS

| Subject | Page |
|--|------|
| Chapter I - Introduction | 1 |
| Chapter II - Review of Literature | 3 |
| 2.1 Introduction | 3 |
| 2.2 Oxidation Rate as a Function of Time | 3 |
| 2.3 Oxidation Rate as a Function of Temperature | 11 |
| 2.4 Oxidation Rate as Function of Oxygen Pressure | 13 |
| 2.5 Reaction of Zirconium with Oxygen | 15 |
| 2.6 Reaction of Zirconium with Nitrogen | 18 |
| 2.7 Reaction of Zirconium with Nitrogen-Oxygen Atmospheres | 19 |
| 2.8 Reaction of Zirconium with Water Vapor-Oxygen Atmospheres | 20 |
| 2.9 Reaction of Zirconium with Gases other than Nitrogen and Oxygen | 20 |
| Chapter III Theory for Parabolic Oxidation and Nitriding of Zirconium. | 23 |
| 3.1 Differential Model for Two-Solid Phase Oxidation and Nitriding | 23 |
| 3.2 Integral Model for Two-Solid Phase Oxidation and Nitriding | 28 |
| 3.3 Differential Model for Three-Solid Phase Oxidation and Nitriding | 29 |
| 3.4 Integral Model for Three-Solid Phase Oxidation and Nitriding | 32 |

| | | |
|---|--|-----|
| 3.5 | Supplementary Restriction on Diffusion Processes | 34 |
| 3.6 | Limitations and Assumptions Relevant to Models | 35 |
| Chapter IV Experimental | | 36 |
| 4.1 | Introduction | 36 |
| 4.2 | Volumetric Apparatus | 36 |
| 4.3 | Procedure | 44 |
| 4.4 | Gravimetric Apparatus and Procedure | 46 |
| 4.5 | Material and Preparations | 46 |
| Chapter V Reaction of Oxygen with Zirconium: Results | | 49 |
| 5.1 | Introduction | 49 |
| 5.2 | Oxidation Measurements at 850°C | 50 |
| 5.3 | Oxidation Measurements at 950°C | 53 |
| 5.4 | Static, Gravimetric Measurements | 62 |
| 5.5 | Microscopic Measurements and Metallography | 62 |
| 5.6 | X-ray Determinations | 70 |
| Chapter VI Reaction of Nitrogen with Zirconium: Results | | 73 |
| 6.1 | Static, Gravimetric Measurements at 750°- 1000°C | 73 |
| 6.2 | Volumetric Measurements at 850° and 950°C | 75 |
| 6.3 | Microscopic and Metallographic Examinations | 75 |
| 6.4 | Microhardness Measurements | 80 |
| 6.5 | X-ray Determinations | 87 |
| Chapter VII Reaction of Zirconium with Gas Atmospheres: Results | | 95 |
| 7.1 | Nitrogen-Oxygen Atmospheres, 850°C | 95 |
| 7.2 | Water Vapor-Oxygen Atmospheres | 101 |

| | | |
|--------------|---|-----|
| Chapter VIII | Discussion | 107 |
| 8.1 | Kinetics of Zirconium-Oxygen and Zirconium Nitrogen Reactions | 107 |
| 8.1.1 | Two-Phase Oxidation (850°C) | 107 |
| 8.1.2 | Three-Phase Oxidation (950°C) | 109 |
| 8.1.3 | Zirconium-Nitrogen Reaction (750°- 1000°C) | 115 |
| 8.2 | Metallography and X-ray Analyses | 120 |
| 8.3 | The "Breakaway" Phenomenon | 123 |
| 8.3.1 | Effect of Stress | 124 |
| 8.3.2 | Sample Thickness | 125 |
| 8.3.3 | Influence of Atmospheres | 126 |
| Chapter IX | Conclusions | 127 |
| Chapter X | Recommendation for Future Work | 130 |
| Appendix | | 131 |
| Literature | | 153 |

LIST OF ILLUSTRATIONS AND TABLES

| Figure | Subject | Page |
|--------|--|-------|
| 1. | Scale-Metal Diffusion Models for Parabolic Reaction Kinetics and Binary Phase Diagrams | 24,27 |
| 2. | General View of the Volumetric Apparatus | 38 |
| 3. | Schematic Diagram of Main Components of the Volumetric Apparatus | 39 |
| 4. | Electrical Circuits Diagram for Taking Continuous Readings | 41 |
| 5. | Oxidation Rate of Zirconium, at 850°C. Sample thickness 2 mm. | 51 |
| 6. | Oxidation Rate of Zirconium, at 850°C. Sample thickness 2 mm. | 52 |
| 7. | Oxidation Rate of Zirconium, at 850°C. Sample thickness 1 mm. | 54 |
| 8. | Topography of Oxidized Zirconium Samples, at 950°C | 55 |
| 9. | Oxidation Rate of Zirconium at 950°C. Sample thickness 2 mm. | 57 |
| 10. | Oxidation Rate of Zirconium at 950°C. Sample thickness 2 mm. | 58 |
| 11. | Oxidation Rate of Zirconium at 950°C. Sample thickness 2 mm. | 59 |
| 12. | Oxidation Rate of Zirconium at 950°C. Sample thickness 2 mm. | 60 |
| 13. | Oxidation Rate of Zirconium at 950°C. Sample thickness 2 mm. | 61 |
| 14. | Oxidation Rate of Zirconium at 950°C, Gravimetric Method, Sample thickness 2 mm. | 63 |
| 15. | Oxide Thickness as a Function of Time for Zirconium Oxidized at 850°C. | 65 |
| 16. | Growth of Zirconium Dioxide with Time, at 950°C. | 66 |

| | | |
|-------|---|-------|
| 17. | Boundary between Alpha Metal-Oxygen Solid Solution and Transformed Beta-Zirconium (lower part) | 67 |
| 18. | Growth of Zirconium Oxide and Alpha phase, at 950°C | 68 |
| 19. | Change of the Ratio of Alpha-Phase Thick./Oxide Thickness, at 950°C. | 69 |
| 20. | Cross Section of Zirconium Samples Oxidized at 950°C. | 71 |
| 21. | X-ray Powder Photographs of Zirconium Dioxide | 72 |
| 22. | Nitriding Rates of Zirconium at 750°- 1000°C. Sample thickness 2 mm. | 74 |
| 23. | Nitriding Rates of Zirconium at 850°- 950°C. Sample thickness 2 mm. | 76 |
| 24. | Thicknesses of Zirconium Nitride and Zirconium-Alpha Phase Solid Solution | 77 |
| 25. | The Sum and Ratio of Thicknesses Given in Fig. 23. | 78 |
| 26. | Metallography of Nitrided Zirconium cooled from 950°C. | 79 |
| 27. | Hardness Profiles in Zirconium-Nitrogen Solid Solution | 82 |
| 28. | Hardness Profiles in Zirconium-Nitrogen Solid Solutions | 83 |
| 29. | Hardness Gradients Normalized with Respect to Time, for Nitrided Zirconium-Alpha Phase | 84 |
| 30. | Hardness Gradients Normalized with Respect to Time, for Nitrided Zirconium-Alpha Phase | 85 |
| 31. | Hardness as a Function of Nitrogen Concentration in Zirconium | 86 |
| 32-38 | Cumulative Normal Distribution of $x/t^{1/2}$ at; 750°, 800°, 850°, 900°, 950° and 1000°C, respectively | 88-91 |
| 39. | Arrhenius Plot for Diffusion of Nitrogen in Alpha-Zirconium | 92 |

| | | |
|------|---|-----|
| 40. | X-Ray Powder Patterns of Zirconium Nitride | 94 |
| 41a. | Reaction Rates of Zirconium in Oxygen-Nitrogen Mixtures, at 850°C. | 96 |
| 41b. | Reaction Rates of Zirconium in Oxygen-Nitrogen Mixtures, at 850°C. | 97 |
| 42. | Time to "Breakaway" Point as a Function of Nitrogen Mole Fraction (N_{N_2}), at 850°C | 99 |
| 43. | Microstructures of Scale and Zirconium Metal, after Cooling from 850°C. | 100 |
| 44. | Oxidation of Zirconium in Oxygen-Water Vapor Atmosphere, at 950°C. | 102 |
| 45. | Oxidation of Zirconium in Oxygen-Water Vapor Atmosphere, at 850°C. | 104 |
| 46. | Metallography of Zirconium Specimens Oxidized in Oxygen-Water Vapor Atmospheres | 105 |

TABLES

| | | |
|-----|--|-----|
| I | Comparison of Calculated and Experimental Values of k_p 's for Zirconium-Oxygen Reaction | 114 |
| II | Nitrogen Concentrations Relevant to the Diffusion Models | 115 |
| III | Intermediate Values Obtained from the Diffusion Model for Zirconium-Nitrogen Reaction. | 117 |
| IV | Comparison of Calculated and Experimental Values of k_p 's for Zirconium-Nitrogen Reaction | 118 |
| 1. | Impurity Contents of Zirconium | 133 |
| 2. | Experimental Test Conditions | 134 |
| 3. | Microscopic Measurements (950°C) | 135 |
| 4. | Weight Measurements (950°C) | 136 |
| 5. | Microscopic Measurements (850°C) | 137 |
| 6. | X-Ray Powder Data for Gray and White Zirconium Dioxide | 138 |

| | | |
|-----|--|-----|
| 7. | Line Equation for Zirconium-Nitrogen Reaction | 140 |
| 8. | Weight Measurements (750° - 1000°C) | 141 |
| 9. | Microscopic Measurements (750° - 1000°C) | 143 |
| 10. | Line Equations for the Thicknesses of Zirconium Nitride and Alpha-Phase as a Function of Time. | 144 |
| 11. | Microhardness Measurements and Diffusion Data | 145 |
| 12. | X-Ray Powder Data for Zirconium Nitride | 149 |
| 13. | Line Equations for Reaction of Zirconium in Nitrogen-Oxygen Atmospheres at 850°C. | 150 |

CHAPTER I

Introduction

Basically, this thesis consists of three parts: the first part comprises the reaction of zirconium with oxygen, the second describes the reaction of zirconium with nitrogen, and finally the last part is a qualitative discussion on experimental results obtained from a combined effect of both gases.

It is the intention of the author to give a brief outline of the fundamental principles and the summary of theories of high temperature oxidation and nitriding insofar as these have been developed to the present, followed by some experimental results from the author's investigations. An attempt has been made to explain the results on the basis of these theories and principles. It is realized, however, that all conclusions cannot be treated unequivocally and that additional investigations are necessary in order to understand the kinetics of oxidation and nitriding for even the most simplified systems.

The writer is aware also that a critical assessment of "most probable values" as one may attempt in thermo-chemistry of metals for instance, is impossible with oxidation and nitriding rates. There are too many major influences of experimental nature: the purity, the physical state and shape of a metal used, the treatment of the surface, the composition of the gas phase, etc. which make comparison of results of various investigators difficult

and may bear on the conclusions drawn. A summary of experimental results of other investigators together with those presented here, nevertheless, may be useful as a guide to practical applications and may prove helpful for derivation of systematic relationships.

The restrictions have been imposed in this thesis to apply the theories for oxidation and nitriding phenomena to zirconium only, and on comparison of the experimental results with those from other investigations pertaining to zirconium and to metals of the Periodic Subgroup IVB. It is apparent from the published literature that these latter metals exhibit close similarities in behaviour towards oxygen and nitrogen. By adopting this approach, the condition has been imposed to confine all considerations and discussions as closely as possible to the topic of this investigation.

CHAPTER II

Review of Literature

2.1 Introduction

The reaction of oxygen with almost all metals occurs spontaneously. From various studies (1-9) it is reasonable to conclude that many oxides form a protective layer and that the transport of oxygen or metal through the oxide at least partially determines the rate of oxidation. The problem therefore reduces to the consideration of the extent to which coatings formed by the reaction with gas are protective, or, in other words, we are faced with the question of the manner and rate of growth of tarnish layers.

Kinetic theory is concerned primarily with the progress of reaction as a function of temperature and concentrations of the reactants. These factors being of most importance, the first task is to find relationships between them. With the exception of the theory for parabolic oxidation of metals, we do not have adequate equations correlating these factors. However, a number of relationships based upon empirical metal-oxide models have been suggested to account for many reaction mechanisms.

2.2 Oxidation Rate as a Function of Time:

The more common equations accounting for oxidation rates are given here in terms of weight increase per unit area Δm , time t and rate constants K, k .

The linear relationship:

$$\Delta m = k_l t \quad (1)$$

is the simplest expression found to correlate experimental data. Generally, the tendency towards oxidation where reaction proceeds at a constant rate can be assessed from the volume ratio of oxide formed to the metal consumed i. e. from the PILLING and BEDWORTH ratio. If the ratio is less than unity the oxide may be under tension which could be relieved by development of cracks. An oxide exhibiting a larger volume than the consumed metal would tend to be of a compact structure and the oxidation kinetics would be diffusion controlled. If this ratio is exceptionally high, however, the formation of non-uniform that is, porous or cracked scales may also be expected due to compressive stresses. These considerations are not without exceptions and probably less significant for oxides that grow by outward migration of matter than for oxides formed by diffusion of material from the surface towards the metal-oxide interface e.g. for oxides of n-type in which oxygen diffuses via vacant anion sites.

A parabolic relationship:

$$\Delta m = (K_p t)^{1/2} = k_p \sqrt{t} \quad (2)$$

or, a modification of this equation expressed as,

$$(\Delta m)^2 = a + K_p t \quad (3)$$

applies to many metals and alloys under service condition ⁽¹⁰⁾ and can be derived from WAGNER'S theory of oxidation ^(11,12). The significance of parabolic equations is not that they provide a method of predicting oxidation rates, but if experimental results agree with these rate equations, the underlying theoretical assumptions concerning the oxidation mechanism may be supported and the complicated reaction kinetics better understood.

It is this theory the application of which to the obtained results will be emphasized in the next chapter.

The cubic relationship:

$$(\Delta m)^3 = K_c t \quad (4)$$

is found to fit the experimental values occasionally. In most cases it applies to intermediate temperatures approx. 400°C , and to thin oxide films of about 1000 \AA . Examples are oxidation of nickel⁽¹³⁾ and titanium⁽¹⁴⁾. This relationship can be theoretically derived and explained by the MOTT-CABRERA mechanism⁽¹⁵⁾ for films consisting of metal deficit oxides e.g. such as Cu_2O . For the thin film region of this type of oxides (p-type) the MOTT-CABRERA mechanism predicts a direct relation between the ion current and the electrical field. The rate controlling step being the diffusion of metal ions in the oxide under the influence of the electrical gradient. ENGELL, HAUFFE and ILSCHNER⁽¹³⁾ have also considered the influence^{of} the electrostatic field in films of thickness of several hundred Angstroms (approx. $100\text{-}1200 \text{ \AA}$) on the concentration gradient of cation vacancies and derived a cubic rate growth equation for the p-type semi-conducting films, e.g. NiO.

However, neither the MOTT-CABRERA nor the ENGELL-HAUFFE-ILSCHNER theory explains the cubic oxidation of metals forming n-type oxides such as titanium and zirconium (see also section 2.4 of this chapter), and it is for these metals that cubic reaction kinetics have mainly been observed (14,16,17).

Finally, the more general logarithmic (or exponential) law:

$$\Delta m = K_e \log (a.t + t_0) \quad (5)$$

and the inverse logarithmic relationship:

$$\frac{1}{\Delta m} = A - K_{11} \cdot \log t \quad (6)$$

predominate usually at low temperature and short oxidation exposures. Here, the relevant model for the region of a very thin film (about 100 Å) has proved to be the one originally proposed by MOTT⁽¹⁵⁾, based on the hypothesis that a strong electric field exists across the oxide film. The gas-oxide interface is assumed to be covered uniformly with oxygen anions. The electrical field is responsible for pulling the ions through the oxide phase. Electrons pass from the metal to the chemisorbed oxygen layer either by thermionic emission or by the tunnel effect to give rise to the electrical charge distribution. For this case, the oxidation rate is determined by the rate of escape of metal ions into the oxide. This means then, that at low temperatures and for very thin film thicknesses the ions do not simply diffuse through the film under the influence of a concentration gradient.

Combination of two or more of the above mentioned relationships into a single oxidation-time curve is also quite common. A metal may start to oxidize parabolically and then continue linearly as for the case of zirconium reported by SMELTZER and AKRAM⁽¹⁸⁾. This relation has been termed paralinear. These investigators have demonstrated that the transition from parabolic to linear oxidation for zirconium is associated with formation of a

duplex scale composed of compact and porous oxides. Assuming the general diffusion equation for a concentration profile of oxygen in the metal maintained at constant gradient with respect to the moving metal-oxide interface at a velocity k_L , i.e.

$$\frac{\partial^2 C}{\partial x^2} + \frac{k_L}{D} \cdot \frac{\partial C}{\partial x} = 0 \quad (7)$$

it was possible to derive an expression correlating the parabolic and linear rate constants for the case where the concentration of oxygen in the atmosphere is equal to the initial concentration of oxygen in the metal.

Solution of equation (7) yields:

$$k_L \cdot \epsilon \cdot C_o^{II} \approx D_o^{II} (C_o^S - C_o^{II}) \quad (8).$$

Assuming a constant oxygen gradient in the oxide, one obtains from equations (7) and (8) for the parabolic growth law of compact oxide:

$$k_p = 2 \Omega D_o^{II} (C_o^S - C_o^{II}) \quad (9).$$

The symbols used in these equations are:

$\frac{\partial C}{\partial x}$ - variation of oxygen concentration with distance into a sample

ϵ - thickness of a compact oxide

Ω - volume of oxide per oxygen ion

$D; D_o^{II}$ - diffusion constants for oxygen in the metal and in the compact oxide film, respectively.

C_o^S, C_o^{II} - concentrations of oxygen in oxide at the porous-compact oxide and oxide-metal interfaces, respectively

$k_L; k_p$ - linear and parabolic rate constants, respectively.

Since the left hand side of equation (8) can be evaluated empirically from the linear rate data and the appropriate phase diagram, we can express k_p in terms of k_L .

Recently, SMELTZER, HAERING and KIRKALDY⁽¹⁹⁾ constructed a phenomenological theory of metal oxidation which is based on the model that oxygen migrates through the oxide lattice under the influence of its concentration gradient as in WAGNER'S model⁽¹²⁾ for parabolic oxidation and that oxygen diffuses also through a random array of a low resistance paths of temporary decreasing density. They assumed a uniform and low oxygen concentration gradient in the film and that interfacial inhibitions could be neglected. The decay law of the available oxygen sites in the array of short circuit path was expressed by the first order rate equation:

$$f(t) = f^0 e^{-kt} \quad (10)$$

and the effective diffusion constant as:

$$D_{\text{eff}} = D_L(1-f) + D_B \cdot t \quad (11).$$

Here:

f^0 ; f - are the initial and total fractions of oxygen sites respectively within the low resistance paths in the oxide film.

D_L ; D_B - are constants for lattice and short circuit oxygen diffusion, respectively.

FICK'S first law is for the above conditions:

$$\frac{dx}{dt} = \Omega \cdot D_{\text{eff}} \cdot \frac{\Delta C}{x} \quad (12)$$

where:

$\frac{dx}{dt}$ - determines the rate of oxide growth

ΔC - represents the concentration difference of oxygen ions across the oxide film, and

Ω - gives the volume of oxide per oxygen ion.

Combining equations (10), (11) and (12) yields:

$$x^2 = k_p \left[t + \frac{D_B \cdot t^0}{D_L \cdot k} (1 - e^{-kt}) \right] \quad (13)$$

which expresses the growth of oxide governed by short circuit and lattice diffusion. As reported, this equation takes account of the oxidation kinetics of metals of subgroup IVB previously represented by a logarithmic and cubic equations separately, over the temperature range 300° - 600°C.

As previously illustrated, many metals oxidize to form thick scales by a parabolic relationship. WAGNER⁽¹²⁾ set forth the working hypothesis that diffusion in oxide, halide and sulphide phases may generally be interpreted as migration processes of ions and electrons whereas migration of electrically neutral atoms or molecules may be neglected. Under the assumption that the various particles migrate independently of each other it is possible to calculate the mobilities of ions and electrons in the tarnish layer either from electrical data or from self diffusion measurements involving isotopes. WAGNER derived the following equation for the formation of a scale:

$$\frac{\dot{n}}{A e q} = \left[\frac{300}{96,500 N_A e} \int_{\mu(x^1)}^{\mu(x^{11})} \frac{1}{z_2} (t_1 + t_2) t_3 \sqrt{d\mu_x} \right] \frac{1}{\Delta x} \quad (14)$$

$$= k_p / \Delta x$$

where: \dot{n}_{eq}/A is the rate of migration of metal ions or non metal ions, Δx is the thickness of the scale, e is the electronic charge, Z_2 is the valence of negatively charged non metal ions, μ_x is the chemical potential of non metal, $\mu(x^1)$ and $\mu(x^{11})$ are the chemical potentials of non metal at the gas/scale and scale/metal interface, respectively, σ is electrical conductivity, and t_1 , t_2 and t_3 are the transference numbers of metal ions, non metal ions and electrons, respectively. The constant k_p , has been named "rational rate constant".

The "rational rate constant" may be expressed also as:

$$k_p = C_{eq} \int_{a(x^1)}^{a(x^{11})} \left(\frac{Z_1}{Z_2} D_1^* + D_2^* \right) d \ln a_x \quad (15)$$

where: $C_{eq} = Z_1 C_1 = |Z_2| C_2$ is the concentration of metal or non metal ions, a_x is the activity of non metal, $a(x^1)$ and $a(x^{11})$ are the activities of non metal at the gas/scale and scale/metal interfaces, respectively, and D_1^* and D_2^* are the self-diffusion coefficients of metal and non metal.

With respect to metal oxidation reactions, this theory has been applied to the scaling of copper at 1050°C and to scaling of iron in the temperature range of 800 - 1100°C. The agreement between the experimentally determined values of k_p and those calculated from the above equations is good.

2.3 Oxidation Rate as Function of Temperature:

The temperature influence on surface reactions as kinetic processes may be expected to approximate to an ARRHENIUS equation:

$$k = A \cdot \exp - Q/RT \quad (16)$$

for which the experimentally determined values of k fit the equation in $\log k$ vs. $1/T$ plot as a straight line.

There are however, some notable exceptions which still await explanation. For example, the reaction of oxygen and zinc displays anomalies with respect to temperature⁽²⁰⁾, or as in the case of reaction of oxygen with cadmium⁽¹⁰⁾ or niobium⁽¹⁰⁾ for intermediate temperatures, where it was found that the oxidation rates decrease with increasing temperature. Since activation energies, Q , cannot be negative these effects cannot be explained by a uniform kinetic process.

It should be mentioned that no unambiguous physical meaning has yet been given to the constant A in equation (14). Moreover, the dimensions of A vary with the oxidation-time law for which the equation is applicable.

GULBRANSEN⁽²¹⁾ considered EYRING'S reaction rate theory⁽²²⁾ for diffusion processes involving the presence of a transition state at the top of the energy barrier between the initial and final states of diffusion to derive an expression correlating the parabolic rate constant with temperature:

$$k = \frac{kT}{h} \cdot \exp - \Delta F^+/RT \quad (17).$$

This expression may be reduced to:

$$k_p = \frac{2kTd^2}{h} \exp \Delta S^+/R \cdot \exp - \Delta H^+/RT \quad (18).$$

Here:

d - is the closest cation distance in cm.

k, h - are Boltzman's and Planck's constants, respectively

$\Delta F^+, \Delta H^+, \Delta S^+$ - are the changes of free energy, enthalpy and entropy, respectively, for formation of activated complexes.

and the term:

$\exp - \Delta F^+ / RT$ - gives the number of activated complexes as a function of the free energy barrier and the absolute temperature.

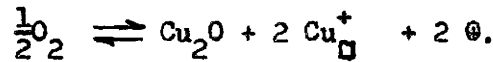
Obviously, equation (18) is related through the parabolic rate constant k_p to the thickness of the oxide film. Also, comparison of equation (18) with equation (16) shows that in this theory A is slightly dependent on temperature. It is almost impossible at the present time to check any considerations regarding ΔH^+ and especially ΔS^+ by means of experimental oxidation data, and future developments along this line will require further arguments and much more accurate experimental values.

The successful approach to the fundamental problem of the mechanism of oxidation probably will continue along the theoretical line presented above. As already mentioned a particular rate law may transform from one form to another with the time of oxidation. There is also some evidence that the rate-law which is followed depends on temperature.

In a recent study by KOFSTAD⁽²³⁾, zirconium was oxidized under a condition of linearly increasing temperature. It was shown that between 650° and 950°C the cubic rate law was obeyed, and between 950° and 1100°C the parabolic rate-law fitted the data best.

2.4 Oxidation Rate as Function of Oxygen Pressure:

The oxides of metals are classified according to their lattice defect structures. Metals forming oxides of the p-type must, when oxidizing according to WAGNER'S mechanism, show a certain dependence on pressure. To the first approximation a relation can be found by applying the mass-action equation to the interaction of oxygen with the oxide. For example, for oxidation of copper the interaction of oxygen with cuprous oxide may be expressed as:



The concentrations of cation vacancies and electron defects (holes) are equal, i.e.

$$C(Cu_{\square}^{+}) = C(\oplus) \quad (19).$$

Using the ideal mass action law we obtain:

$$(Po_2)^{1/2} / [C(Cu_{\square}^{+})]^2 \cdot [C(\oplus)]^2 = \text{const} \quad (20)$$

under the assumption that the activity coefficients are unity,

Equation (19) combined with equation (20) yields:

$$C(\oplus) = C(Cu_{\square}^{+}) = \text{const.} (Po_2)^{1/8} \quad (21).$$

Since the diffusion rate depends directly on the number of defects, the oxidation rate of copper would also depend on the 8-th root of Po_2 . Actual experimental values of WAGNER and GRUENEWALD⁽²⁴⁾ confirm that the parabolic constant, k_p , for oxidation of copper is a linear function of the 7-th root of oxygen pressure at 1000°C, giving thus approximate agreement.

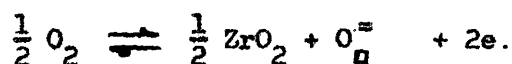
Similarly, following the same reasoning, it can be shown that the concentration of nickel vacancies in nickel oxide may be expressed by equation:

$$C(\oplus) = C(\text{Ni}_{\square}^{++}) = \text{const. } (P_{\text{O}_2})^{1/6} \quad (22)$$

which again was confirmed by WAGNER and GRUENEWALD⁽²⁴⁾. These considerations also apply to metal sulfides. In the case of iron sulfidization in gaseous sulphur a close check of pressure dependence as predicted by the defect structure of FeS was obtained by HAUFFE and RAHMEL⁽²⁵⁾.

If the surface compound is of an n-type semiconductor such as ZrO_2 or TiO_2 , the number of defects at the oxide-gas interface may be expected to be negligibly small at moderate temperatures and pressures, and consequently the oxidation rate should be nearly independent of the partial pressure of oxygen. This has in fact been confirmed at certain pressure ranges for several metals forming n-type oxides at temperatures where oxidation is parabolic, e.g. for reaction of zirconium with oxygen by GULBRANSEN and ANDREW⁽²⁶⁾, by CUBICCIOTTI⁽³⁾, by HUSSEY and SMELTZER⁽²⁷⁾; and for oxidation of titanium by JENKINS⁽²⁸⁾.

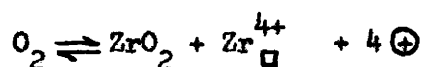
In a most recent investigation VEST et al⁽²⁹⁾ discuss more fully the defect structure of monoclinic zirconia at 1000°C . They found, from electrical conductivity measurements, that at low oxygen pressures and at compositions far removed from stoichiometry, ZrO_{2-x} , the conductivity may be due to completely ionized oxygen vacancies. The lattice defect equation for this consideration is



Accordingly,

$$C(e) \propto (P_{O_2})^{-1/6} \quad (23).$$

However, at high oxygen pressures, for compositions removed from stoichiometry in the reverse sense, ZrO_{2+x} , the conductivity may be attributed to the formation of completely ionized zirconium vacancies. That is,



hence

$$C(\oplus) \propto (P_{O_2})^{1/5} \quad (24).$$

At a composition near stoichiometry zirconia was shown to be an amphoteric semiconductor, at a given oxygen partial pressure.

2.5 Reaction of Zirconium with Oxygen:

Although the elevated temperature oxidation of zirconium in dry oxygen has undergone extensive investigation in the past decade, the literature is replete with controversy as to the set of kinetics best descriptive of the extended reaction. The proponents of the parabolic rate law appear to be offset by a similar number of authors reporting a cubic oxidation process.

BELLE and MALLETT⁽¹⁷⁾ and CHARLES et al⁽³⁰⁾ have shown that during oxidation of zirconium in the temperature range 350°-950°C the results were best fitted to a cubic equation. WESTERMAN⁽³¹⁾ found that zirconium and Zircaloy 2 oxidize in oxygen and water vapor at comparable rates according to the cubic rate law, in the temperature range of 600° - 800°C and under a pressure of 25 mm Hg. Regardless of temperature and environment zirconium did not exhibit a transition in oxidation kinetics in tests of 25 hr. duration.

PEMSLER⁽³²⁾ in a recent investigation has shown that the dissolution of oxygen in zirconium in the temperature range 840°-975°C obeyed diffusion kinetics and remained parabolic for sufficiently thick samples. The film growth conformed to a parabolic rate growth after approx. 9 hrs; the initial rate growth could be expressed best by a quadratic equation. The over-all weight gain curves could be fitted to the parabolic relationship after an initial period of more rapid reaction.

HUSSEY and SMELTZER⁽³³⁾ obtained similar relationship for the temperature range of 400°-850°C. These investigators report that the oxidation kinetics of zirconium at long times obeyed a parabolic rate equation which was best described in terms of a diffusion model for both the oxide and metal. From microhardness measurements, they determined the diffusivity of oxygen in alpha-zirconium, as: $D = 28.8 \exp(-53,400/RT)$.

DEBUIGNE and LEHR⁽³⁴⁾ conducted measurements on oxidation of zirconium in the temperature range of 600°-850°C and found that to a good approximation a parabolic relationship was satisfied. Based on the assumption of a diffusion controlled reaction, they derived a mathematical treatment for evaluating the diffusivity of oxygen in alpha-zirconium. The calculated value was shown to be: $D = 22.4 \exp(-59700/RT)$ for temperatures higher than 700°C. For temperatures lower than 650°C they assumed from the discontinuity in the slope of the Arrhenius plot of D vs. $1/T$ that grain boundary diffusion became preferred.

KEARNS and CHIRICOS⁽³⁵⁾ employing hardness measurements have determined the diffusivity of oxygen in alpha-zirconium for the temperature range

622°-840°C. They report that the average value of diffusivity based on their own results and those of PEMSLER⁽³⁶⁾ and MALLETT et al.⁽³⁷⁾ can be expressed as: $D = 5.4 \exp(-50800/RT)$.

At present, the diffusion coefficient of oxygen in beta-zirconium is not known. To a good approximation the value of oxygen diffusivity reported by MALLETT, ALBRECHT and WILSON⁽³⁷⁾ i.e. $D = 0.0453 \exp(-28200 \pm 2400)/RT$ for the case of beta-Zircaloy 2 may be taken into consideration. For justification of this recommendation the reader is referred to a study by PEMSLER⁽³⁶⁾.

All of the above mentioned investigators report the formation of gray zirconium dioxide only, during the reaction of zirconium with oxygen. There is, however, some evidence in the literature^(18,38,39) that after prolonged exposures white oxide commences to appear and the oxidation rate of zirconium increases accordingly.

ARONSON⁽⁴⁰⁾ and SARKISOV et al.⁽⁴¹⁾ have shown that both oxides possess the same monoclinic structure and that during conversion of white oxide into gray oxide the color changes from white to gray as oxygen is being removed, and that the reverse process is also true. Both authors observed a slight difference in the position of lines on X-ray and electron diffraction patterns. However, they did not attempt to determine quantitatively the changes in lattice parameters of the respective cell. SAUR et al.⁽⁴²⁾ explain the change of color in terms of optical properties associated with the physical state of the oxide, i.e. with the thickness of the oxide layer. Their arguments do not appear to be very convincing.

COX⁽⁴³⁾ discusses the wide variation in stoichiometry of ZrO_2 . He points out that none of the studies of non-stoichiometry of ZrO_2 in the literature can be accepted without reserve and that the pretransition gray oxide formed on zirconium is hypo-stoichiometric. It is difficult to give precise deviations from stoichiometry without stating the specific conditions of examinations. Generally, the reported value is from ZrO_{2-x} where: $x < 0.001$ to $ZrO_{1.9}$ for temperatures up to $1500^\circ C$. There is no evidence of hyper-stoichiometry for zirconium oxide formed during the reaction of zirconium with pure oxygen.

2.6 Reaction of Zirconium with Nitrogen:

The reaction of zirconium with nitrogen has been described by GULBRANSEN and ANDREW⁽²⁶⁾ in the temperature range $400^\circ - 825^\circ C$ and by DRAVNIKES⁽⁴⁴⁾ at 860° to $1050^\circ C$. Both investigators showed that the reaction obeyed a parabolic relationship and that the reaction rate was much slower than with oxygen. They also report that the zirconium-nitrogen reaction is nearly independent of pressure in the range of 15-760 mm Hg.

MALLETT, BELLE and CLELAND⁽⁴⁵⁾ investigated the zirconium-nitrogen reaction over a wide range of temperatures ($975^\circ - 1640^\circ C$) at 1 atm and found that the reaction conforms strictly to a parabolic law and the parabolic rate constant in $(ml/cm^2)^2/sec$ could be calculated to give: $k_p = 5.0 \times 10^3 \exp \left[\frac{-48000 \pm 1500}{RT} \right]$. They also determined the diffusion of nitrogen from the gaseous phase into beta-zirconium containing 0.015 wt.% hafnium. The samples were degassed in vacuum and then heated in nitrogen.

Layers were removed and analysed for nitrogen. The values obtained could be correlated by the equation: $D = 1.5 \times 10^{-2} \exp \left[\frac{-30.700 \pm 1000}{RT} \right]$.

In the above investigations it has been assumed that the scale consists of zirconium nitride. In all likelihood this nitride would correspond closely to ZrN.

2.7 Reaction of Zirconium with Nitrogen-Oxygen Atmospheres:

Even small amounts of nitrogen in the presence of oxygen have a detrimental effect on corrosion resistance of zirconium. The deleterious effect of nitrogen according to LOEVENSTEIN and GILBERT⁽⁴⁶⁾ could possibly be explained by the replacement of some oxygen atoms in the oxide lattice, the exchange being in the ratio 2/3; that is, 2 N³⁻ ions would replace 3 O²⁻ ions. Therefore, in an n-type oxide the presence of nitrogen would increase the number of vacant oxygen sites. Since the parabolic rate constant is directly related to the concentration of vacancies, this increased concentration would increase the oxidation rate in the parabolic range.

HAYES and ROBERTSON⁽⁴⁷⁾ oxidized zirconium samples in air. They found that the scales formed were blue-black at first, and turned white later. Samples completely covered with white scale were obtained in 24 hrs. at 700°C and 4 hrs. at 800°C. The weight increase followed first a parabolic law and deviations towards more rapid scaling kinetics occurred after formation of white oxide.

Similarly, PHALNIKAR and BALDWIN⁽³⁸⁾ report that black scales preceded the white scales during oxidizing zirconium in air. Before the advent of

white scales a quasi parabolic law of oxidation was obeyed, this was followed by a sharply increased rate for tests below 1050°C.

2.8 Reaction of Zirconium with Water Vapor-Oxygen Mixtures:

The scaling behaviour of high-purity zirconium in water vapor at 25mm pressure and 600°-800°C was investigated by WESTERMAN⁽³¹⁾. The kinetic curves were best fitted by a cubic rate law. No deviation from this rate-relationship occurred even at long exposures, up to 25 hr. duration. When compared with the oxidation rates of zirconium in pure oxygen under the same conditions, the scaling rates in water vapour were slightly slower.

Data available in the literature and concerning the combined effect of water vapour and oxygen on zirconium are indeed very scarce. The only reported investigation is that by AMBARTSUMYAN et al.⁽⁴⁸⁾. They investigated the simultaneous influence of oxygen and steam on zirconium at 450°C and test durations up to 810 hr. The oxygen pressure was 380 mm Hg. and the remaining 380 mm Hg. was due to steam. The rates of scaling under the influence of the mixture were about the same as the rates of scaling of zirconium in steam at 760 mm Hg. However, the behaviour of Zr - 1.0% Nb and Zr-2.5% Nb alloys was quite different. The alloys oxidized much faster in the mixture than in pure steam, under the same conditions.

2.9 Reactions of Zirconium with Gases other than Nitrogen and Oxygen:

HALL et al.⁽⁴⁹⁾, and MARTIN and REES⁽⁵⁰⁾ have developed a theory based on statistical mechanics to account for the solubility of hydrogen

in zirconium as a function of hydrogen pressure. The good agreement between the experimental evidence of solubility and theoretical predictions and between the observed and evaluated values of heats of ZrH_2 formation provide satisfactory justification for the theoretical basis of their interpretation. They also explain the fact that the saturation solubility decreases with temperature in terms of order-disorder phenomenon in the metal lattice.

The negative influence of hydrogen on oxidation resistance of zirconium is of a secondary nature. Hydrogen may form a hydride under the oxide layer and detach the oxide which would otherwise protect the metal substrate. Provided no hydride is formed, hydrogen in solid solution has no direct effect on corrosion as reported by LOEVENSTEIN and GILBERT⁽⁴⁶⁾.

Zirconium is attacked by carbon dioxide and carbon monoxide more strongly than by oxygen but less than by water vapour, at 600° - $1000^{\circ}C$. When the pressure was 0.6 mm Hg and the temperature $986^{\circ}C$ the following sequence with regard to attack was found by DRAVNIEKS⁽⁵¹⁾: oxygen, air, water vapour and carbon dioxide. HUSSEY and SMELTZER⁽⁵¹⁾ in a recent study on the reaction of zirconium with carbon dioxide and carbon monoxide at $850^{\circ}C$ found that the kinetic curve for zirconium-carbon dioxide reaction exhibited three distinct parts: an initial decreasing rate, an intermediate rapid increasing rate, and a final decreasing rate. After about 16 hrs. the weight gain was to a good approximation the same as for the zirconium-oxygen reaction and conformed to the parabolic law. The oxidation kinetics of zirconium with carbon monoxide were in the form of continuously decreasing rate curve and up to about 16 hrs. the weight gain was approximately the same as for oxygen. At times in excess of 16 hrs. a transition to more rapid oxidation rates occurred.

MALLETT, ALBRECHT and BENNETT⁽⁵³⁾ found that the reaction of iodide zirconium with water vapour at a pressure of 33 mm Hg and for the temperature range 300°-600°C obeys a cubic law and that only a single-phase oxide could be seen under the microscope, which means that adsorption of hydrogen by the metal must have been negligible.

Due to corrosion problems in nuclear reactors, a considerable amount of work has been carried on the oxidation of zirconium and several of its alloys in steam. This work does not directly relate to the present study and the reader is referred to recent review articles on this subject^(31,54,48,55).

CHAPTER III

Theory for Parabolic Oxidation and Nitriding of Zirconium

3.1 Differential Model for Two-Solid Phase Oxidation and Nitriding:

Oxidation and nitriding of zirconium at temperatures less than 862°C, the allotropic transformation temperature for alpha to beta zirconium, takes place by interstitial dissolution of the gaseous reactant in the alpha metal phase up to the saturation limits and simultaneous formation of the scale. Provided that scale growth and oxygen solution in the metal are governed by lattice diffusion of oxygen this gives rise to a solid two-phase diffusion system. A diffusion model applicable to this type of system has been advanced by WAGNER⁽⁵⁶⁾ where one of the phases (metal phase) is treated as an infinite plate.

The appropriate diffusion model for oxidation or nitriding is shown schematically in Fig. 1a . For concurrent scale growth and gas dissolution the total rate of oxygen or nitrogen uptake is:

$$\frac{d}{dt} \left(\frac{\Delta m}{A} \right) = - D_{II} \left(\frac{\partial C}{\partial x} \right)_{x < \epsilon} = (C_{II}^I - C_I^{II}) \frac{d\epsilon}{dt} - D_I \left(\frac{\partial C}{\partial x} \right)_{x > \epsilon} \quad (25)$$

where:

$$\frac{d\epsilon}{dt} = \gamma_{\epsilon} \sqrt{D_{II}} / \sqrt{t} \quad (26)$$

and the concentration of the gaseous reactant at any point in the

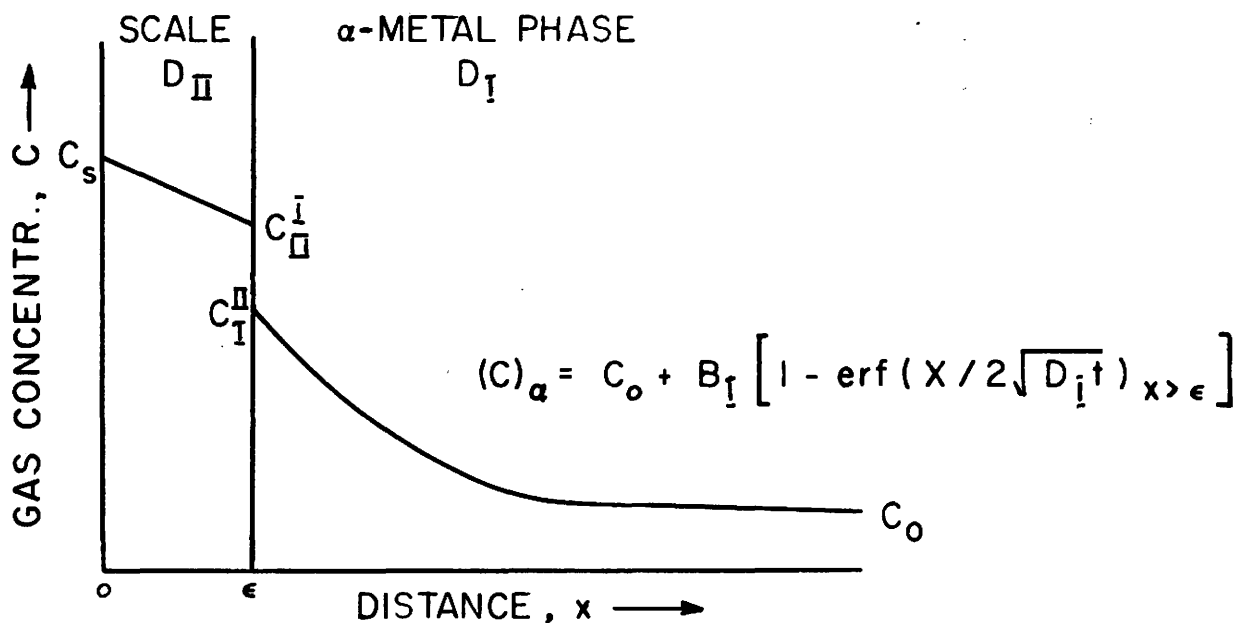
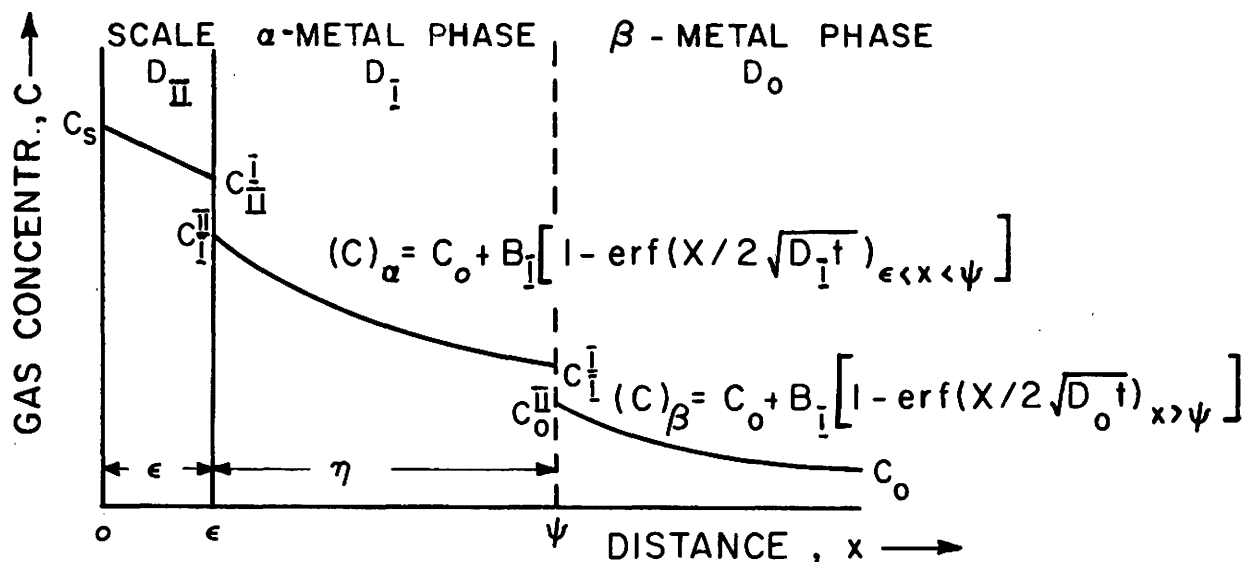
(a) TWO-PHASE SOLID DIFFUSION MODEL, $T = \text{CONST.}$ (b) THREE-PHASE SOLID DIFFUSION MODEL, $T = \text{CONST.}$

FIG. I. SCALE-METAL DIFFUSION MODELS FOR PARABOLIC REACTION KINETICS & BINARY PHASE DIAGRAMS.

metal phase is given as an error function relation:

$$(C)_\alpha = C_o + B_I \left[1 - \operatorname{erf} \left(\frac{x}{2\sqrt{D_I t}} \right) \right]_{x>\epsilon} \quad (27)$$

Therefore:

$$\left(\frac{\partial C}{\partial x} \right)_{x=\epsilon} = -B_I / \sqrt{\pi D_I t} \cdot \exp - \frac{\gamma_\epsilon^2 D_{II}}{D_I} \quad (28)$$

Substituting equation (26) and (28) into (25) yields upon integration:

$$\frac{\Delta m}{A} = 2 \left[(C_{II}^I - C_I^{II}) \gamma_\epsilon \sqrt{D_{II}} + B_I \sqrt{D_I/\pi} \exp - \gamma_\epsilon^2 \cdot \frac{D_{II}}{D_I} \right] t^{1/2} \quad (2)$$

where:

$$2 (C_{II}^I - C_I^{II}) \gamma_\epsilon \sqrt{D_{II}} = k_{p(\text{scale})} \quad (30)$$

and

$$2 B_I \sqrt{D_I/\pi} \cdot \exp - \gamma_\epsilon^2 \frac{D_{II}}{D_I} = k_{p(\text{metal})} \quad (31)$$

Therefore:

$$\frac{\Delta m}{A} = (k_{p(\text{scale})} + k_{p(\text{metal})}) \cdot \sqrt{t} = k_{p(\text{total})} \cdot t^{1/2} \quad (32)$$

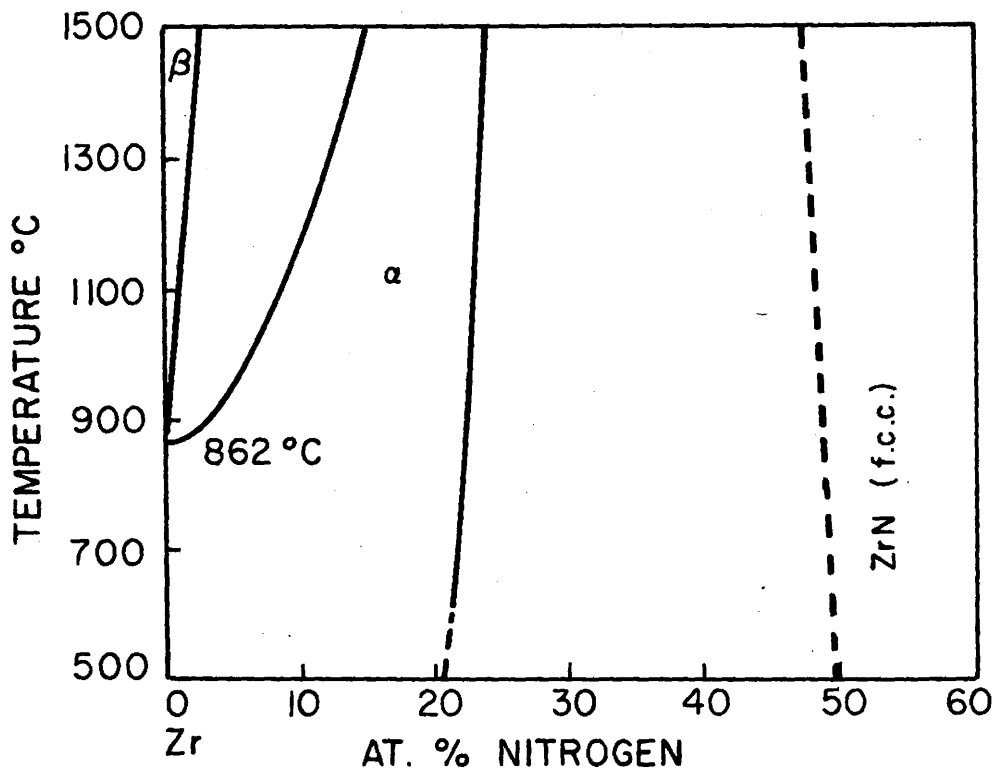
is consistent with the parabolic relationship, equation (2), and accounts functionally for the scaling of a metal forming a two-phase semi-infinite diffusion couple.

In these equations: ϵ is the scale thickness at time t , x is the distance from the scale/gas interface, D_{II} and D_I are diffusivities of oxygen or nitrogen in the oxide or nitride scale and metal respectively, C_{II}^I and C_I^{II} are oxygen or nitrogen concentrations in the scale and metal at the metal-scale interface respectively, and B_I

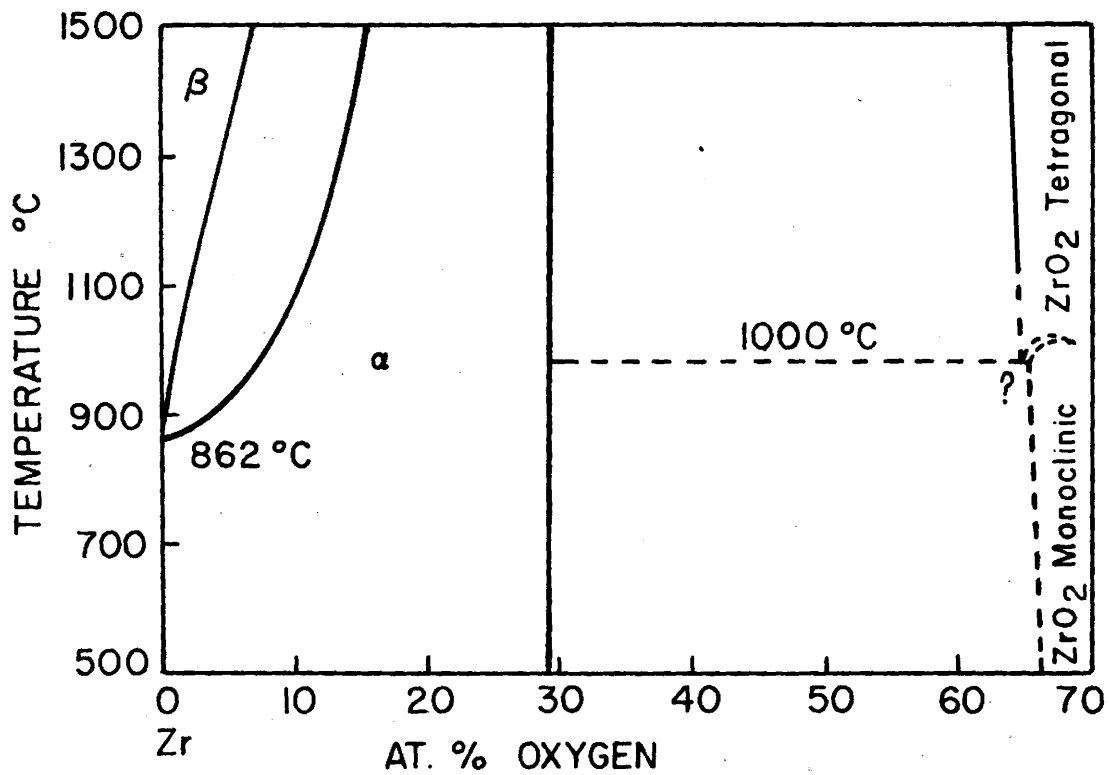
and γ_{ξ} are constants. C_o and C_{α} in equation (27) are the concentrations of oxygen or nitrogen initially in the metal and at any distance $x > \xi$, respectively.

Combining equation (26) with (30) one can evaluate the parabolic rate constant from the movement of the metal-scale interface, providing the values of gaseous concentrations at this interface are known. These can be obtained from the appropriate zirconium-oxygen phase diagrams, e.g. by HANSEN⁽⁵⁷⁾. The movement of the scale-metal interface or in other words the thickness ξ of the scale for a given time, t , can be measured microscopically.

The binary zirconium-oxygen and zirconium-nitrogen phase diagrams are shown in Figure 1 c,d. to the temperature of 1500°C. Zirconium exhibits an exceptionally large solubility for both oxygen and nitrogen, the solubility limits being larger than 20at %. It is to be noted that the solution of oxygen or nitrogen into the metal increases the temperature for stability of the alpha phase. Accordingly, the above discussed two phase solid diffusion model for oxidation or nitriding of zirconium is applicable only to the allotropic transformation temperature of 862°C. If appropriate diffusion data are available, these data may be employed with concentrations from the appropriate phase diagram to evaluate the parabolic oxidation or nitriding constants.



(c) ZIRCONIUM - NITROGEN EQUILIBRIUM DIAGRAM



(d) ZIRCONIUM - OXYGEN EQUILIBRIUM DIAGRAM

3.2 Integral Model for Two-Solid Phase Oxidation and Nitriding

The total oxygen or nitrogen uptake at a given time, $t > 0$ is equal to:

$$\left(\frac{\Delta m}{A}\right)_{\text{total}} = \left(\frac{\Delta m}{A}\right)_{\text{scale}} + \left(\frac{\Delta m}{A}\right)_{\text{Zr-a}}$$

If the oxide is treated as a finite plate of uniform oxygen concentration, integration over the respective fields of fig. 1a yields:

$$\left(\frac{\Delta m}{A}\right)_{\text{total}} = \int_0^{\epsilon} \int_{C_I^{II}}^{C_{II}^I} c dx + \int_{\epsilon}^{\infty} \int_{C_0}^{C_a} c dx + \int_0^{\epsilon} \int_{C_0}^{C_I^{II}} c dx \quad (33)$$

and when making use of equation (27):

$$\left(\frac{\Delta m}{A}\right)_{\text{total}} = (C_{II}^I - C_0) \epsilon + B_I \int_{\epsilon/2}^{\infty} \operatorname{erfc} \frac{x}{2\sqrt{D_I t}} dx \quad (34)$$

Let: $\xi = \frac{x}{2\sqrt{D_I t}}$ then $dx = 2\sqrt{D_I t} \cdot d\xi$, which when

substituted into equation (34) and taking into account equation (26) gives upon integration:

$$\left(\frac{\Delta m}{A}\right)_{\text{total}} = 2 \left[(C_{II}^I - C_0) \gamma_{\epsilon} \sqrt{D_{II}} + B_I \sqrt{D_I} \cdot \operatorname{ierfc} \gamma_{\epsilon} \sqrt{\frac{D_{II}}{D_I}} \right] \sqrt{t} \quad (35)$$

which is the explicit expression for a two-phase diffusion model i.e. below the alpha-beta allotropic transformation ($\sim 862^{\circ}\text{C}$).

Here, the values for k_p 's are given by:

$$(k_p)_{\text{scale}} = 2 (C_{II}^I - C_I^{II}) \gamma_{\epsilon} \sqrt{D_{II}} \quad (36)$$

which is the same as in equation (30), and

$$(k_p)_{\text{alpha-Zr}} = 2 \left[B_I \sqrt{D_I} \operatorname{ierfc} \gamma_\epsilon \sqrt{\frac{D_{II}}{D_I}} + (C_I^{II} - C_o) \gamma_\epsilon \sqrt{D_{II}} \right] \quad (37)$$

Thus, we are able to evaluate again the total parabolic rate constant and compare it with the experimentally obtained value.

3.3 Differential Model for Three-Solid Phase Oxidation and Nitriding

At temperatures above the alpha-beta allotropic transformation temperature of zirconium, dissolution of oxygen or nitrogen into the metal stabilizes the alpha solid solution phase, Fig. 1e,d. Accordingly a superficial scale and an intermediate of the stabilized alpha phase are formed on beta zirconium during oxidation or nitriding. It is possible to extend the previously presented diffusion principles to these more complex systems.

The diffusion model governing formation of three solid phases during reaction is shown in Fig. 1b. Let us retain the same notation as for the two-phase model, with the following supplementary designations: the alpha/beta interface will be Ψ , the thickness of the alpha phase will be denoted as η , C_I^I and C_o^{II} will represent the gas concentrations in the alpha phase and beta phase at the phase boundary Ψ , respectively. Let D_o indicate the diffusivity of oxygen or nitrogen in the beta phase and C_o the initial amount of oxygen or nitrogen in the metal.

For the situation shown, equations:

$$(C)_\alpha = C_o + B_I \operatorname{erfc} \left(\frac{x}{2 \sqrt{D_I t}} \right) \quad \epsilon < x < \Psi \quad (38)$$

$$(C)_\beta = C_o + B_o \operatorname{erfc} \left(\frac{x}{2 \sqrt{D_o t}} \right) \quad x > \Psi \quad (39)$$

express the variation of gas concentration in each of the given metal phases for the implied conditions of x .

The mass balance at the interface ξ is:

$$-D_{II} \left(\frac{\partial C}{\partial x} \right)_{x=\xi-0} = (C_{II}^I - C_I^{II}) \frac{d\xi}{dt} - D_I \left(\frac{\partial C}{\partial x} \right)_{x=\xi+0} \quad (40)$$

and at the interface ψ :

$$-D_I \left(\frac{\partial C}{\partial x} \right)_{x=\psi-0} = (C_I^I - C_o^{II}) \frac{d\psi}{dt} - D_o \left(\frac{\partial C}{\partial x} \right)_{x=\psi+0} \quad (41).$$

Correlation between equations (40) and (41) is found to be:

$$\left(\frac{\partial C}{\partial x} \right)_{x=\psi-0} = \left(\frac{\partial C}{\partial x} \right)_{x=\xi+0} + \int_{\xi}^{\psi} \left(\frac{\partial^2 C}{\partial x^2} \right) dx \quad (42).$$

Differentiation of equation (38) with respect to x gives:

$$\frac{\partial^2 C}{\partial x^2} = \frac{B_I x}{2\sqrt{\pi D_I t} D_I t} \cdot \exp - \frac{x^2}{4D_I t} \quad (43).$$

Substituting this into equation (42) and after solving the integral one obtains:

$$\left(\frac{\partial C}{\partial x} \right)_{x=\psi-0} = \left(\frac{\partial C}{\partial x} \right)_{x=\xi+0} + \frac{B_I}{\sqrt{\pi D_I t}} \left(\exp - \frac{\xi^2}{4D_I t} - \exp - \frac{\psi^2}{4D_I t} \right) \quad (44).$$

Substituting this equation into equation (41) yields:

$$-D_I \left(\frac{\partial C}{\partial x} \right)_{x=\xi+0} - \frac{B_I \sqrt{D_I}}{\sqrt{\pi t}} \left(\exp - \frac{\xi^2}{4D_I t} - \exp - \frac{\psi^2}{4D_I t} \right) = (C_I^I - C_o^{II}) \frac{d\psi}{dt} - D_o \left(\frac{\partial C}{\partial x} \right)_{x=\psi+0} \quad (45),$$

which when solved with respect to: $-D_I \left(\frac{\partial C}{\partial x} \right)_{x=\xi+0}$ and combined with equation (40) gives:

$$\begin{aligned} -D_{II} \left(\frac{\partial C}{\partial x} \right)_{x=\xi-0} = & (C_{II}^I - C_I^{II}) \frac{d\xi}{dt} + (C_I^I - C_o^{II}) \frac{d\psi}{dt} + \frac{B_I \sqrt{D_I}}{\sqrt{\pi t}} \left(\exp - \frac{\xi^2}{4D_I t} - \exp - \frac{\psi^2}{4D_I t} \right) + \\ & - \frac{B_o \sqrt{D_o}}{\sqrt{\pi t}} \exp - \frac{\psi^2}{4D_o t} \end{aligned} \quad (46),$$

where the last term of this equation has been obtained by differentiation of equation (39) for $x=\Psi$.

Since the total amount of oxygen or nitrogen Δm per area A taken up by the sample in time t is equal to:

$$\frac{d}{dt} \left(\frac{\Delta m}{A} \right) = - D_{II} \left(\frac{\partial C}{\partial x} \right)_{x=\epsilon=0} \quad (47)$$

and;

$$\frac{d\epsilon}{dt} = \gamma_{\epsilon} \cdot \sqrt{D_{II}} / \sqrt{t} \quad (48)$$

$$\frac{d\Psi}{dt} = \gamma_{\Psi} \cdot \sqrt{D_I} / \sqrt{t} \quad (49)$$

substitution of these three equations into equation (46) gives the total gas uptake:

$$\begin{aligned} \frac{\Delta m}{A} = 2 \left[(C_{II}^I - C_I^{II}) \gamma_{\epsilon} \cdot \sqrt{D_{II}} + (C_I^I - C_o^{II}) \gamma_{\Psi} \cdot \sqrt{D_I} + B_I \sqrt{D_I/\pi} \left(\exp - \frac{\gamma_{\epsilon}^2 D_{II}}{D_I} - \exp - \gamma_{\Psi}^2 \right) + \right. \\ \left. + B_o \sqrt{D_o/\pi} \exp - \frac{\gamma_{\Psi}^2 D_I}{D_o} \right] \sqrt{t} \quad (50). \end{aligned}$$

Obviously, equation (50) reduces to equation (29) for $\epsilon < x < \Psi$ and becomes an explicit expression for a two phase system.

Similarly to equation (32) applicable to two-phase diffusion, equation (50) can be expressed as:

$$\frac{\Delta m}{A} = (k_{p(\text{scale})} + k_{p(\alpha\text{-phase})} + k_{p(\beta\text{-phase})}) t^{1/2} = k_{p(\text{total})} \cdot t^{1/2} \quad (51)$$

where:

$$2(C_{II}^I - C_I^{II}) \gamma_{\epsilon} \sqrt{D_{II}} = k_{p(\text{oxide})} \quad (52)$$

$$2 (C_I^I - C_o^{II}) \gamma_{\Psi} \sqrt{D_I} + B_I \sqrt{D_I/\pi} (\exp - \gamma_{\epsilon}^2 D_{II}/D_I - \exp - \gamma_{\Psi}^2) = k_p(\alpha\text{-phase}) \quad (53)$$

and

$$2 B_o \sqrt{D_o/\pi} \exp - \gamma_{\Psi}^2 D_I/D_o = k_p(\beta\text{-phase}) \quad (54).$$

Experimental evaluation of equation (50) follows the same patterns as those outlined already for the two-phase model and will not be discussed again. The experimental check on the applicability of the derived equations for a three-phase system will be given in Chapter 8.1.2.

3.4 Integral Model for Three-Solid Phase Oxidation and Nitriding

Consider again the zirconium-oxygen or zirconium-nitrogen equilibrium phase diagrams (Fig. 1c,d) and the associated diffusion model at temperature above 862°C and time, $t > 0$, as shown in Fig. 1b. The total gas uptake would be:

$$\left(\frac{\Delta m}{A}\right)_{\text{total}} = \left(\frac{\Delta m}{A}\right)_{\text{scale}} + \left(\frac{\Delta m}{A}\right)_{\text{Zr-alpha}} + \left(\frac{\Delta m}{A}\right)_{\text{Zr-beta}} \quad (55),$$

or upon integrating the appropriate fields and making use of equations (38) and (39):

$$\left(\frac{\Delta m}{A}\right)_{\text{total}} = (C_{II}^I - C_I^{II}) \epsilon + B_I \int_{\epsilon/2 \sqrt{D_I t}}^{\Psi/2 \sqrt{D_I t}} \operatorname{erfc}\left(\frac{x}{2 \sqrt{D_I t}}\right) dx + (C_I^{II} - C_o^{II}) \epsilon - (C_o^{II} - C_o^o).$$

$$\cdot (\Psi - \epsilon) + B_o \int_{\Psi/2 \sqrt{D_o t}}^{\infty} \operatorname{erfc}\left(\frac{x}{2 \sqrt{D_o t}}\right) dx + (C_o^{II} - C_o^o) \Psi \quad (56).$$

Let: $\xi = \frac{x}{2 \sqrt{D_I t}}$, therefore $dx = 2 \sqrt{D_I t} \cdot d\xi$

and $\xi' = \frac{x}{2\sqrt{D_0 t}}$, therefore $dx = 2\sqrt{D_0 t} \cdot d\xi'$.

Substituting these terms for the integrands and dx 's of equation (56) one obtains:

$$2 B_I \sqrt{D_I t} \left(\int_{\xi/2\sqrt{D_I t}}^{\infty} \operatorname{erfc} \xi \, d\xi - \int_{\psi/2\sqrt{D_I t}}^{\infty} \operatorname{erfc} \xi \, d\xi \right) + 2B_0 \sqrt{D_0 t} \int_{\psi/2\sqrt{D_0 t}}^{\infty} \operatorname{erf} \xi' \, d\xi',$$

as part of equation (56). With the aid of this expression, integration of equation (56) gives:

$$\begin{aligned} \left(\frac{\Delta m}{A}\right)_{\text{total}} = 2 \left[(C_{II}^I - C_0) \gamma_{\xi} \sqrt{D_{II}} + B_I \sqrt{D_I} (\operatorname{ierfc} \gamma_{\xi} \sqrt{D_{II}/D_I} - \operatorname{ierfc} \gamma_{\psi}) + \right. \\ \left. + B_0 \sqrt{D_0} \cdot \operatorname{ierfc} \gamma_{\psi} \sqrt{D_I/D_0} \right] \cdot \sqrt{t} \end{aligned} \quad (57),$$

where the movement of the interfaces ξ and ψ has been given in terms of relationships (48) and (49).

Equation (57) is the final expression for the total gas uptake by a system consisting of three phases. It is immediately apparent that this expression reduces to two-phase diffusion system, viz. equation (35), for the condition $\xi < x < \psi$.

Finally, the values of the parabolic rate constants for the appropriate phases are:

$$k_{p(\text{scale})} = 2(C_{II}^I - C_I^{II}) \gamma_{\xi} \sqrt{D_{II}} \quad (58)$$

which is, of course, identical with equation (36) derived from a two-phase oxidation model;

$$k_p(\text{alpha-Zr}) = 2 \left[B_I \sqrt{D_I} (\text{ierfc } \gamma_\xi \sqrt{D_{II}/D_I} - \text{ierfc } \gamma_\Psi) + (C_I^{II} - C_o) \gamma_\xi \sqrt{D_{II}} - (C_o^{II} - C_o) \gamma_\Psi \sqrt{D_I} \right] \quad (59)$$

and

$$k_p(\text{beta-Zr}) = 2 \left[B_o \sqrt{D_o} \text{ierfc } \gamma_\Psi \sqrt{D_I/D_o} + (C_o^{II} - C_o) \gamma_\Psi \sqrt{D_I} \right] \quad (60).$$

Thus, following the outlined already procedure we are able to calculate the total uptake of gas and compare this evaluation with experimental evidence. Comparison of the two three-phase models reveals that the expressions for k_p 's for the scale are identical. In the appendix, Problem 1, it has been shown that the identity between the remaining terms for k_p 's exists also.

3.5 Supplementary Restriction on Diffusion Processes:

Should the oxidation or nitriding phenomena be a purely diffusion controlled reaction, then according to KIDSON⁽⁵⁹⁾ the following has to hold:

$$\xi = B_\xi \cdot \sqrt{t}$$

and

$$\eta = B_\eta \cdot \sqrt{t}.$$

Therefore, at a given temperature, T,:

$$\xi/\eta = B_\xi / B_\eta = \text{constant} \quad (61)$$

where:

ξ and η - are the thicknesses of the scale and alpha-phase at time

t , and

B_ξ , B_η - are constants for the respective phases.

The plot of equation (61) vs. \sqrt{t} should yield a straight line and any deviation from linearity can be interpreted either by the experimental error involved or in terms of some other process associated with the diffusion phenomenon.

3.6 Limitations and Assumptions Relevant to Models:

1. From the expressions for k_p 's of the oxide it follows that we approximate our calculations by neglecting the error function curve of phase II. This assumption is necessary because we do not know the value of C_s . The small gradient $(C_s - C_{II}^I)/\xi$ should not introduce an appreciable error.
2. For a kinetic system the value of gas concentration in the alpha-phase at the ξ interface should lie between C_I^{II} and C_{II}^I . Similarly the value for the beta-phase at the interface Ψ should be between C_o^{II} and C_I^I . This deviation from the equilibrium values arises from the fact that a small degree of supersaturation is needed in order to form and to continue the growth of the appearing new phase. We neglect these deviations.
3. The mathematical treatment derived above is only valid for the condition where the volume of the forming new phase (II and I) is exactly equal to the volume of the disappearing phase.

CHAPTER IV

Experimental

4.1 Introduction:

Various methods have been employed for investigating the oxidation rates and for examining the nature of oxidation products formed on metals. The simplest and most direct methods, gravimetric, manometric, volumetric, electrometric, have been commonly used. Descriptions of these methods can be found in texts dealing with corrosion. It is therefore not the object of this section to review these procedures.

In this experiment the volumetric method has been chosen as a procedure for measuring the oxidation and nitriding rates. By adopting this method it was expected that larger samples than those used in gravimetric measurements could be utilized.

4.2 Volumetric Apparatus:

One of the apparatuses used for determination of gas volumes adsorbed by zirconium specimens at various temperatures and gas pressures combines basically two concepts: that used by JENKINS⁽⁶²⁾ for measuring oxidation rates of titanium and that utilized by SMELTZER et al.⁽⁶³⁾ for estimation of amounts of oxygen adsorbed by silver catalysts.

Essentially the whole arrangement is comprised of four main parts: equipment for determinations of large volumes of oxygen adsorbed together with the furnace assembly and its control, oxygen supply system, air admittance system, and an assembly for measurements of small volumes of gases consumed by the metals.

Fig. 2 is an over-all picture of the apparatus and Fig. 3 represents a schematic diagram of main components.

A suitable prepared specimen was placed into a demountable silica chamber (2). Since it was suggested by DALGAARD⁽⁶⁴⁾ that zirconium may become contaminated by silicon at high temperatures while in contact with a silica-glass tube, the sample was supported at both ends by platinum wire wrapped around it. To decrease the "dead" space of the reaction chamber an evacuated silica tube (3) was placed concentrically inside the glass tube (2), thus increasing the sensitivity of the apparatus. The "dead" volume between these two tubes was calibrated by the amount of water displaced at room temperature and turned out to be: 58 cc. A water-cooled joint (4) was incorporated in order to maintain a good vacuum seal at the operating temperatures from 750° to 1000°C.

The furnace (1), which was positioned around the reaction assembly by a vertical slide, consisted of two independently controlled heating elements. The inner, 36 x 2 1/2 in. in diameter closely wound Nichrome coil acted as the main heating source. The purpose of the outer coil, which was concentrically wound at both ends on the top of the first one, was to extend the uniform temperature zone. This somewhat superfluous precaution appeared to be justified when one considers the large effect of the SORET-type diffusion

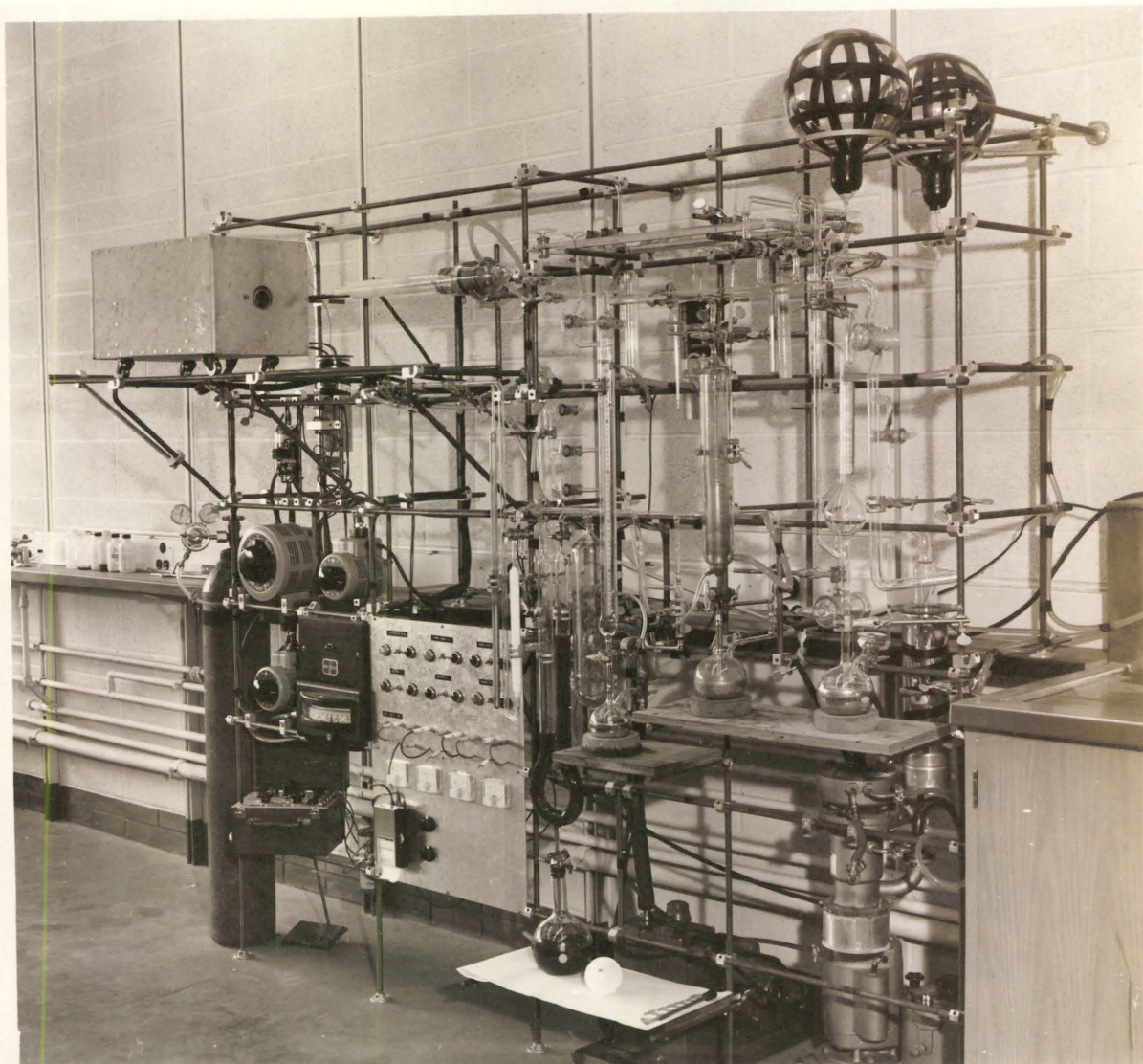


Fig. 2 General view of the volumetric apparatus.

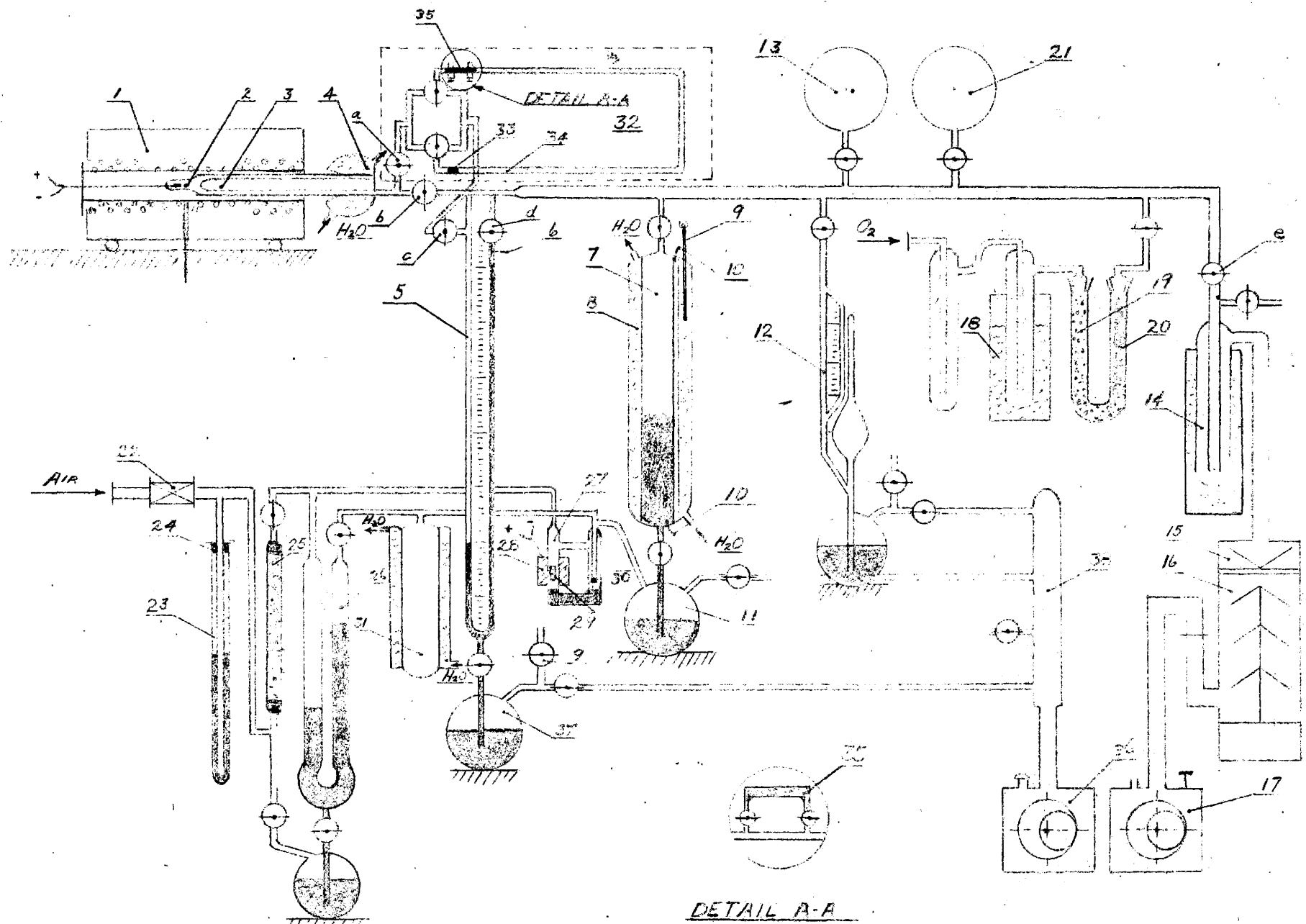


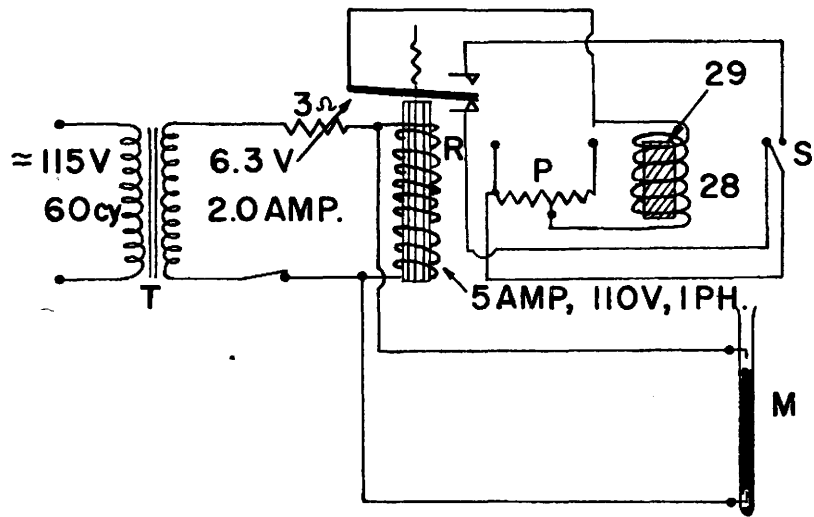
Fig. 3 Schematic diagram of main components of the volumetric apparatus.

of oxygen or nitrogen in zirconium. RIECK and BRUNING⁽⁶⁵⁾ have demonstrated that either of the gases moves quite readily under the influence of a temperature gradient to that part of the metal which has the lower temperature.

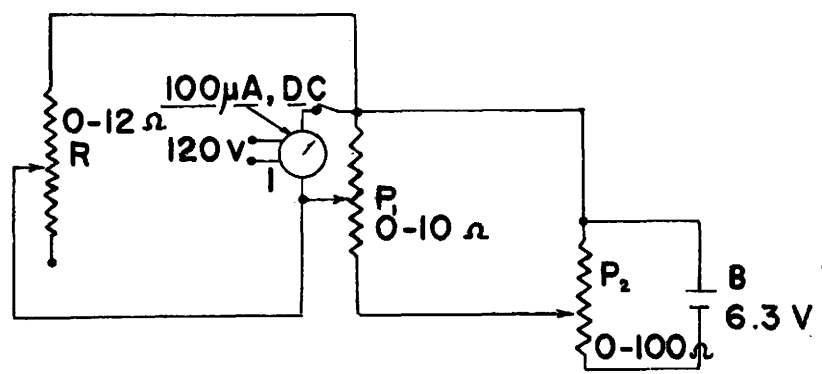
The uniform temperature zone was 2 1/2 in. in length at 850°C with the temperature variation of $\pm 2.3^{\circ}\text{C}$ within it. The fluctuation of temperature was limited by the sensitivity of the controlling BRISTOL indicator. The temperature of the adsorption cell was measured by two standardized chromel-alumel thermocouples, one of which was placed very close to the specimen in a cavity purposely designed for this reason, as shown in Fig. 3 .

The glass-chamber (2) was connected by means of a capillary tube to the mercury manometer (5) which in turn was joined with the calibrated 250 cc. glass-burette (7). To permit burette readings in rapid successions (at constant pressure) the manometer was equipped with sealed-in electrical contacts (6) and these were connected to the relay winding (R) as shown in Fig. 4a .

A water jacket (8) placed around the burette prevented excessive changes of gas volumes due to variations in the room temperature. The water temperature was controlled by the inserted thermometer (9) and the rate of water flow was regulated accordingly. A high resistance thin wire (10) was vacuum sealed into the burette with the intention of continuously recording the movement of mercury column on the basis of resistance changes. Fig. 4b shows the electrical circuit diagram designed for this purpose,



(a)



(b)

Fig. 4 Electrical circuit diagram for taking continuous readings.

where (R) represents the high-resistance Nichrome wire (10), (I) the indicator and recorder, and (P_1) and (P_2) are the parallel connected sensitizing potentiometers. A standard dry cell of 6.3V was used as the current source. Since the direct readings taken from the gas-burette with the accuracy of 0.25cc. of oxygen displaced were more precise than those registered by the recorder (I), the present sensitizing circuit was inadequate. It should be replaced possibly by a Wheatstone bridge-type balancing arrangement or some other controlling equipment.

The whole assembly was evacuated by BALTZER'S oil diffusion pump (16) coupled with a rotary mechanical 'DUO-SEAL' pump (17). To obtain a better vacuum by hindering the "back-streaming" of hot vapour molecules of oil and by condensing the water vapour, the water-cooled trap (15) and a liquid-air trap (14) have been incorporated into the system. A standard McLeod gauge (12) was utilized for measuring vacuum. Pressures ranging from 6×10^{-7} to 5×10^{-5} mm Hg could be achieved depending on the degassing time and type of oil used. Container (13) served as a vacuum reservoir.

Chemically pure, medical grade oxygen was used as environment for the oxidation studies and prepurified nitrogen for nitriding kinetics. Before entering the system the gases were passed through the expansion trap and cold-trap (18) and through purifiers (19) containing silica-gel for removing moisture and (20) containing phosphorous pentoxide for

removing the residual water vapour. Since there is evidence in the literature, as alluded to in Chapter II, about the detrimental effects of hydrogen and water vapor on the kinetics and mechanism of zirconium oxidation these excessive precautions were justified. The admitted oxygen or nitrogen was stored in cylinder (21) of such volume that it permitted the use of the same gas for 4-5 experimental runs.

Laboratory air, passing through dust remover (22) and moisture adsorber (25) containing magnesium perchlorate, exerted pressure on one side of the U-tube (26) filled with vacuum oil. The pressure difference could be adjusted at will in two ways: either by the position of the mercury bubbler (23), which was covered with a cotton stopper to prevent the harmful particles of mercury from contaminating the surrounding, or by evacuating the right-hand side of the U-tube by the mechanical pump (36). Moisture-free air enters the automatically operated mercury valve (27). In the case of a gap between the mercury level and the upper wire connection (6) as shown in Fig. 3 or Fig. 4a and for the position of the double pole-double throw switch (c) as in Fig. 4a, the solenoid (28) becomes energized and lifts plunger (29). Mercury in (27) levels up and exposes the porous plug (30) to air which when passing through it "breaks" the vacuum in container (11) and raises the mercury level in burette (7). Simultaneously the gap between the mercury column and the electrical contact is closed. The cycle repeats itself while the gas is being displaced by the oxidizing zirconium sample. To hinder "overshooting" of mercury in the automatic pressure manometer a damping volume (31) was incorporated into the glass circuit.

Part (32) of this apparatus was designed for the use of fine and short-time measurements. A drop of dibutyl phthalate (33) moves along the calibrated capillary tube (34). The movement is brought about by the decrease of pressure due to the adsorbed oxygen or nitrogen. On the other side of the drop a constant pressure is maintained by manometer (5). The dibutyl phthalate drop is replaced from time to time from container (35) shown as detail A-A at the bottom of Fig. 3. The motion could be read to the accuracy of 1 mm which corresponds from the calibration data to 0.02 mg of gas displaced.

4.3 Procedure:

An attempt is not made to give exact descriptions of the separate parts or to delineate in detail the operating instruction. Only a superficial and approximate description of the operating procedures will be outlined in this section.

After obtaining a suitable vacuum, approx. of 1×10^{-6} mm Hg, the furnace was positioned around the reaction cell. At this time the temperature was 6° to 10°C above the test temperature. The positive deviation from the testing temperature was maintained purposely in order to equalize the temperature distribution across the cell in the shortest time possible. During this period, which was about 8 min., the final outgassing operation takes place by heating the walls of the oxidation vessel. When the temperature decreased to the required value e.g. 850°C , 950°C etc., it was maintained at that value.

The pressure in manometer (5) was adjusted to the desired value, e.g. in the present case to 400 mm Hg, by admitting the proper amount of mercury to the manometer with the aid of stopcock (f) and (g) and mechanical pump (36). The mercury level in cylinder (7) was raised by admitting air through the mercury valve (27) to previously evacuated container (11). After closing stopcocks (b), (d) and (e) oxygen or nitrogen was let in from bulb (21). To compensate for the known volume of the reaction cell an additional amount of gas was admitted.

Since the mercury level in burette (7) may be initially below its "0" reference mark the mercury column could be raised either by admitting air from manifold (38) or through valve (27). It is obvious that the first alternative is not recommended because the air contains moisture which may effect the subsequent readings. To open the valve (27) while connections (6) are short-circuited the switch (s) in Fig. 4a has to be thrown to energize solenoid (28) and purified air may then pass the porous plug (30). When mercury has been brought close to the "0" reference mark, opening of stopcock (b) eliminates the excess of pressure mentioned before and permits to take subsequent continuous readings.

Where fine measurements are required, one can make use of part (32). Closing stopcocks (b) and opening (a) and (c) puts it into operation. Reversing periodically the three-way stopcocks causes movement of the dibutyl phthalate drop back and forth providing again opportunity for taking continuous readings.

4.4 Gravimetric Apparatus and Procedure:

The oxidation kinetics of zirconium in oxygen-water vapour environment were determined by using a gravimetric assembly containing a McBain type spiral spring balance. The equipment used was very similar to that described by AKRAM and SMELTZER⁽¹⁸⁾. Cathetometer measurements of spring elongation were reproducible to 0.15 mm and this corresponded to a reproducibility of 0.5 mg for a specimen weighing 1.6-1.8 gm. In most cases the thickness of specimens used was the same as for volumetric measurements, i.e. 2.0 mm.

For injecting water vapor into the system, an attached bulb containing de-aerated distilled water was immersed in a bath maintained at the appropriate temperature. By altering the temperature of the bath it was possible to change the concentration of water-vapour in the gaseous surrounding.

The apparatus was capable of maintaining a residual pressure of 10^{-6} mm Hg. Prior to admitting oxygen the specimens were subjected to vacuum of 10^{-6} mm Hg. for a period of 12 hr. at room temperature. The furnace at the predetermined temperature of 850° or 950°C was then drawn over the reaction tube and oxygen admitted to a pressure of 400 mm Hg. The type of oxygen used and the purifying system were the same as already described for the volumetric measurements. Temperatures were controlled to $\pm 2.5^{\circ}\text{C}$.

4.5 Material and Preparations:

Pure zirconium from the VAN ARKEL process was used in this investigation. It was supplied in cold rolled and vacuum annealed condition by A.E.C.L.

the composition of the metal is recorded in Table 1 in the appendix.

Samples for oxidation and nitriding tests, approx. 2 x 1 x 0.2 cm, were prepared by wet-abrasion on 220, 320, 400 and 600-grit silicon-carbide papers followed by final polishing on 8 and 1 μ diamond laps and acetone washing and careful drying. The averages of three measurements of the sample size were taken as basic values for further calculations. Most samples were weighed before and after the oxidation or nitriding test.

To prevent local excessive overheating at edges and hence possible structure changes, specimens for microscopic examinations were cut under an air-blast. For the same reason and in order to avoid a gap between the metal and mounting material, whenever microscopic measurements of oxide thickness had to be taken, most samples were cold mounted in HYSOL self-setting epoxy resin and prepared for metallography by using methods advised by EVENS⁽⁶⁰⁾. Final polishing was performed on rotating wheels impregnated with 8-micron and 1-micron diamond dust, followed by vibrator polishing with gamma alumina-oxide solution. Whenever edge preservation was of importance, e.g. in oxide and nitride thickness determinations, the procedures outlined by CPREK⁽⁶¹⁾ were adopted.

Measurements of the nitride thickness were made using a filar micrometer eyepiece on normal sections of the polished specimens. To delineate distinctly the boundary between the mount and specimen, the nitrified surface was coated with dyed "Eastman 910" adhesive diluted in "GA-1A" accelerator and allowed to harden for 2-4hr., and cold mounted afterwards. Dark-blue recorder ink was used as an dye. The zirconium-nitride although quite thin

covered the metal substrate uniformly; no appreciable edge or corner effects could be observed. The thickness of the alpha-phase was measured by projecting it on a metallographic glass-screen.

Since zirconium possesses a hexagonal structure and anisotropic surfaces can be readily prepared, the polarized light renders a high degree of contrast between areas of different orientations and thus delineates clearly the grain boundaries. Accordingly, it was expected that application of polarized light techniques would be suitable for examination of the metal and scale structures.

X-ray determinations were made of scale constituents. To dissolve metal beneath the gray oxide, samples were subjected to the chemical etchant: 45 ml H_2O , 45 ml HNO_3 (conc.) and about 10 ml HF (52%) for 2-4 hr, and rinsed in distilled water afterwards. The residue was ground to powder and prepared for X-ray examination by conventional techniques. White oxide or nitride powders were obtained by scratching the surface of heavily scaled samples.

In order to determine the nitrogen concentrations in nitrided zirconium specimens, hardness profiles in the metal substrate beneath the nitride layer was determined with a Reichert microhardness indenter using the standard 124° diamond under a 30 gm load.

CHAPTER V

Reaction of Oxygen with Zirconium. Results

5.1 Introduction

Results of oxidation tests from volumetric measurements at 850° and 950°C will be presented in conjunction with static weight-gain determinations, metallographic observations and microscopic measurements. All values of oxygen uptake are expressed as weight gains of specimens, mg. O/cm².

In one set of experiments, the temperature 850°C was chosen because our aim was not only to test the applicability of equations (29) and (35) to the oxidation kinetics of alpha zirconium but also to reach the "breakaway point" in the shortest possible time. Reasons for choosing the temperature 950°C for the second set of experiments were twofold: to show the applicability of equation (61) to the oxidation kinetics of beta zirconium and to minimize the time to the "breakaway point" for a better definition of the expected deviations in the kinetic curves. Also, verification of equations (50) and (59) could be gained.

The upper range of this test temperature was limited by the reluctance to allow the formation of the tetragonal modification of ZrO₂. Although the zirconium-oxygen equilibrium phase diagram by HANSEN⁽⁵⁷⁾ shows that the

transformation occurs at approximately 1000°C , DIETZEL and TOBER⁽⁶⁶⁾ report that the monoclinic structure prevails up to 950°C only. GELLER and YAVORSKY⁽⁶⁷⁾ mention that the transformation takes place in the range from 983° to 1039°C , and MURRAY and ALLISON⁽⁶⁸⁾, who made a thorough study of the transformation under constant-heating-rate conditions by means of differential thermal analysis and by a dilatometric method, extend the possible range of transition to 950° - 850°C on cooling and from 1100° - 1190°C for the case of the forward transformation.

5.2 Oxidation Measurements at 850°C :

Fig. 5 shows the oxidation-time relationship. The plot of oxygen uptake in mg per unit area in cm^2 vs. square root of time, $\text{hrs}^{1/2}$, is a straight line indicating that oxidation behaves parabolically within the experimental time. The oxide was dark grey and no white coloration could be seen on the surface and edges or corners of the sample. Similarly, Fig. 6 gives evidence of parabolic oxidation up to approximately 160 and 300 hr; thereafter a not well defined deviation from the parabolic relation occurs and the oxidation rate somewhat increases.

Since it was possible that plastic deformation of the metal might have an effect on the oxidation kinetics, a sample designated as "run IV" was normally prepared and bent to approx. 30° . From the graph it may be seen that this degree of plastic deformation did not have a pronounced influence

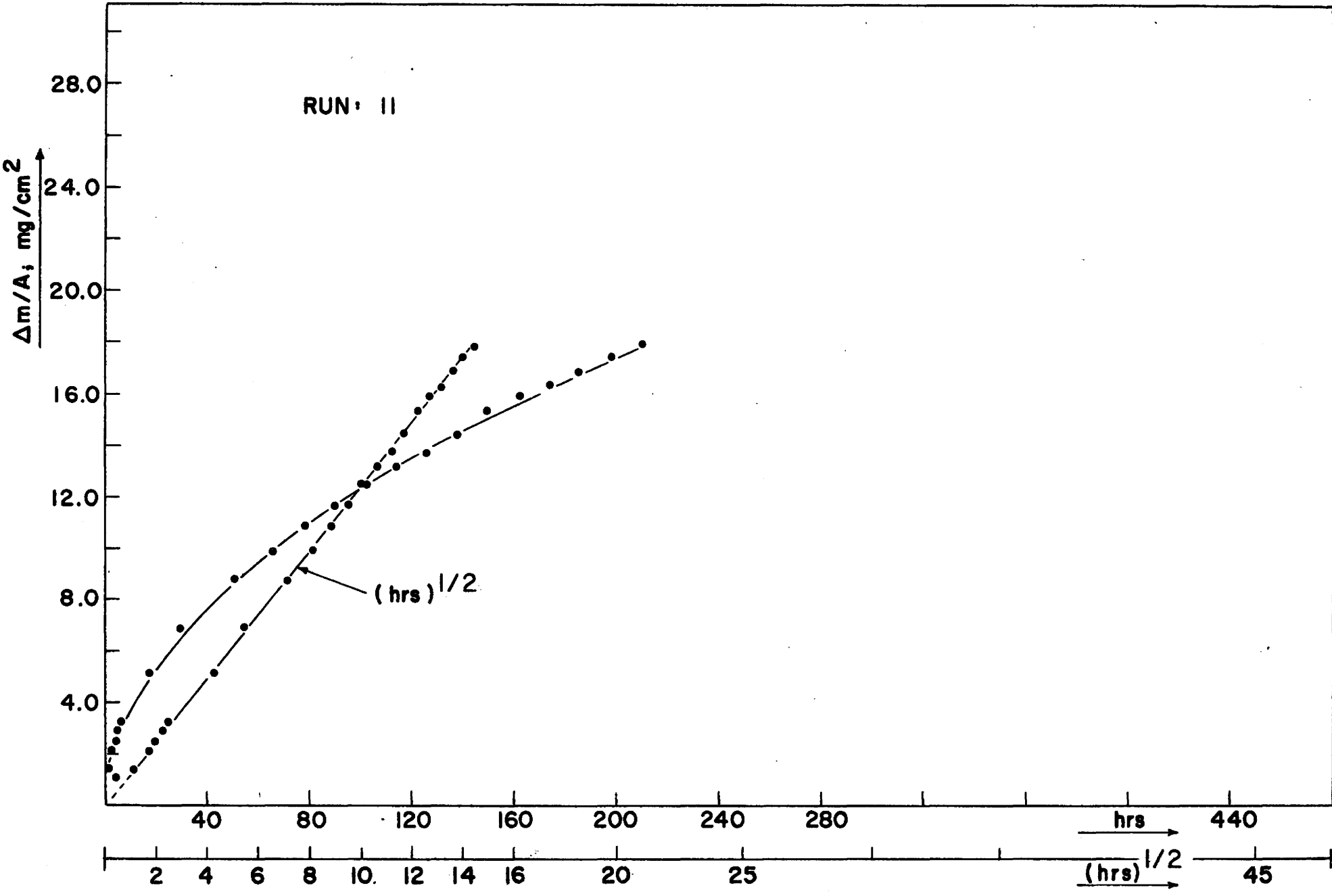


Fig. 5 Oxidation Rate of Zr, at 850°C. Sample thickness 2 mm.

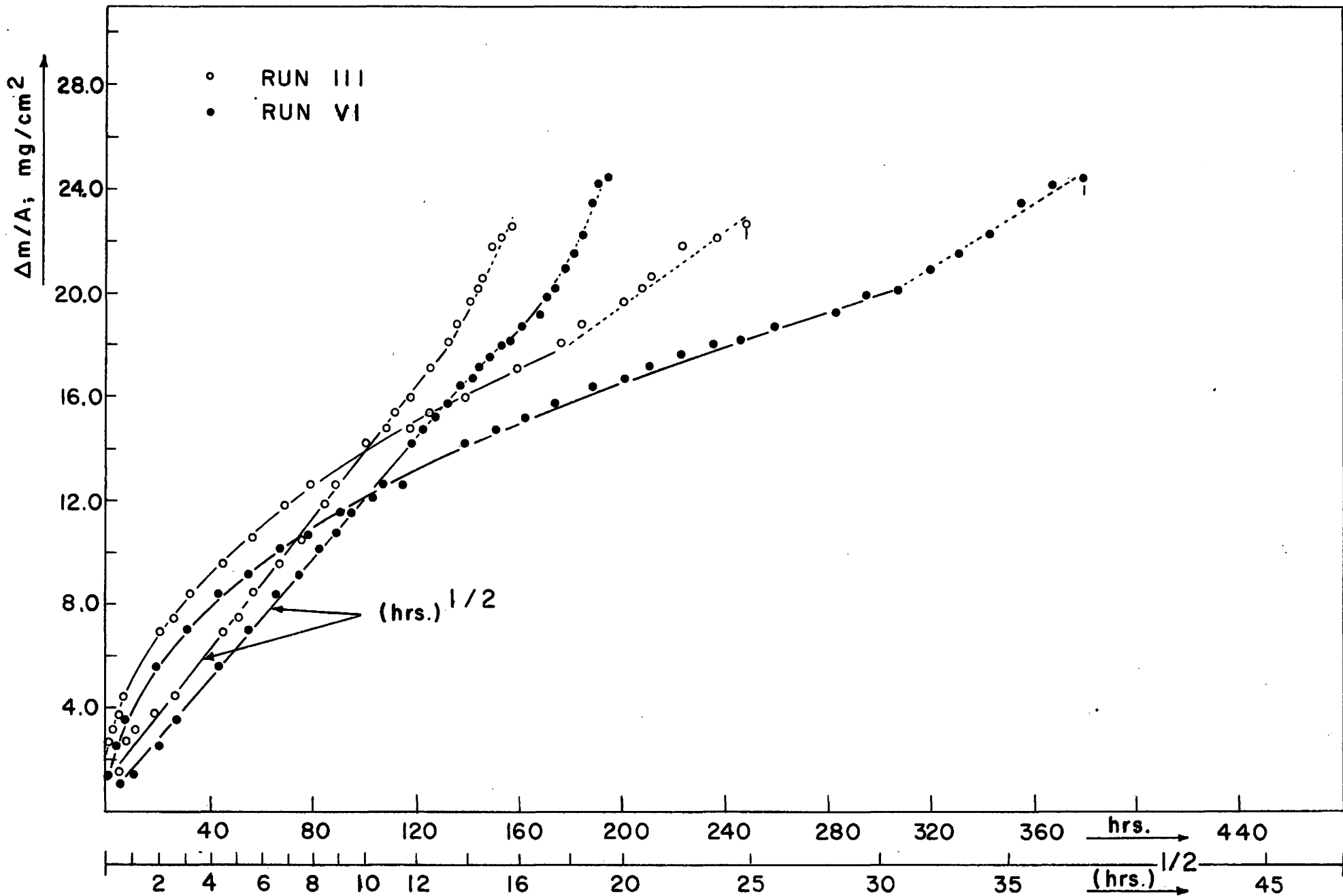


Fig. 6. Oxidation Rate of Zr, at 850°C. Sample thickness 2 mm.

on the oxidation rate. Both specimens from the above two tests exhibited some white oxide on edges and corners.

Fig. 7 represents oxidation data for samples with thicknesses approx. half of those normally used, i.e. 1 mm. From the oxygen penetration curve one would expect that if white oxide formation is a function of oxygen concentration in the metal, then the time interval to the "breakaway point" should be shorter for samples with smaller thicknesses. Indeed, it is evident from this graph that deviation from the parabolic relationship starts at about 120 hr, which is approx. 0.5 of the time required for regular samples, viz, Fig. 6. White oxide formation on edges of these samples could be well distinguished.

Table 2 in the appendix summarizes the experimental conditions under which each sample was tested together with calculated equations for the continuous curves. These equations were computed by the "least squares" method.

5.3 Oxidation Measurements at 950°C:

For clarity of presentation, the oxidation data are presented in an arrangement based upon the visual surface properties of the oxidized specimens. Fig. 8 represents the topography of oxidized samples. Based on visual appearance they have been divided into three groups. The Roman numbers correspond to the test number and the Arabic numbers indicate time, hrs, for which the sample was oxidized. The upper row shows the

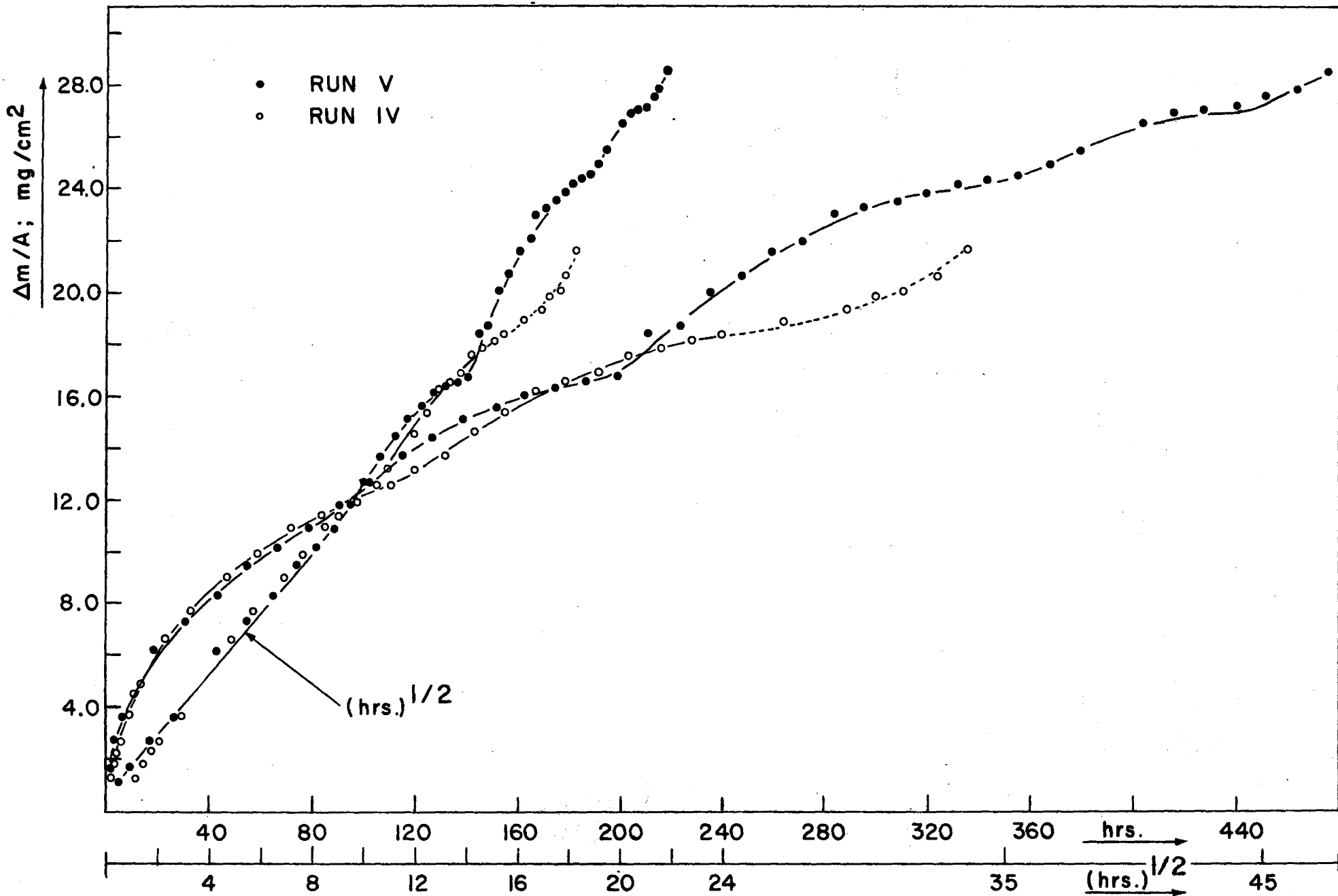


Fig. 7 Oxidation Rate of Zr, at 850°C. Sample thickness 1 mm.

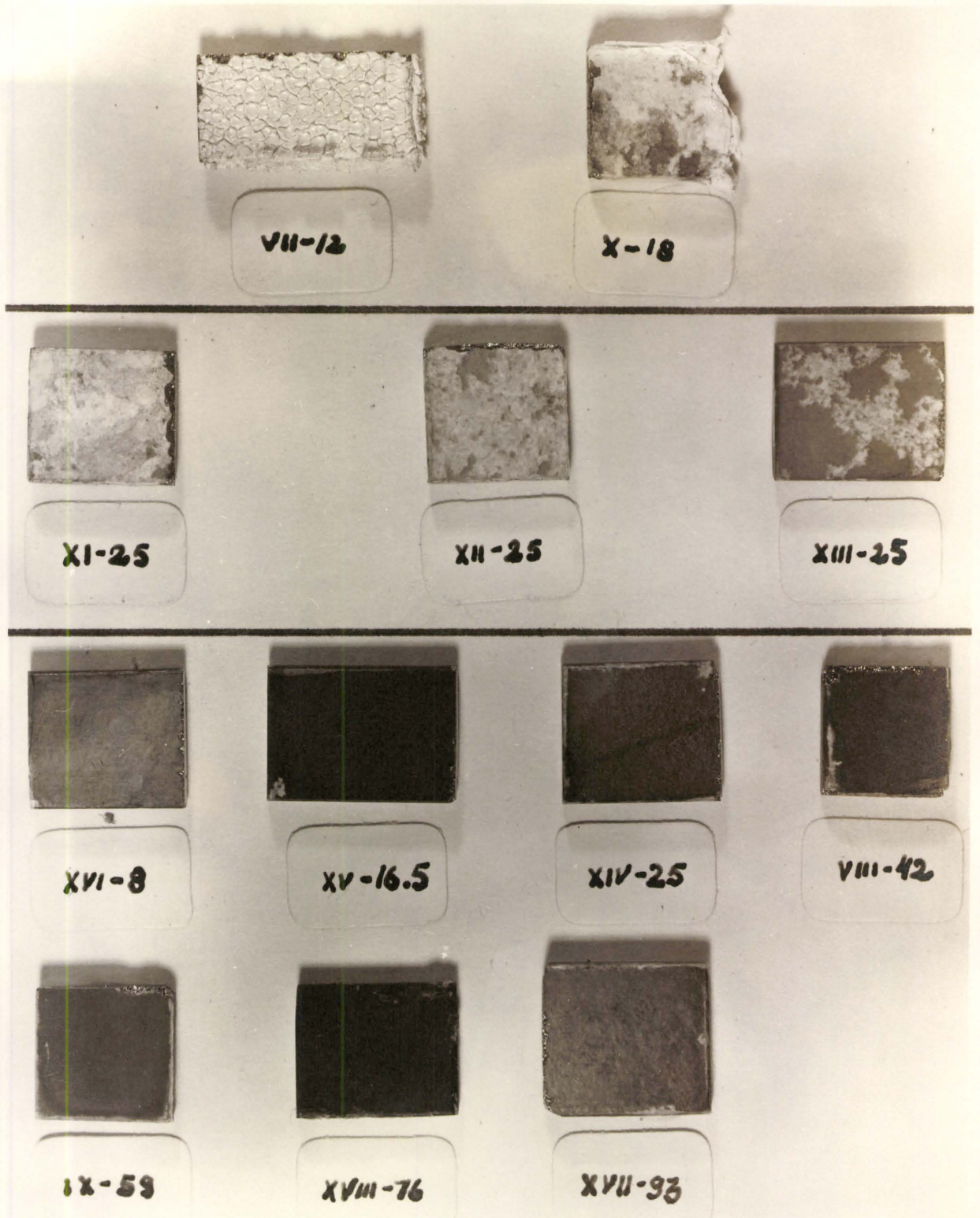


Fig. 8 Topography of oxidized Zirconium samples, at 950°C. Magnification 2 1/2x

formation of thick white oxide scale, those in the middle illustrate the example of transition from gray to white oxide, and those at the bottom exemplify the surface appearance of samples covered with gray oxide only.

Fig. 9 shows the plot of oxygen uptake vs. time for specimens displayed in the upper row of Fig. 8 and undergoing breakaway oxidation. Here, the parabolic relationship is followed by a linear dependence. This behaviour was found when samples were pre-annealed prior to oxidation in a vacuum of 5×10^{-4} mm Hg.

Figs. 10 and 11 represent data for the transition state. The dashed lines represent interpolated parabolic relations calculated by the "least squares" method. From these graphical representations and from those at 850°C , it can be postulated that deviation from strictly parabolic oxidation commences whenever white oxide begins to appear. Furthermore, the formation of this oxide was found on specimens pre-annealed prior to oxidation in a residual vacuum of 10^{-5} mm Hg, viz. Table 2. The above findings imply that degassing (vacuum) of a system prior to oxidation must be controlled precisely.

The results from volumetric measurements, under the restricted experimental conditions for annealing at 10^{-6} mm Hg prior to oxidation are given in Figs. 12 and 13. During oxidation exposures to 100 hr, only minute amounts of white oxide formed on edges and corners of these samples. This can be seen from the macrographs in Fig. 8.

Table 2 in the appendix summarizes the test conditions and some of the values calculated from data obtained at 950°C .

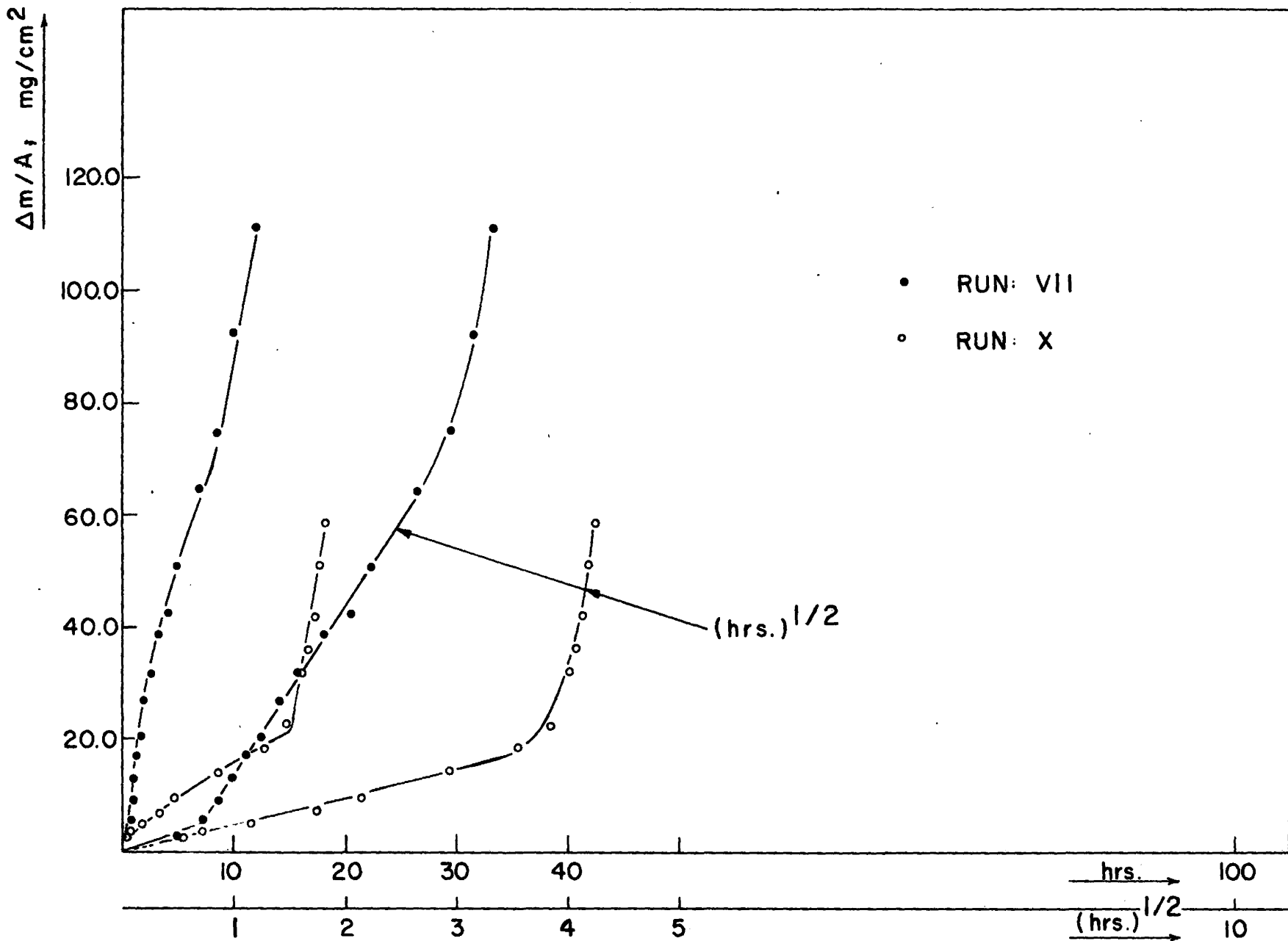


Fig. 9. Oxidation Rate of Zr at 950°C. Sample thickness 2mm.

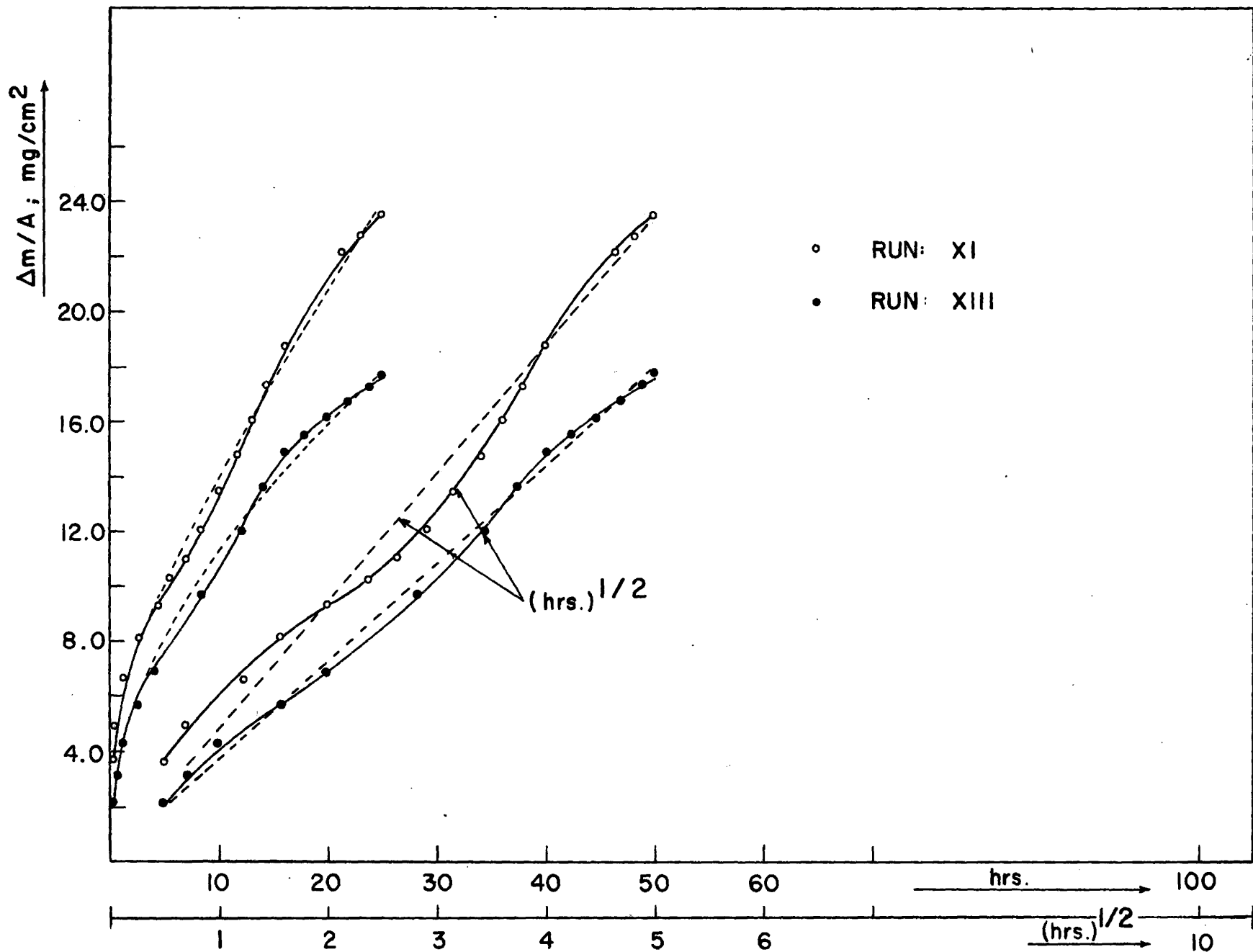


Fig. 10. Oxidation Rate of Zr. at 950°C, sample thickness 2mm.

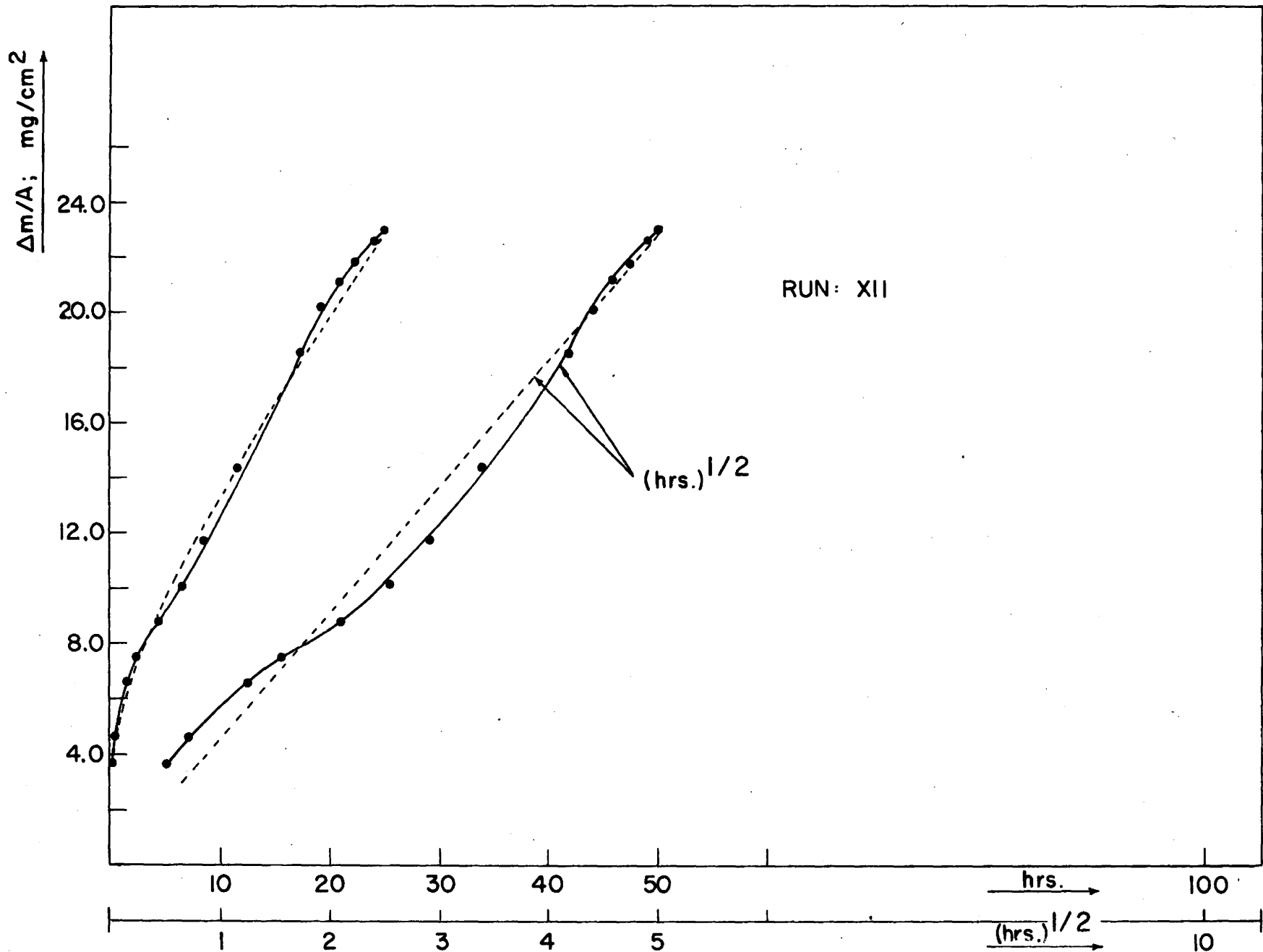


Fig. 11 Oxidation Rate of Zr. at 950°C. Sample thickness 2mm.

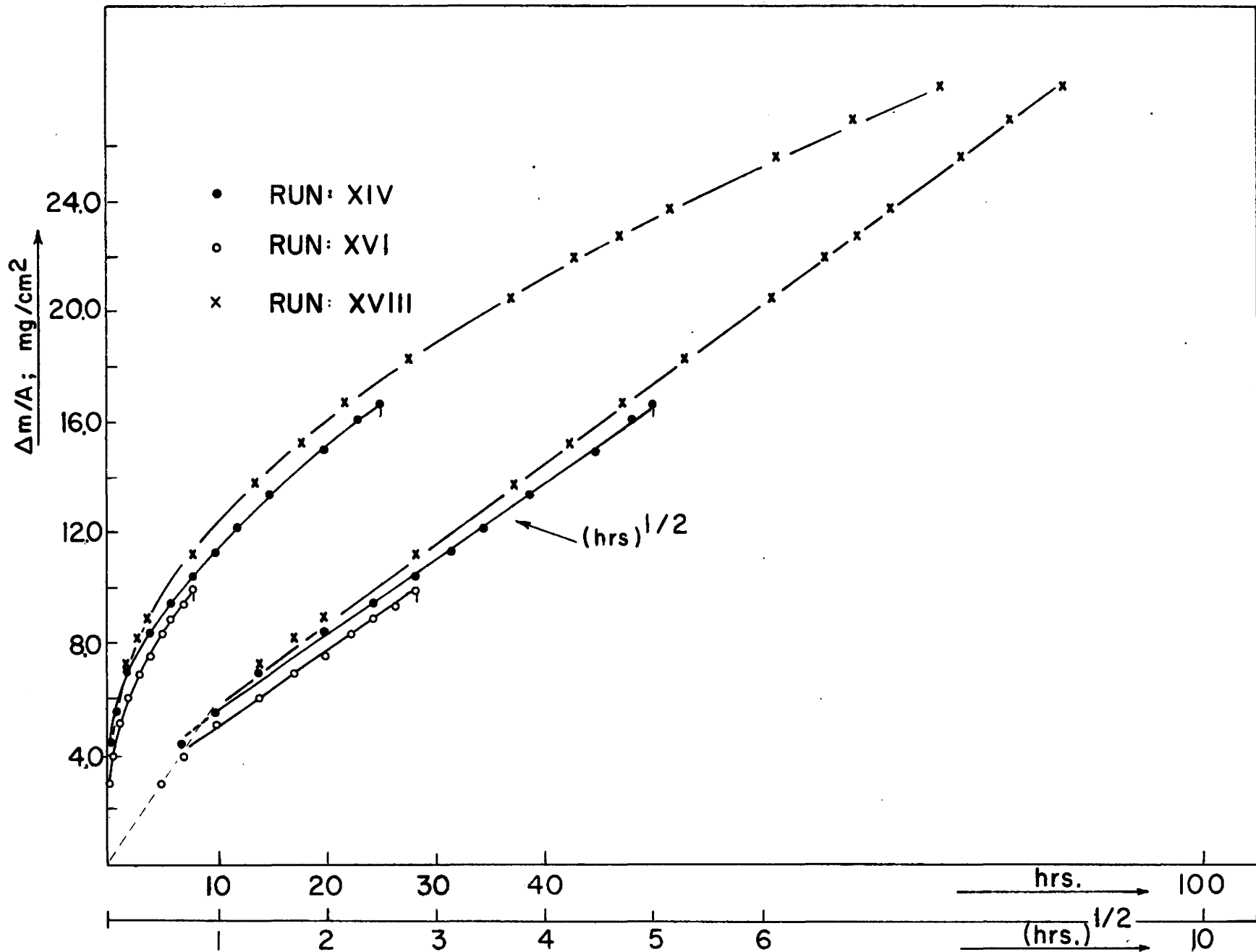


Fig. 12 Oxidation Rate of Zr. at 950°C. Sample thickness 2mm.

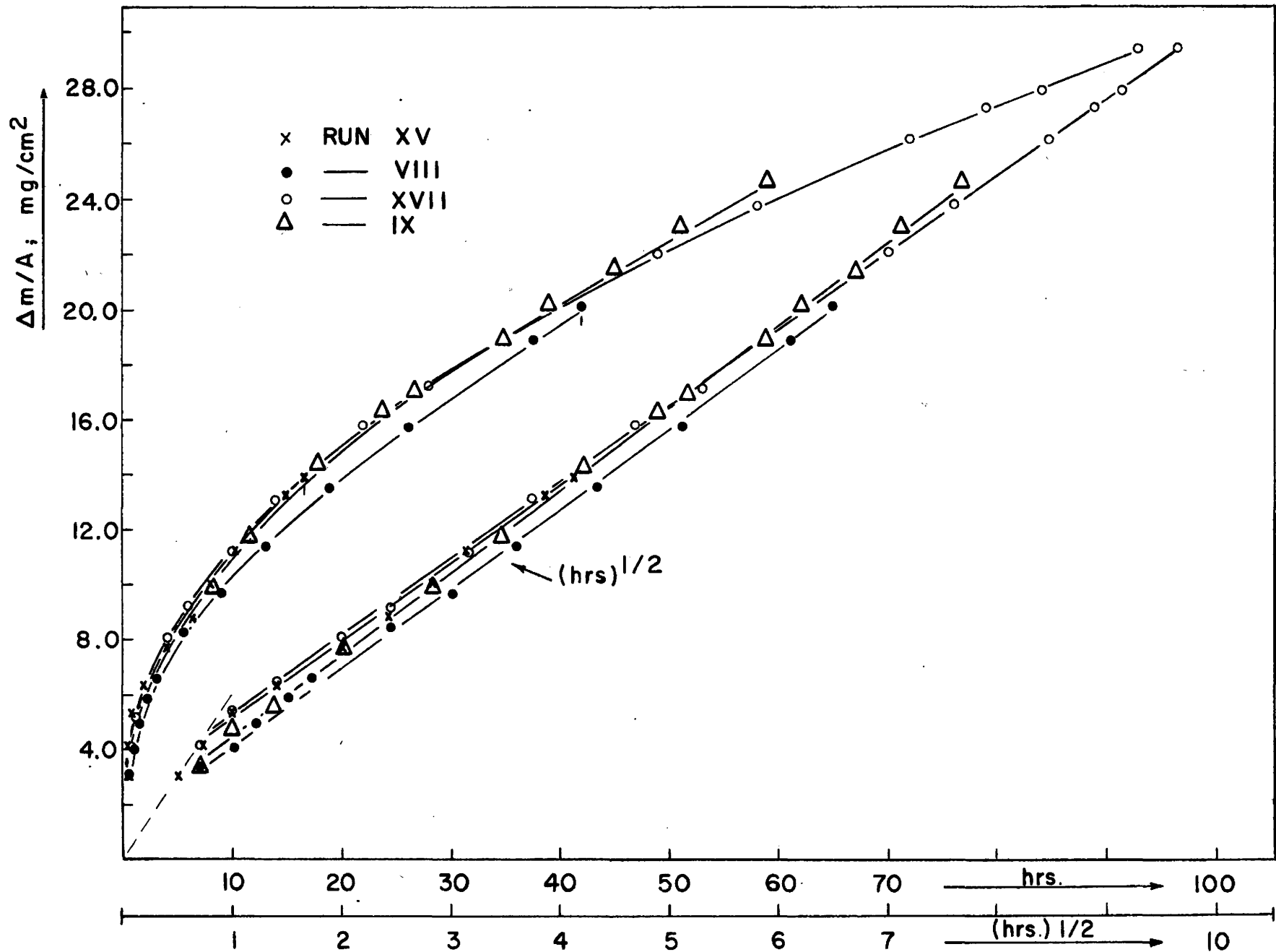


Fig. 13 Oxidation Rate of Zr. at 950°C. Sample thickness 2mm.

5.4 Static Gravimetric Measurements:

In the series of oxidation tests at 950°C each sample was weighed before and after oxidation. The weight gain $(\Delta m)_w$ per unit area, A, vs. time has been plotted in Fig. 14. To a good approximation the parabolic oxidation relationship is obeyed and after the initial period of deviation the curve satisfies the equation: $(\Delta m)_w/A = (4.43 \pm 0.27) \times 10^{-5} \sqrt{t}$ gO/cm², for time, t, expressed in seconds. Within the experimental reproducibility these results agree with those from the volumetric method. The values from the gravimetric determinations are given in Table 3 in the appendix.

5.5 Microscopic Measurements and Metallography:

The results in this section and the metallographic premises are pertinent to measurements and observations at room temperature on the oxide scales and zirconium-oxygen solid solution phases formed at the oxidation temperatures of 850° and 950°C.

According to HAYES and KAUFMANN⁽⁶⁹⁾ the peritectic beta-zirconium phase cannot be retained at room temperature even by quenching. It seems reasonable to adopt an alternative nomenclature for the resulting beta-phase. We shall call this new phase the "transformed beta", which in appearance resembles a serrated-like alpha-phase. The author does not wish to speculate whether the zirconium-oxygen solid solution (approx. 2-7 at.% of oxygen) transforms to the new phase by a martensitic process or whether the resulting "transformed beta" phase forms by nucleation and growth.

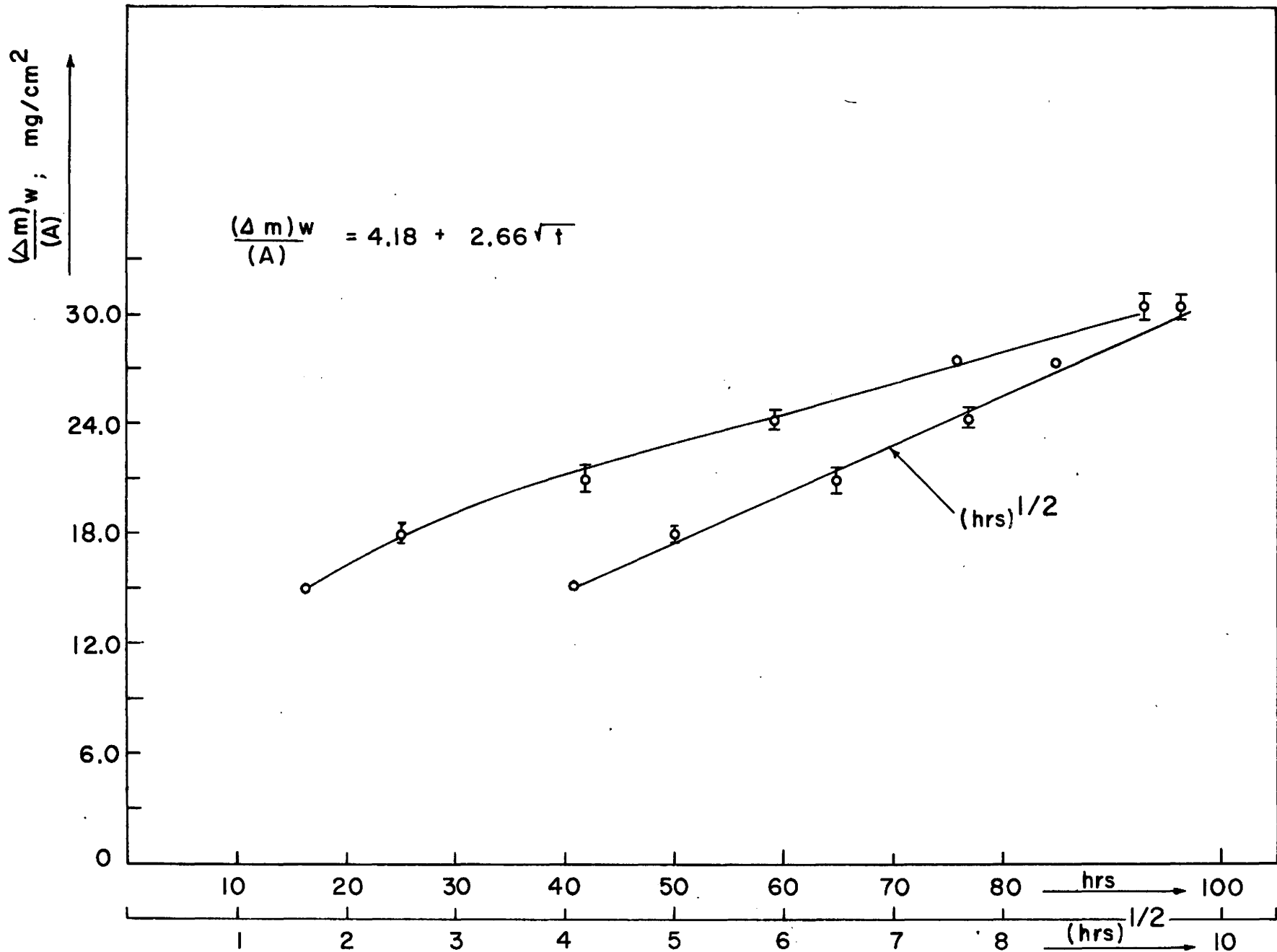


Fig. 14 Oxidation Rate of Zr. at 950°C. Samples thickness 2mm. Gravimetric method.

Fig. 15 shows the thickness measurements of the oxide scale as a function of time for exposures to approximately 300 hrs at 850°C. Also, results from three other investigations (33, 34, 70) are included in this figure. The growth of scale obeys a parabolic relationship and the parabolic constant is recorded in Table 5. Microscopic examination of the scale showed it to be compact and of uniform thickness.

Fig. 16 shows the growth of oxide with time, at 950°C. The topography of these specimens was shown in the bottom row of Fig. 8, where the Arabic numbers (i.e. time in hrs) correspond to the letters (a-g) in an increasing order. It can be seen from these pictures that voids develop in the oxide layer. These voids tend to hinder the oxidation of the underlying metal. A tentative explanation of their formation and their influence on corrosion rate will be discussed later. The faint visible lines in the metal substrate are cracks. Whether they form on cooling or during the oxidation test has not been established explicitly.

Fig. 17 shows the alpha metal-oxygen solid solution layer overlying the beta-metal phase here shown as "transformed beta", after an oxidation exposure at 950°C. It is apparent from this photomicrograph that the thickness of the alpha-phase may be readily measured.

The thickness measurements of the oxide layers depicted in Fig. 16 and the thickness of the alpha-zirconium phase together with the sum of both values have been plotted in Fig. 18. These parameters are also tabulated in Table 4, in the appendix. In Fig. 19 a plot is shown of the thickness ratio of the alpha and oxide layer. After approximately 30 hrs this ratio attains a constant value.

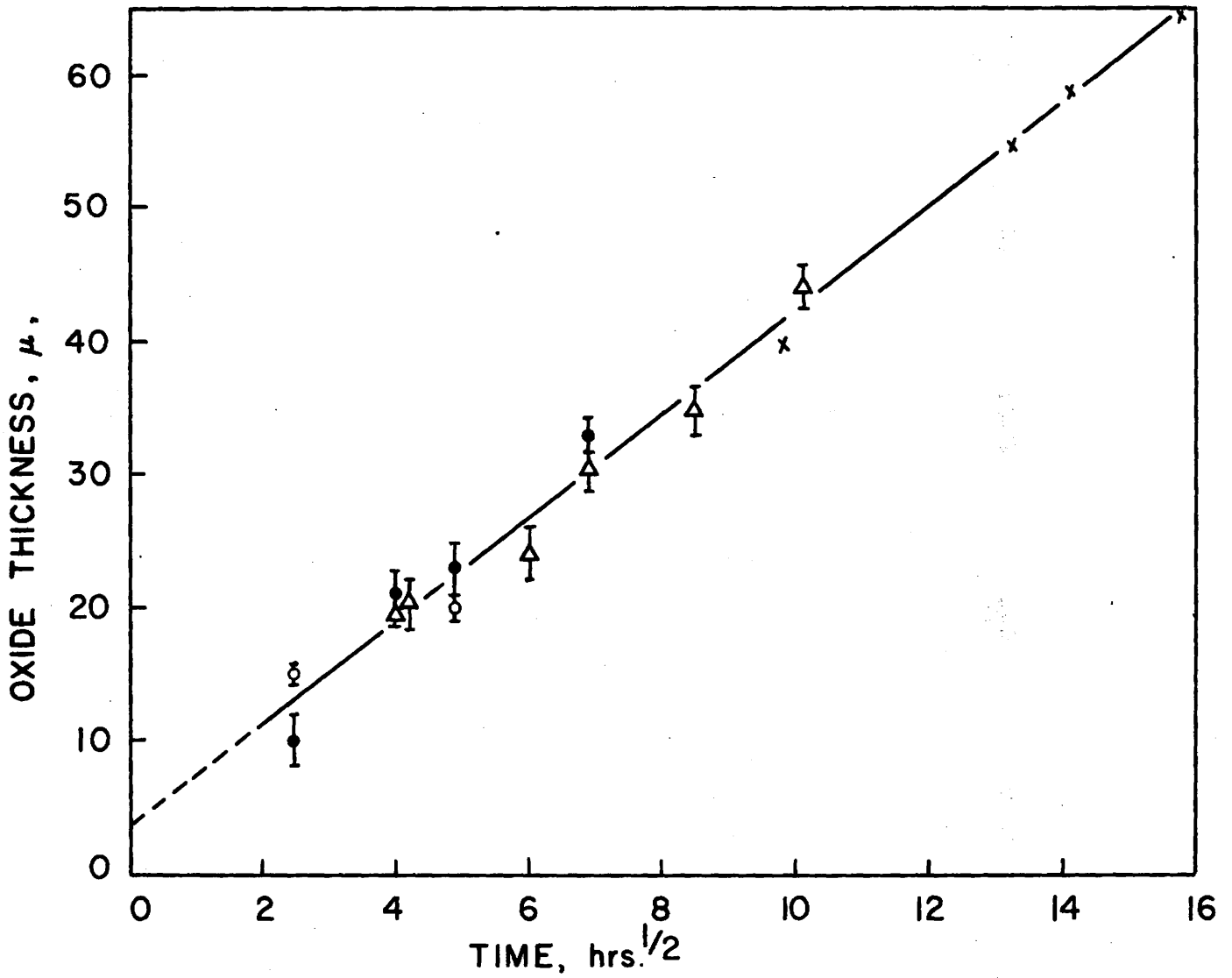


FIG. 15 OXIDE THICKNESS AS A FUNCTION OF TIME FOR ZIRCONIUM OXIDIZED AT 850°C.

- DEBUIGNE & LEHR (34)
- HUSSEY & SMELTZER (33)
- × WALLWORK et al. (70)
- △ PRESENT INVESTIGATION

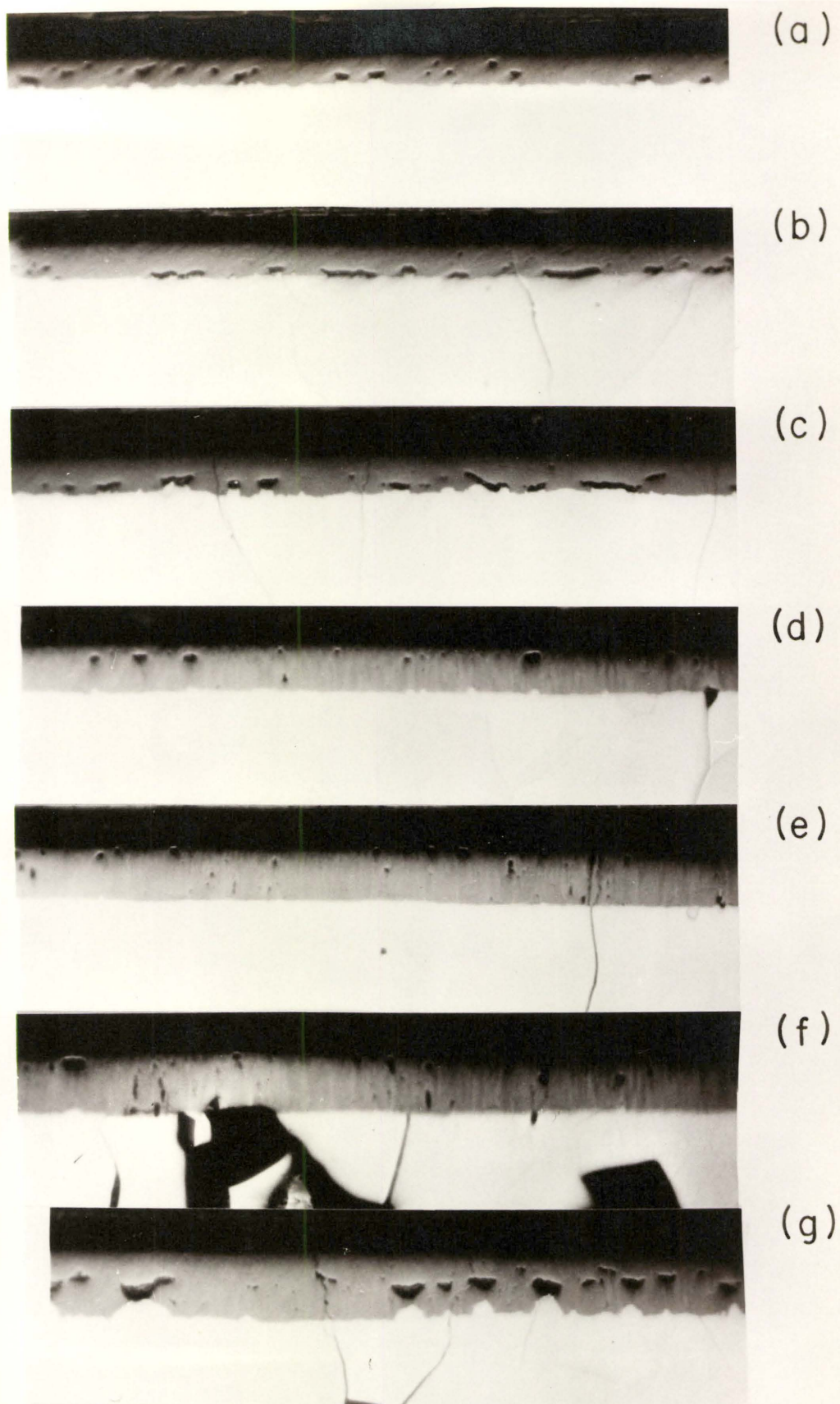


Fig. 16 Growth of Zirconium dioxide with time, at 950°C . Magnification 250x.

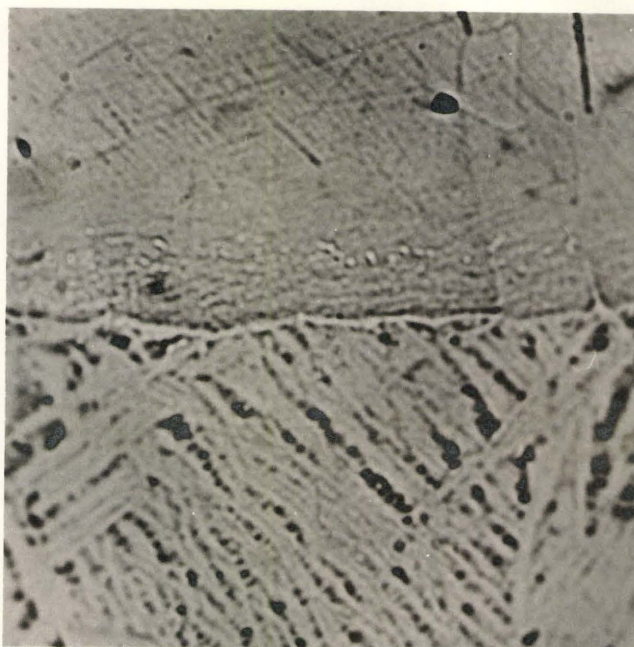


Fig. 17 Boundary between alpha-metal-oxygen solid solution and transformed beta-zirconium (lower part). Oblique illumination. $\times 150$. Magnification of reproduction 1.1x.

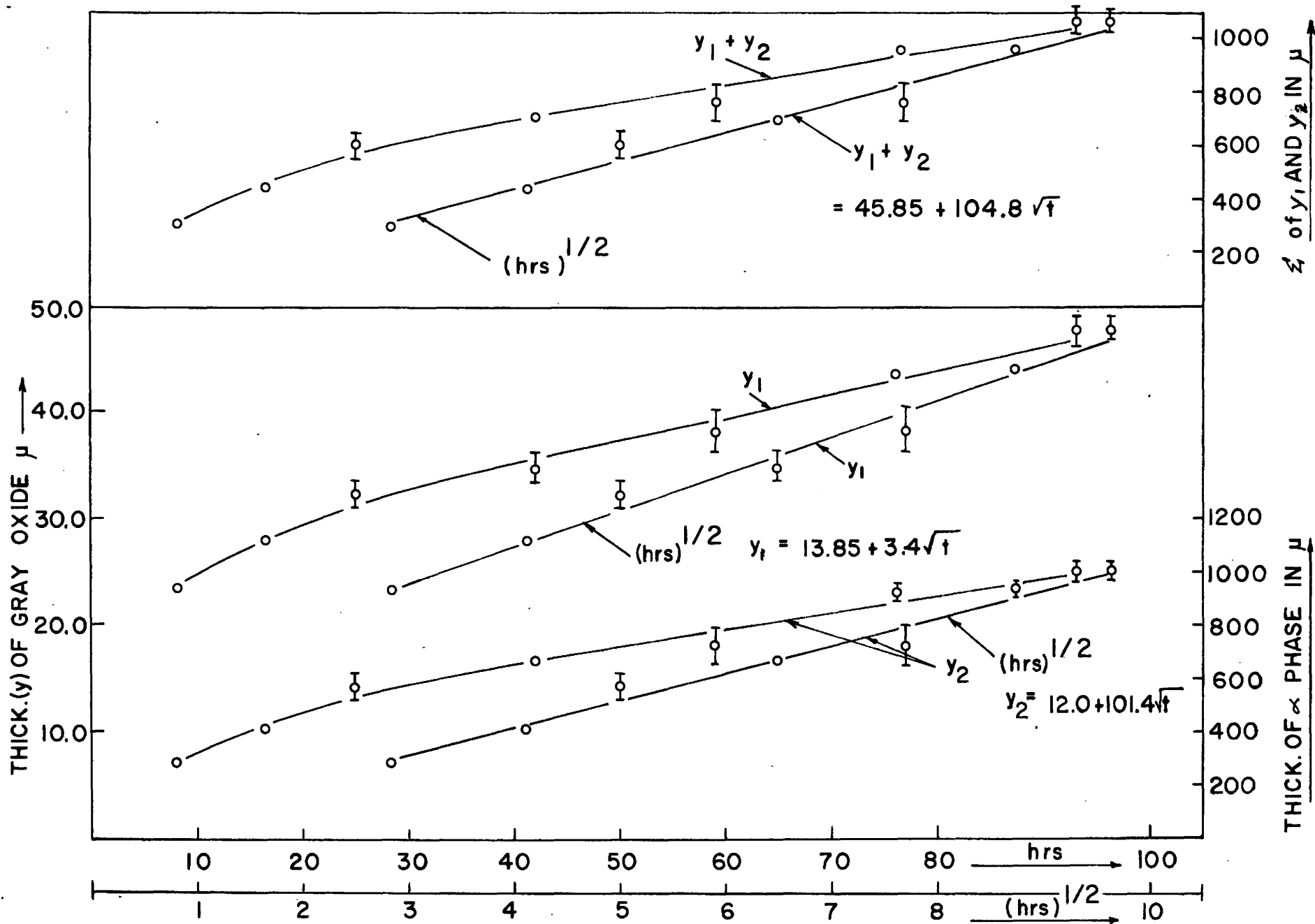


Fig. 18 Growth of Zirconium oxide and alpha phase, at 950°C.

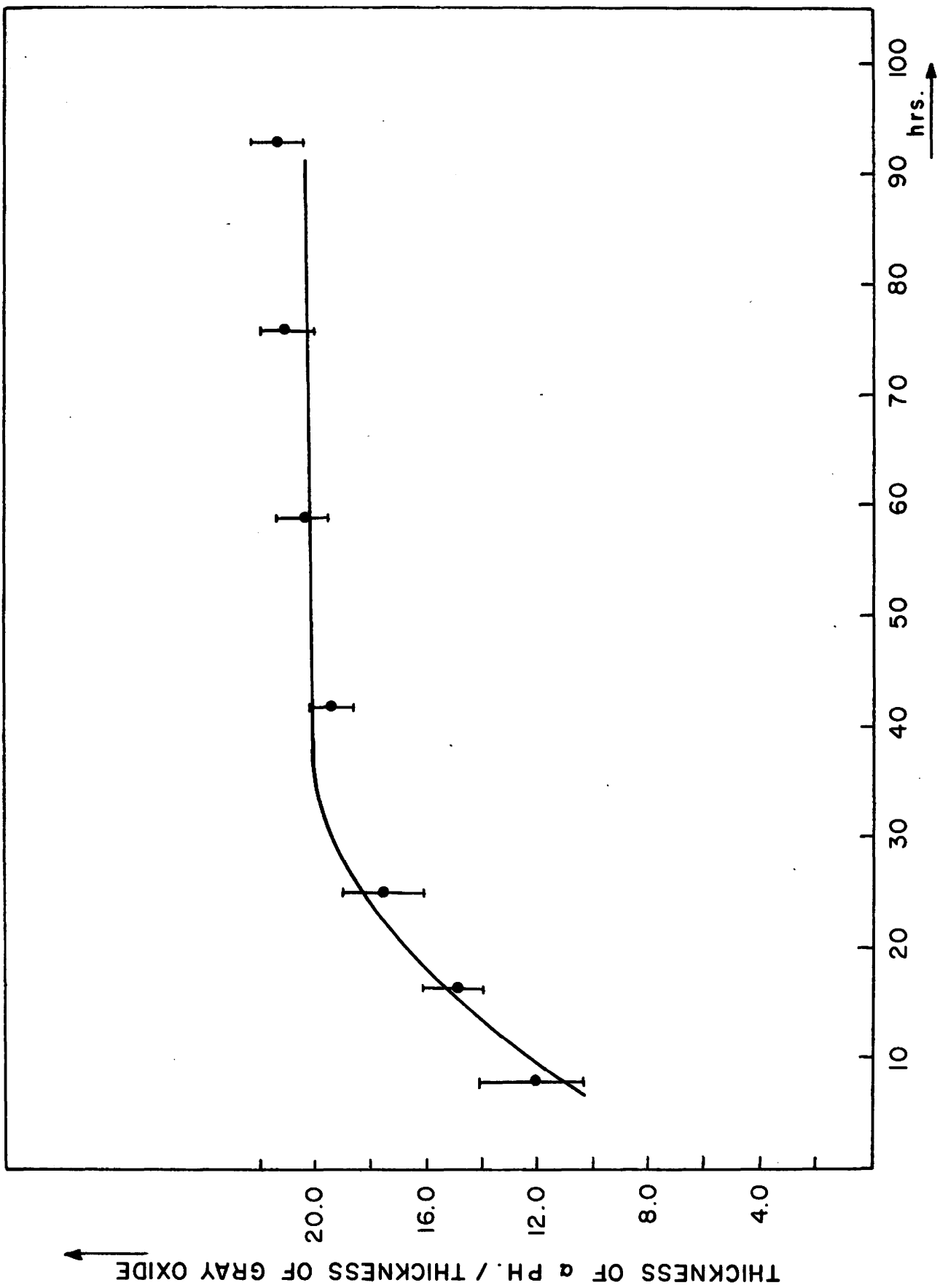


FIG. 19 CHANGE OF THE RATIO OF α -PH. THICK. / OXIDE THICKNESS AT 950°C.

Fig. 20 represents pictures taken under polarized light conditions at the University of Toronto by courtesy of Dr. W. C. Winegard. Pictures (a) and (b) show the cross sections of gray oxide and match with pictures (d) and (c) in Fig. 16 respectively, which were taken under bright-light illumination. Pictures (c), (d) and (e) represent what was called the "transition" state and correspond to specimens shown in the middle row of Fig. 8, in a proper sequence. Here the formation of double oxide scale is apparent. Finally, picture (f) shows the edge effect and the formation of white oxide on the expense of gray oxide is clearly evident.

5.6 X-ray Determinations:

Debye-Scherrer photographs of gray and white oxide obtained by employing nickel filtered copper radiation for exposures of approx. 26 hrs. are shown in Fig. 21. Both oxides exhibit monoclinic structures and the same plane spacings (d), within the experimental error.

Some of the values obtained are given in Table 6, (appendix).

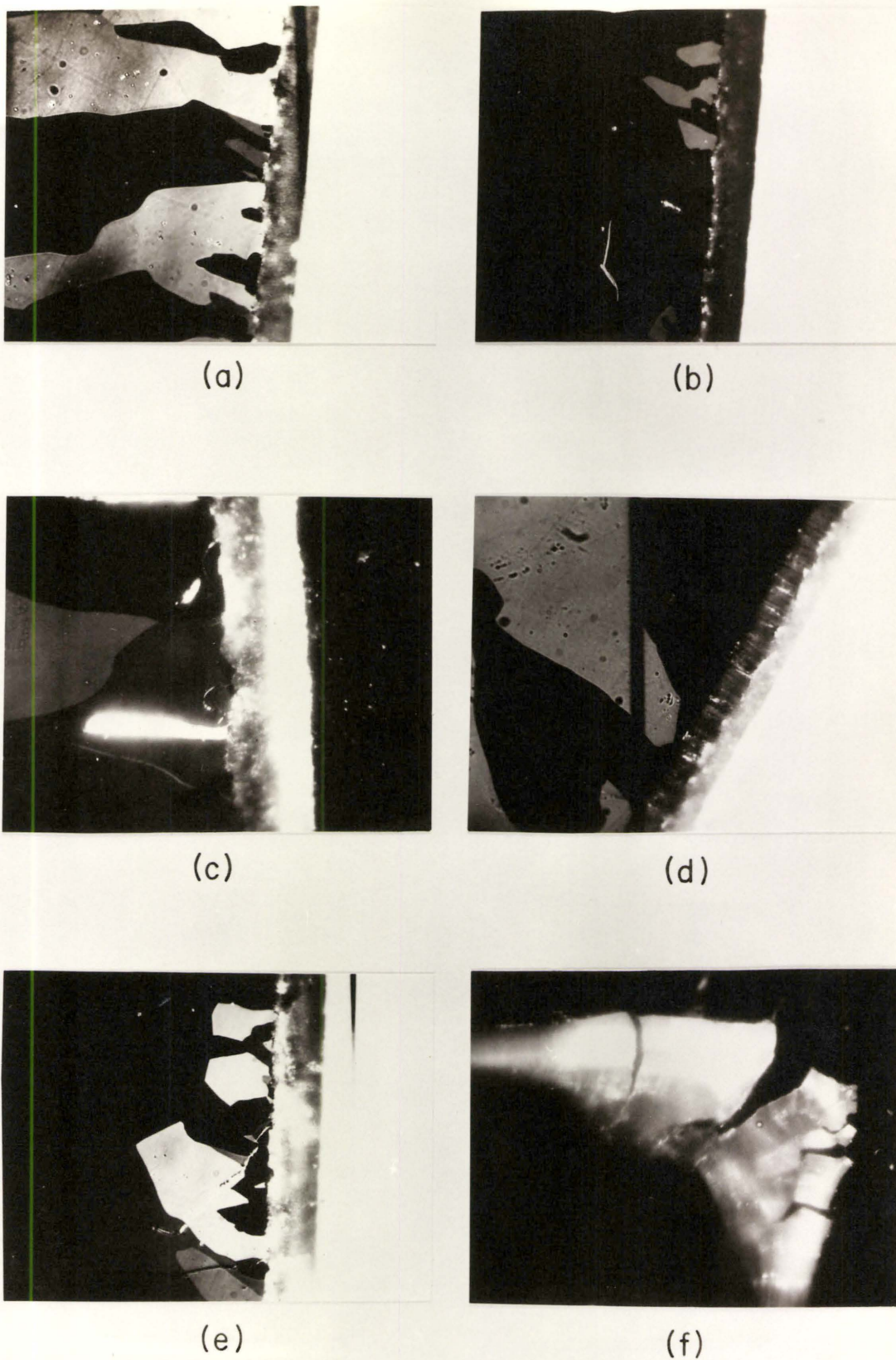


Fig. 20 Cross section of Zirconium samples oxidized at 950°C. Polarized light
200 x,

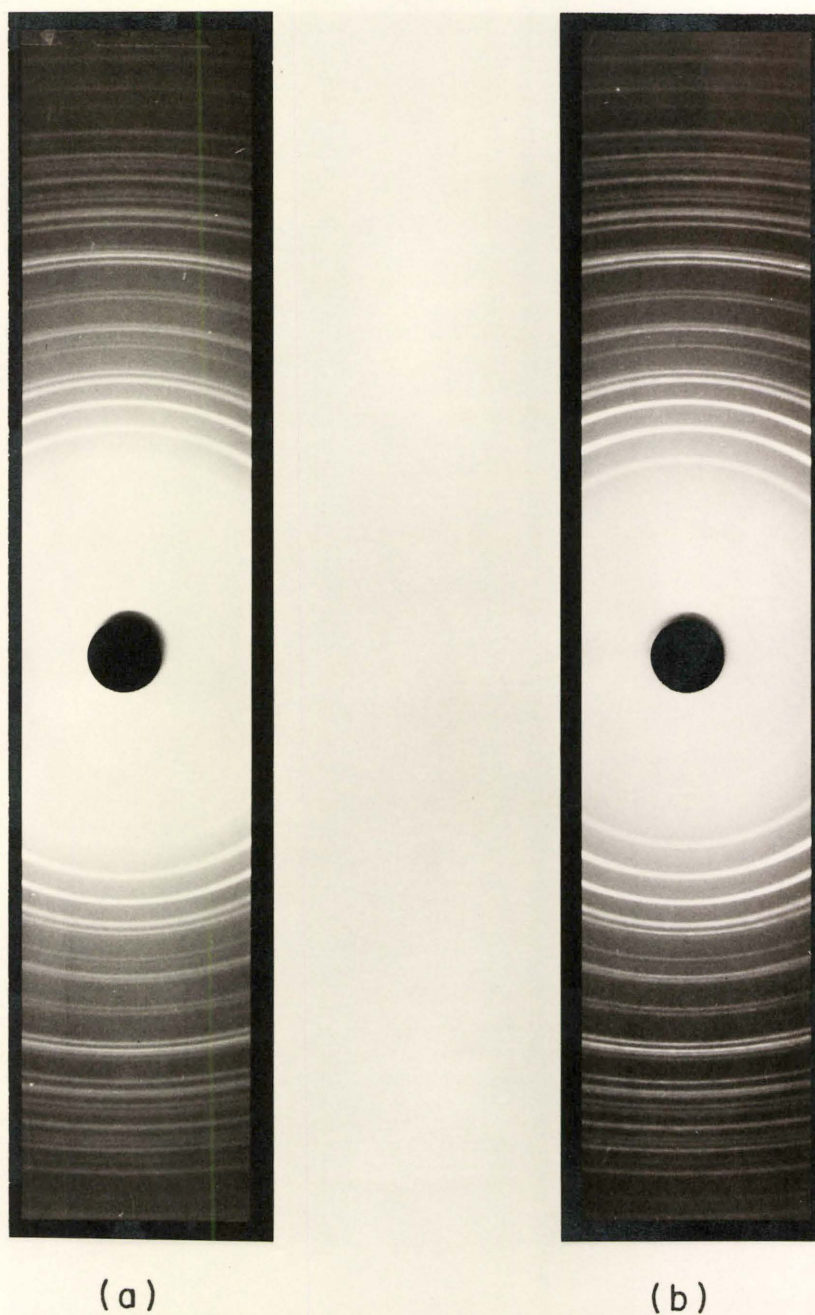


Fig. 21 X-Ray powder photographs of Zirconium Dioxide. Straumanis method. Filtered Cu radiation. Camera dia. = 10.4 cm.
(a) Gray oxide. Corresponds to sample XVIII, 76 hr.
(b) White oxide. Corresponds to sample VII, 12 hr.

CHAPTER VI

Reaction of Nitrogen with Zirconium. Results

6.1 Static, Gravimetric Measurements at 750° - 1000°C:

The zirconium-nitrogen reaction has not attracted the interest of many investigators. Although data available in the literature describing the kinetics of nitriding are limited, those published agree that the reaction obeys a parabolic relationship. Since the Pilling-Bedworth ratio for zirconium nitride (1.05) is more favorable than that for zirconium dioxide, it was decided to investigate this system more vigorously with respect to the application of the previously derived diffusion equations.

Fig. 22 represents the weight-gain vs. time relationship expressed by equations calculated by the "least squares" method. The values for these equations are recorded in Table 7. A plot of weight-gain as a function of temperature, °K, is shown also. The dashed lines were obtained from extrapolations of the appropriate rate equations. The parabolic nitriding rates demonstrate that the reaction is probably a diffusion controlled process.

All samples for the nitriding tests were prepared by the same procedures as already described for the zirconium-oxygen reaction. Values of the gravimetric results together with the final results from continuous volumetric measurements are listed in Table 8.

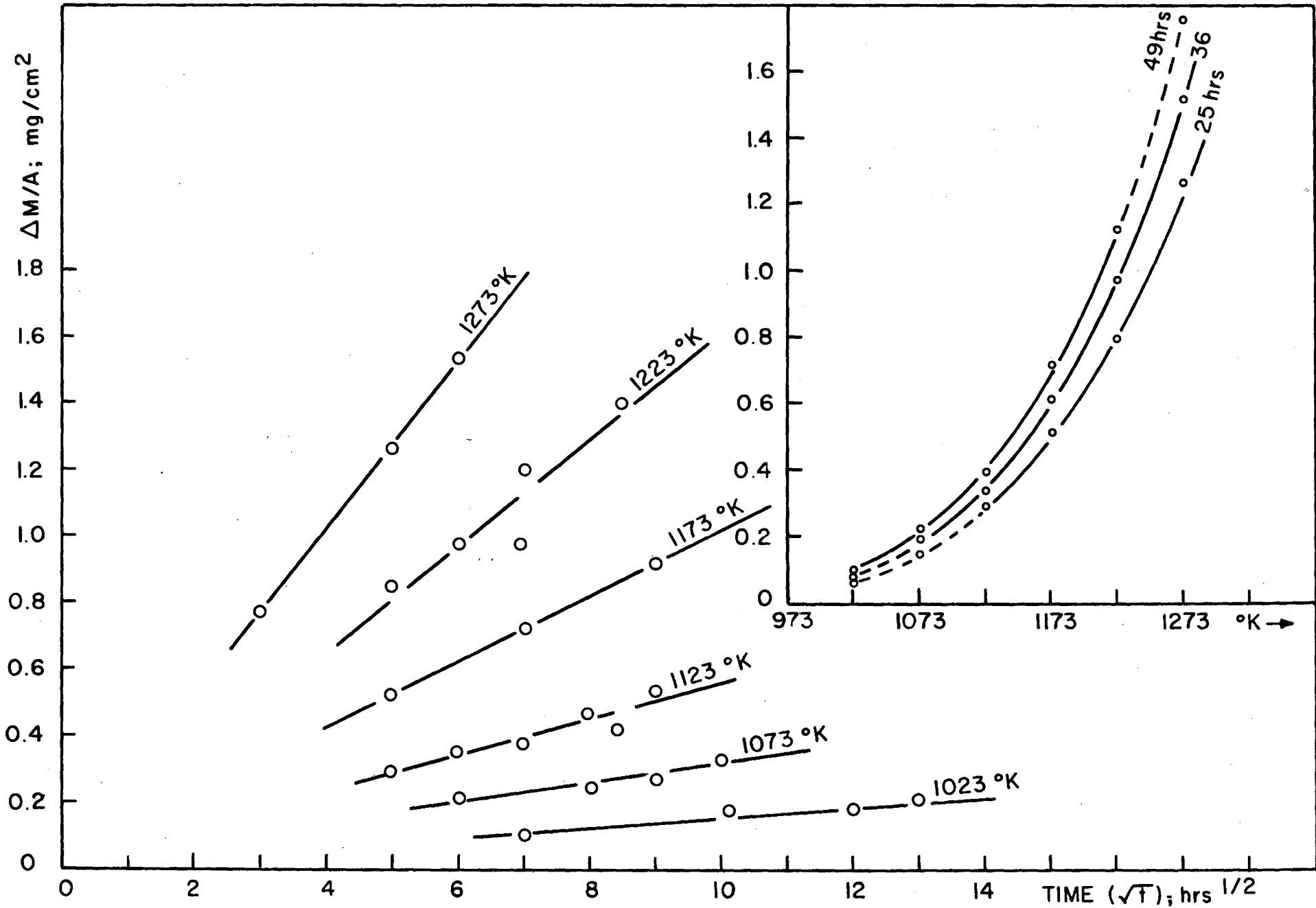


Fig. 22 Nitriding Rates of Zirconium at 750° - 1000°C. Sample Thickness 2mm.

6.2 Volumetric measurements at 850° and 950°C:

Fig. 23 shows the nitriding rates at 850° and 950°C from continuous volumetric measurements. To duplicate the reproducibility three nitriding runs were performed at 950°C. The small deviations for runs at 950°C is within the accuracy of the technique. Comparison of these determinations with those of Fig. 22 shows that both types of measurements give the same results to a good approximation. The appropriate values for the parabolic equation at each temperature are recorded in Table 7.

6.3 Microscopic and Metallographic Examinations:

Fig. 24 shows the obtained values for the thicknesses of nitride and alpha-phase and Fig. 25 is a plot of the sum and ratio of these thicknesses. Table 9, in the appendix lists the values used and Table 10 gives the equations of the curves.

Fig. 26 demonstrates the metallography of nitrided zirconium samples. Picture 26a shows the topography of typical ZrN, which under normal visual inspection appears goldish in colour. Picture 26b is the normal cross section of the nitride layer. It will be noted that in this case we do not find voids, which were typical for the oxygen-zirconium system, Fig. 16. Picture 26c represents the alpha-beta interface. This picture has been taken under oblique illumination purposely, in order to reveal distinctively the boundary between the two phases and under low magnification in order to show the smoothness of this boundary over larger distances.

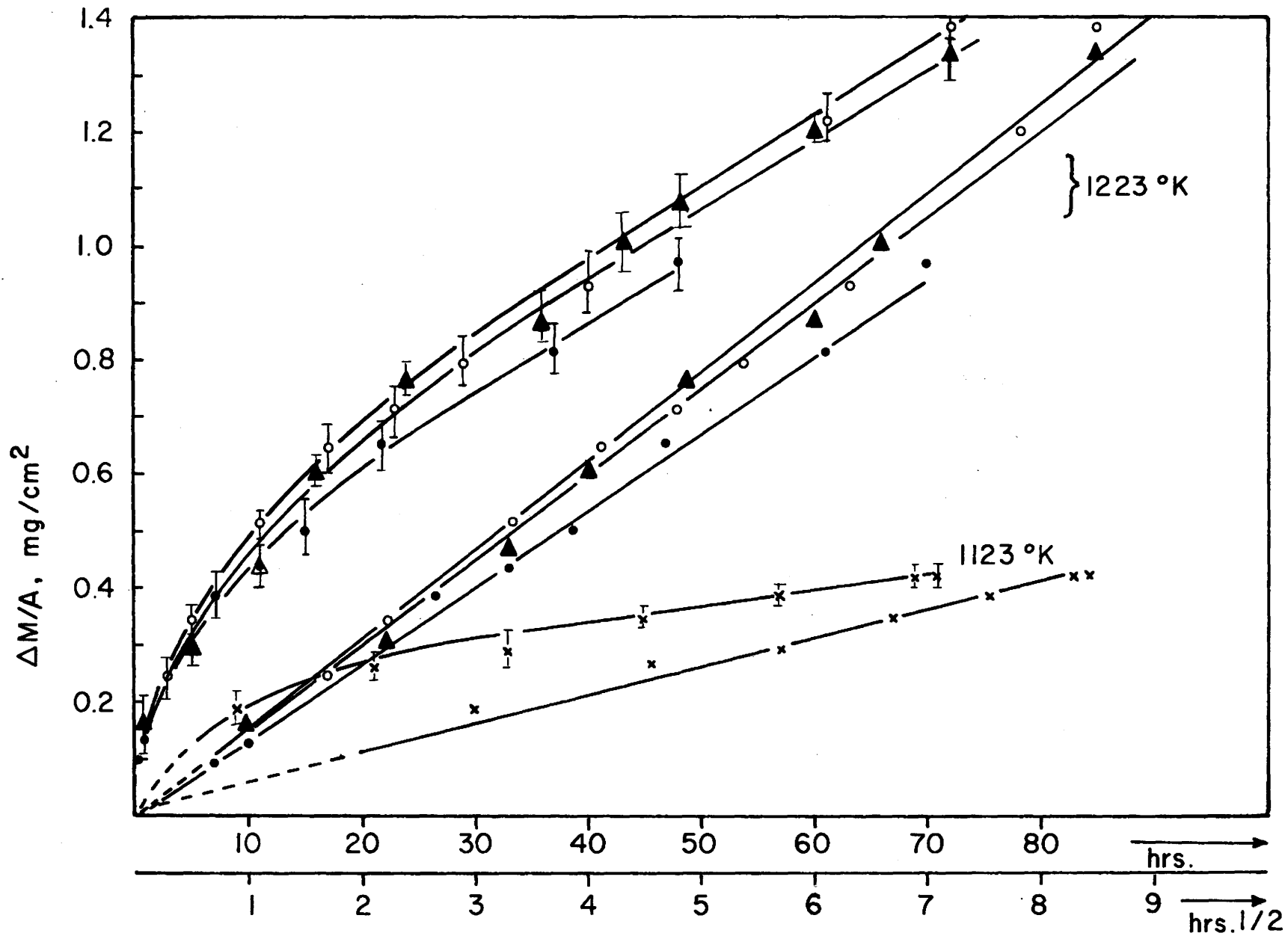


Fig. 23 Nitriding Rates of Zirconium at 850° and 950°C . Sample Thickness 2mm.

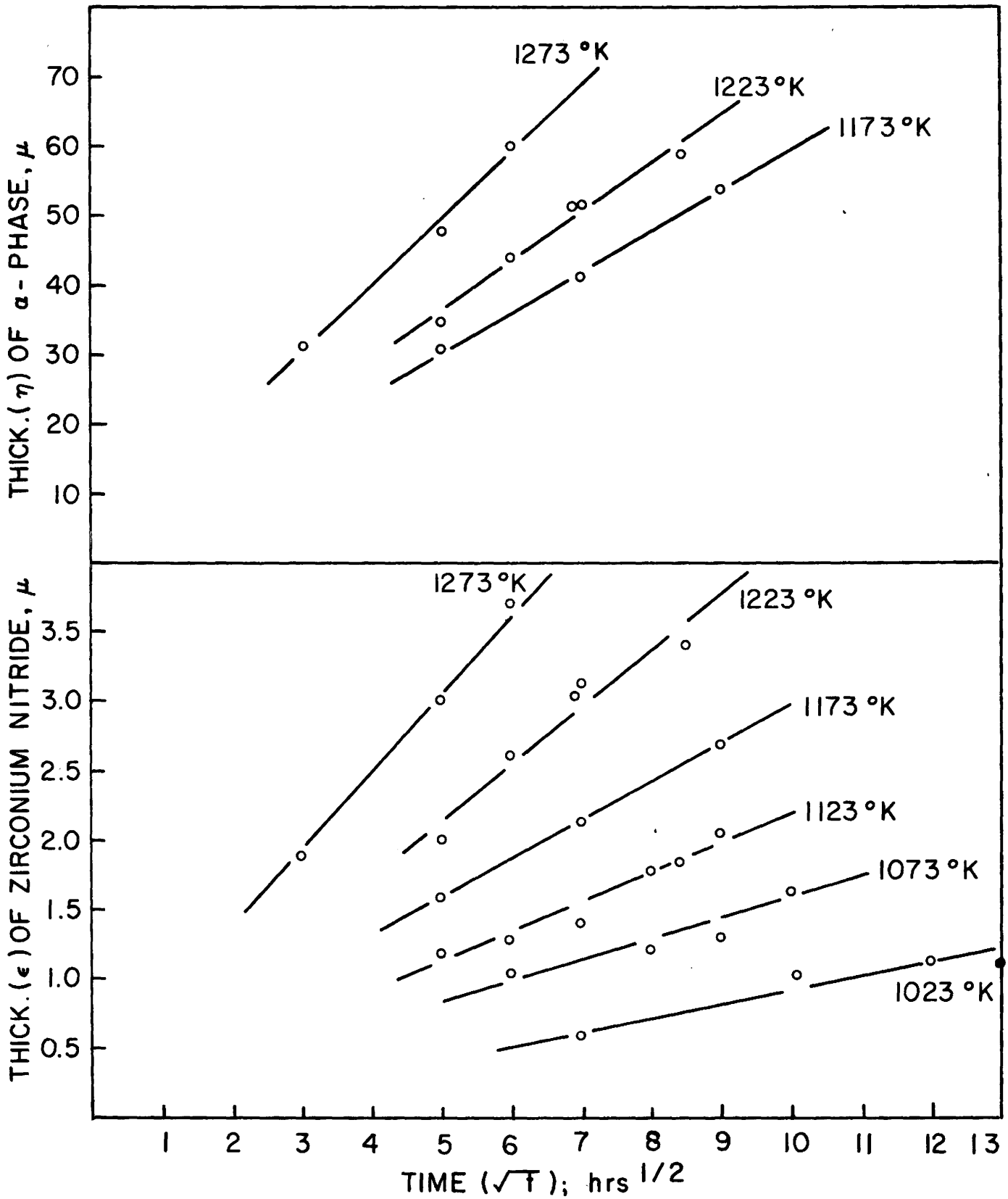


Fig. 24 Thicknesses of Zirconium Nitride and Zirconium-Alpha Phase Solid Solution

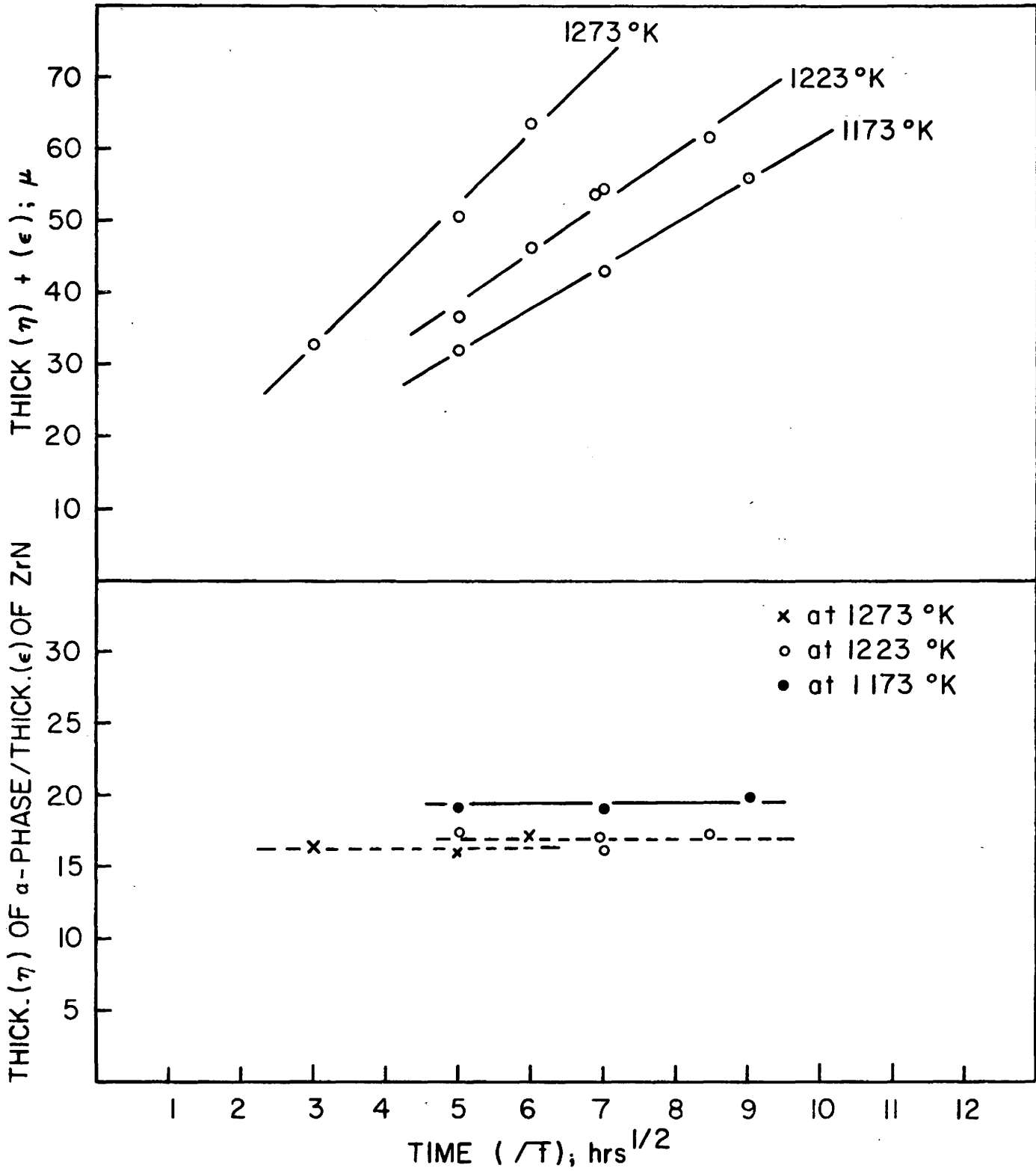


Fig. 25 The Sum and Ratio of Thicknesses Given in Fig. 24

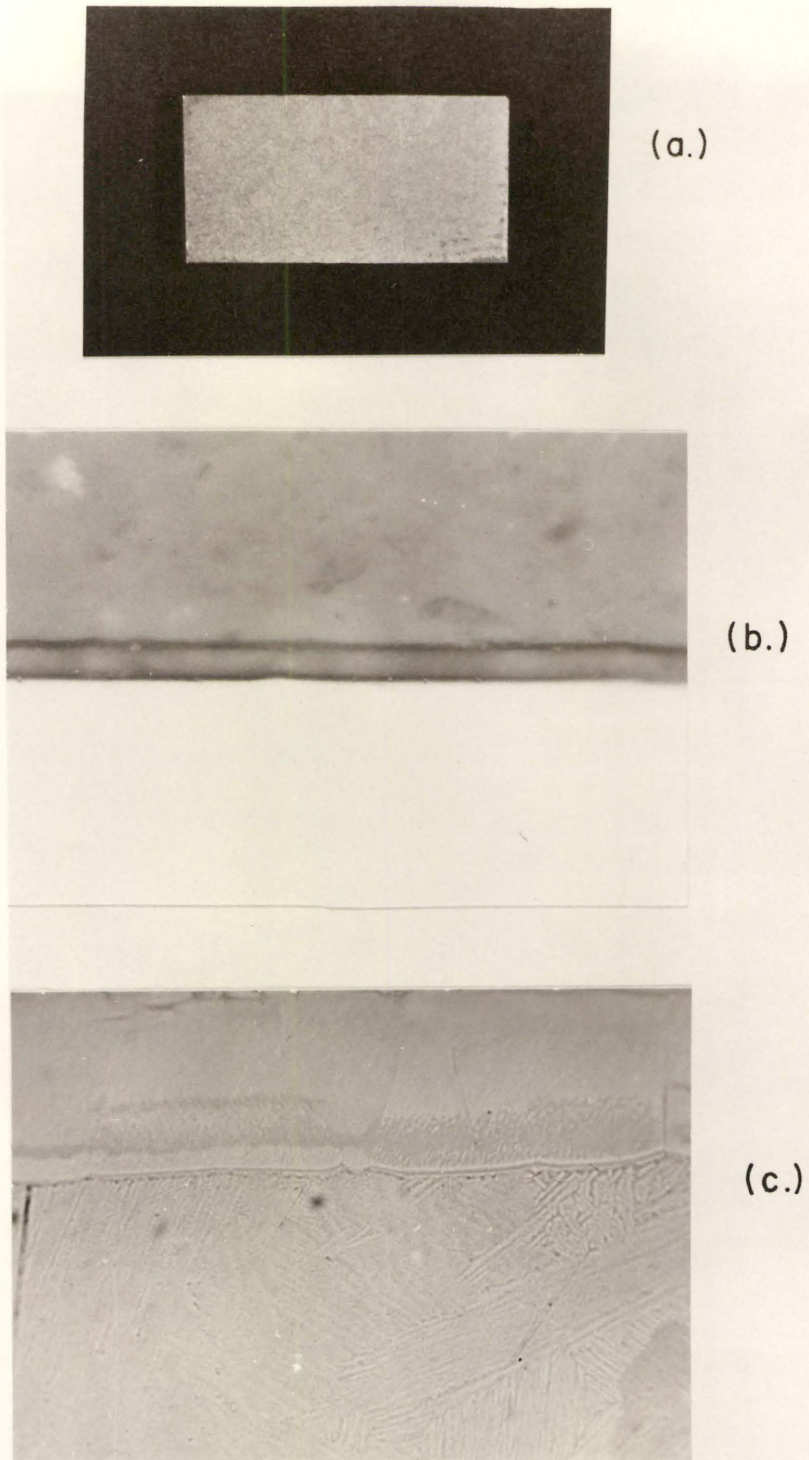


Fig. 26 Metallography of Nitrided Zirconium; cooled from 950°C .
(a) Topography of zirconium nitride, 100x. Reproduction 2x.
(b) Zirconium nitride film and underlying alpha, 400x
(c) Alpha-beta (lower part) interface, 250x, Oblique illumination.

6.4 Microhardness Measurements:

To calculate the uptake of nitrogen by the metal, it follows from equation (31) that one has to know the value for diffusivity, D_I , of nitrogen in alpha-zirconium. A review of the literature reveals that this value has not been published; the only value reported is that of SAMSONOV⁽⁷¹⁾ for diffusion of nitrogen into alpha-zirconium powder compacts. This author reports $D_I = 7.47 \times 10^{-5} \exp (-1000/T)$ for the range of 500° - 600°C. The density of a compact was only 99.6% of the theoretical value; and obviously such data for D_I cannot be very reliable. It was decided, therefore, to determine the diffusivity by the available techniques.

The microhardness method is a commonly employed technique⁽⁷²⁾. The depth of the microprint depends on concentration and usually the microhardness of pure metal is smaller than that of a solid solution in which the metal serves as a base and increases with increasing concentration of the dissolved substance. It is most convenient to use this method at low concentrations.

TERCO⁽⁷³⁾ has shown that the hardness of zirconium is very sensitive to small amounts of oxygen, while GEBHARDT and SEGHEZZI⁽⁷⁴⁾ found a large and linear dependence between the microhardness of tantalum solid solution and the concentration of nitrogen, for the range of 0.0 - 2.6 at % N_2

From relationship:

$$C(x) = C_o + B_I \operatorname{erfc} \frac{x}{2 \sqrt{D_I t}} \tag{62}$$

it is possible to evaluate the value for D_I providing that the variation of hardness, H , vs. concentration, $C(x)$, of nitrogen is known. This we do not know, except for the initial nitrogen content, C_0 . However, we can gain information from the values of H 's resulting from extrapolation of hardness curves to the alpha-beta interfaces and from the measured surface hardnesses for samples nitrided at different temperatures, because the equilibrium concentrations at these boundaries are given by the nitrogen-zirconium phase diagram e.g. by DOMAGALA and McPHERSON⁽⁷⁵⁾ or HANSEN⁽⁵⁷⁾.

Fig. 27 and 28 show a direct plot of hardness (D.P.N.) vs. distance, x , into a sample from the nitride-alpha zirconium interface, for different nitriding times and temperatures. Each value plotted represents the average of three readings taken from the same indentation. The dashed vertical lines in Fig. 28 represent positions of the alpha-beta boundary and were drawn on the basis of microscopic observation, see Table 9.

Equation (62) implies that the concentration gradients for different times become coincident on a normalized graph of $C(x)$ vs. x/\sqrt{t} . If the concentration of nitrogen in the metal is proportional to its hardness a test may be made of this relationship by plotting: $H(x)$ vs. x/\sqrt{t} . Figs. 29 and 30 show this test at different temperatures. It is apparent from these tests that the above relationship is valid within the accuracy in measuring hardness as a function of the indentation size.

As illustrated by the plot in Fig. 31, there is a linear relationship between hardness and nitrogen concentration in the metal. Assuming this relationship between hardness and nitrogen concentration, equation (62) may be

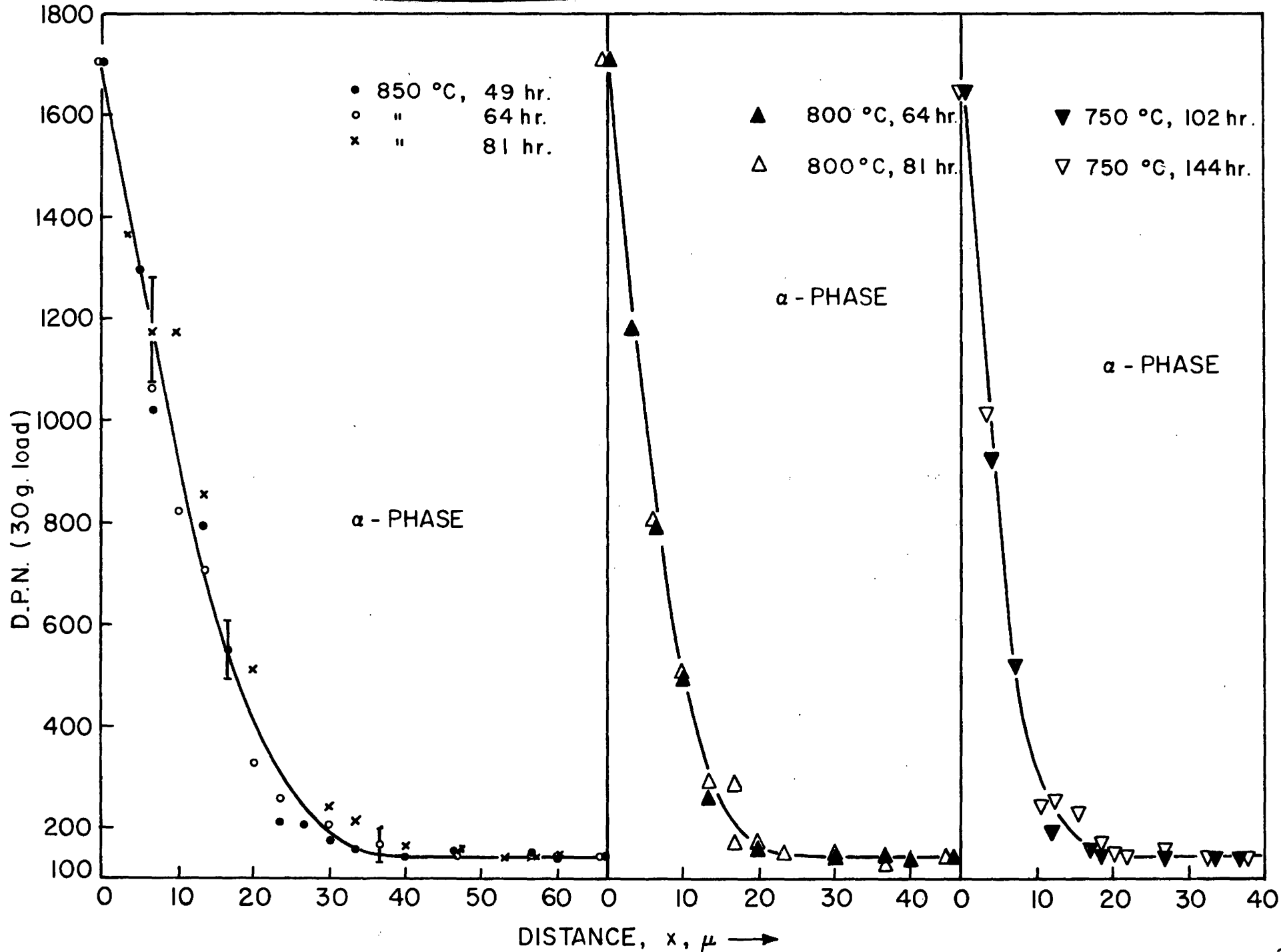


Fig. 27 Hardness Profiles in Zirconium-Nitrogen Solid Solution

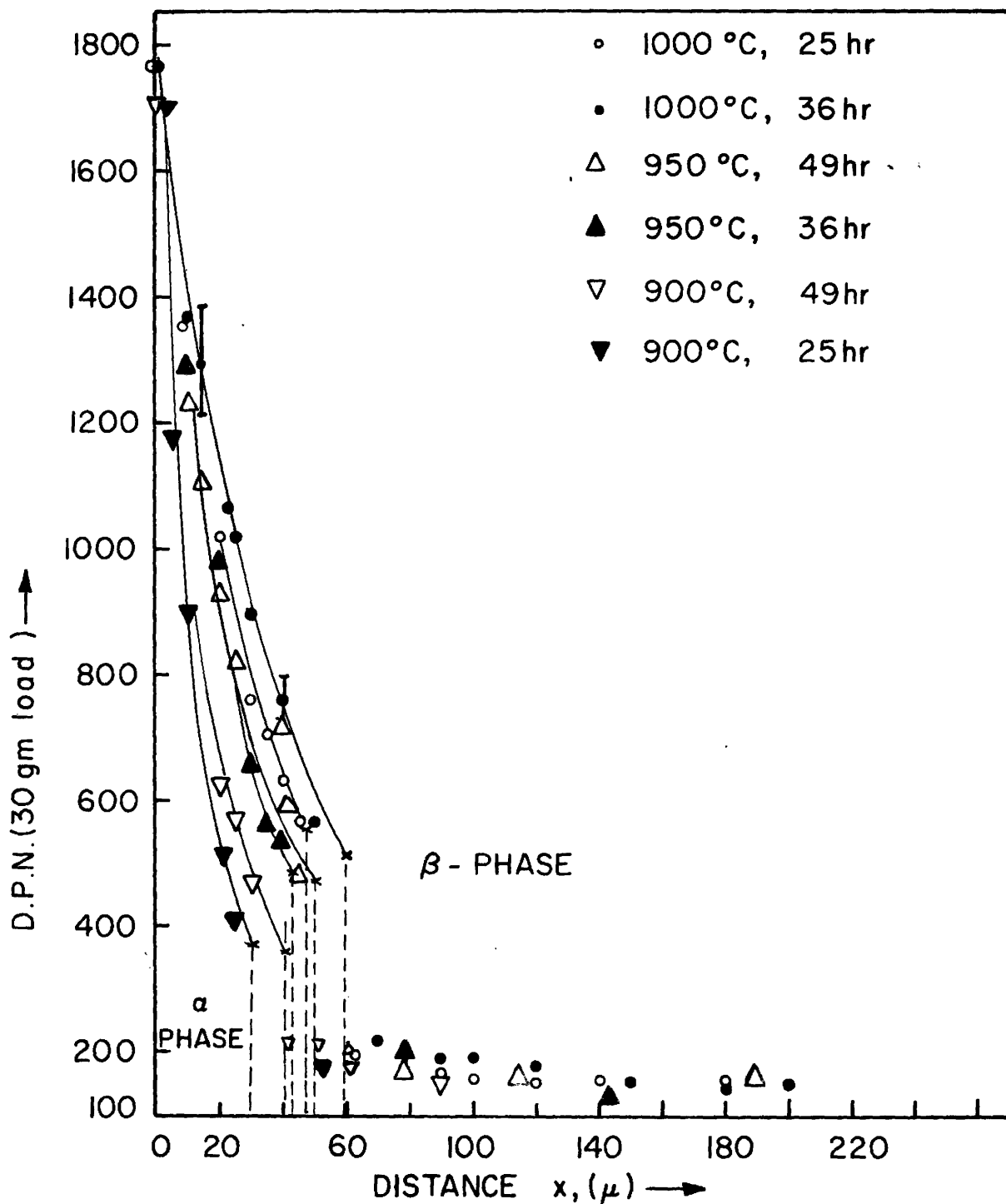


Fig. 28. Hardness Profiles in Zirconium-Nitrogen Solid Solutions

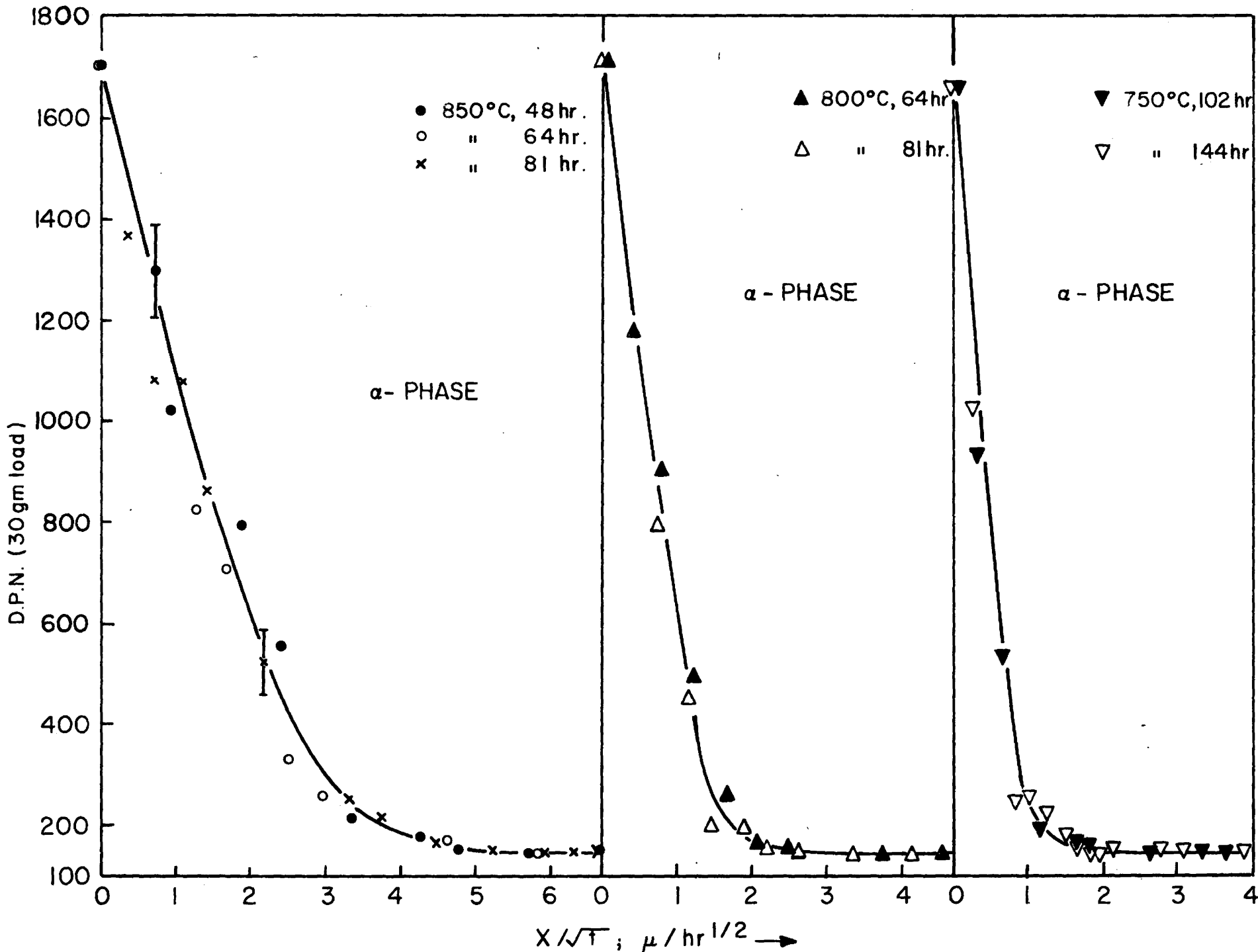


Fig. 29 Hardness Gradients Normalized with Respect to Time, for Nitrided Zirconium-Alpha Phase.

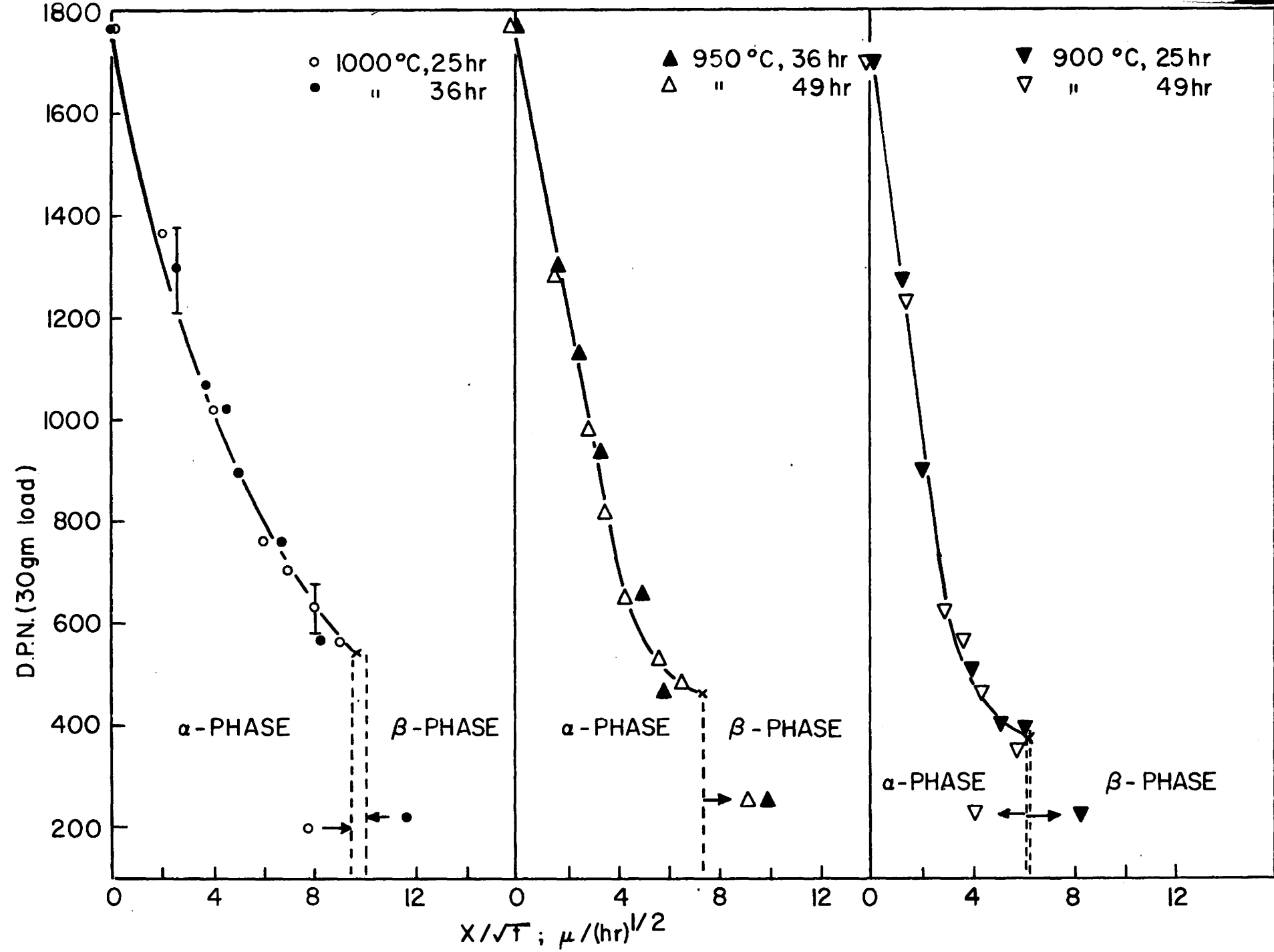


Fig. 30 Hardness Gradients Normalized with Respect to Time for Nitrided Zirconium Alpha Phase.

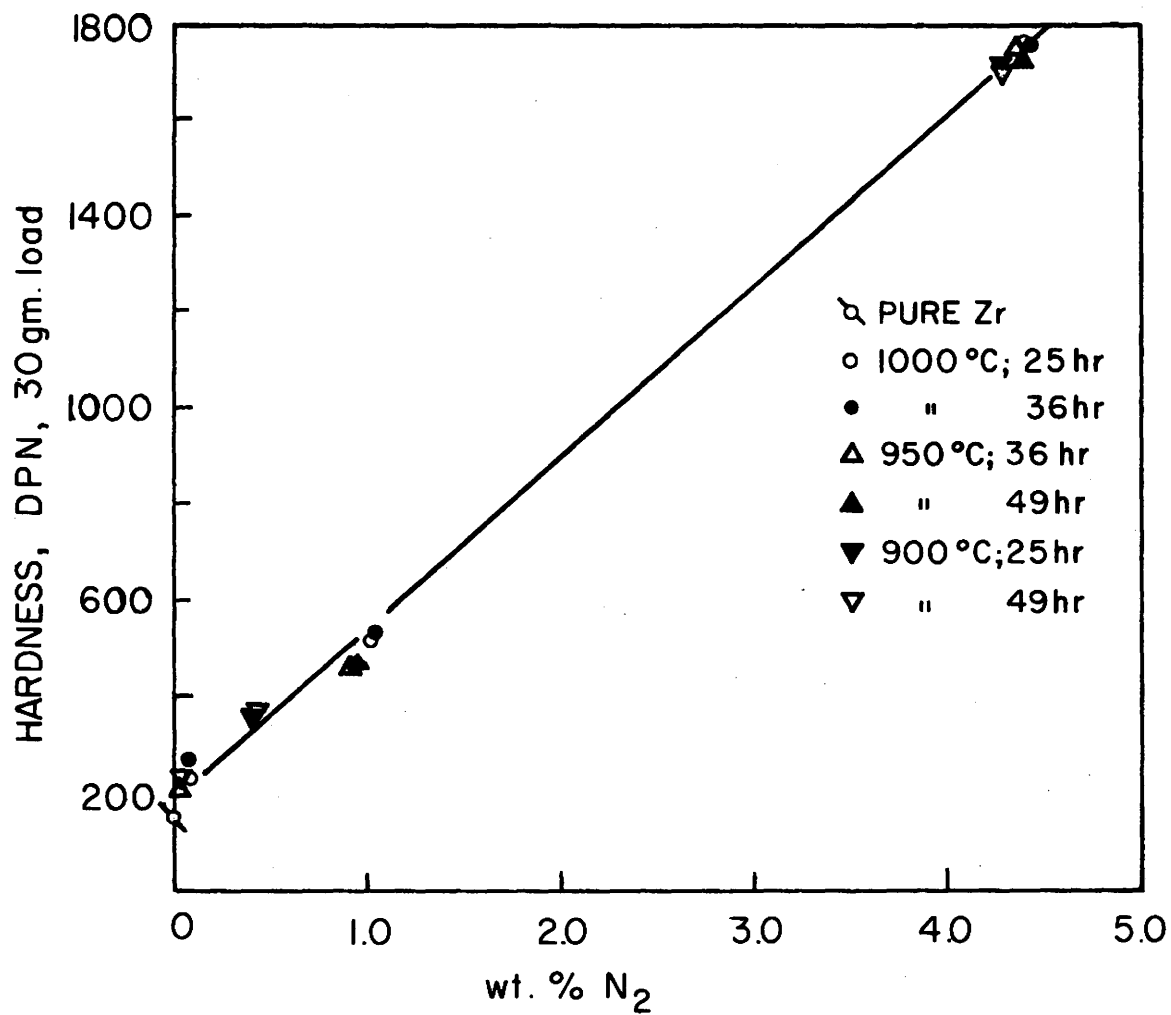


Fig. 31 Hardness as a Function of Nitrogen Concentration in Zirconium

plotted as $(H(x) - H_0)/H(0) - H_0$ vs. x/\sqrt{t} . The linear plot of a hardness gradient should pass through the mid-point at $x/\sqrt{t} = 0$, and at a given temperature the hardness gradients should become coincident on probability paper irrespective of nitriding time. Figs. 32 to 38 show such plots.

If the linear correlation is properly fitted to the experimental data then only one reading of $(H(x) - H_0)/H(0) - H_0$ for any chosen value of x/\sqrt{t} is necessary to solve,

$$\operatorname{erf} \frac{x}{2\sqrt{D_I t}} = 1 - \left[\frac{H(x) - H_0}{H(0) - H_0} \right] \quad (63)$$

directly for D_I , at a given temperature. An alternative method is to take slopes for each experimental value to obtain the individual D_I 's by virtue of equation (63), and take the average as the reliable value for diffusion of nitrogen into alpha zirconium, at a fixed temperature. The diffusion constants calculated in this way are summarized in Table 11 in the appendix.

Having obtained $D_I = f(T)$ we make use of the Arrhenius relation to obtain an expression for the diffusion constant. This relationship is shown in Fig. 39. Utilizing the "least squares" method, the diffusion constant in the temperature range $750^\circ - 1000^\circ\text{C}$ may be expressed as: $D_I(\text{cm}^2/\text{sec}) = 0.15 \exp \left[\frac{(-54100 \pm 2000)}{RT} \right]$.

6.5 X-ray Determinations:

So far, it was assumed tentatively that the nitride formed during the nitrogen-zirconium reaction corresponded to the chemical formula: ZrN . The only justification for this premise was the golden-yellow colour of the surface

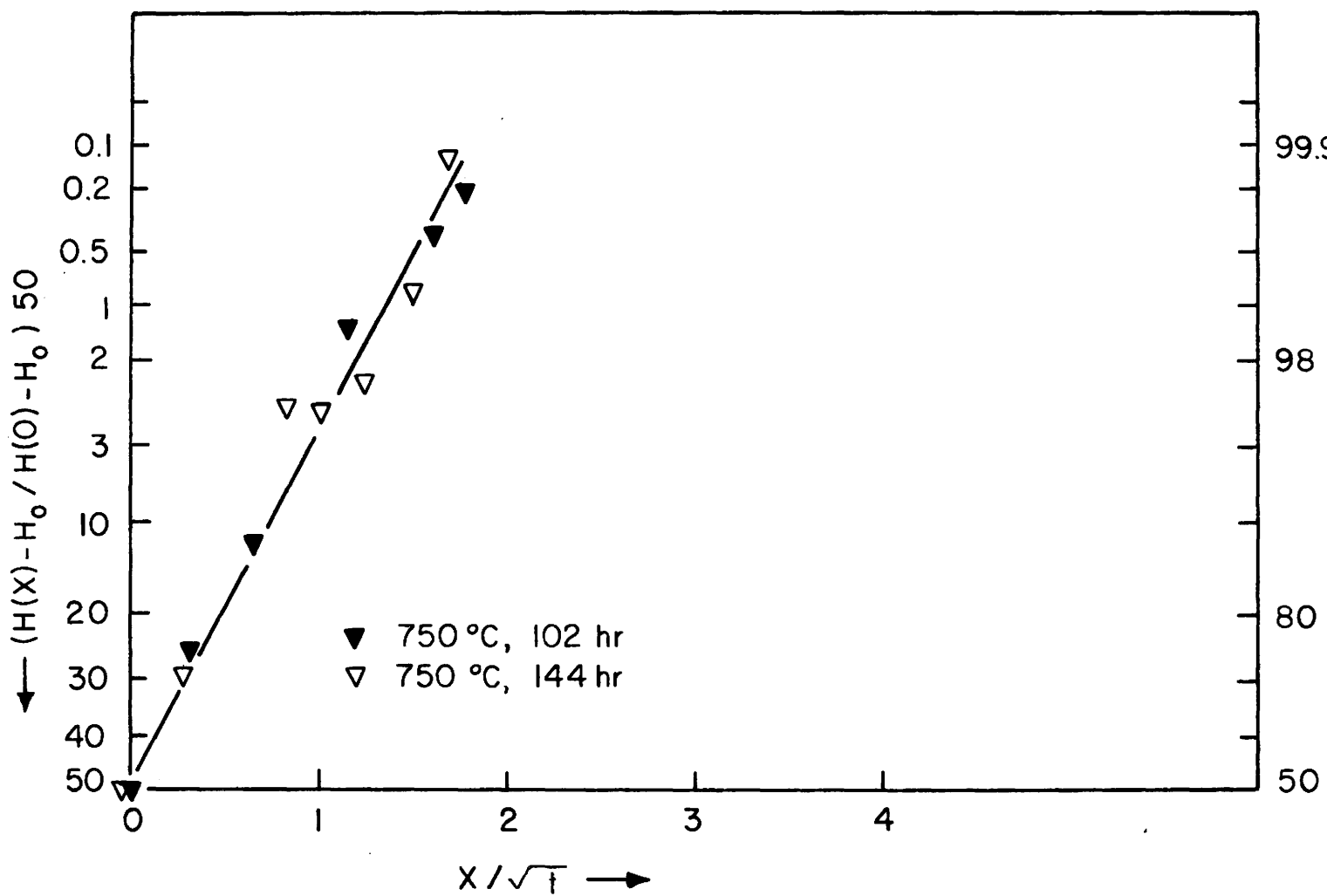


Fig. 32 Cumulative Normal Distribution of $x/t^{1/2}$; 750°C .

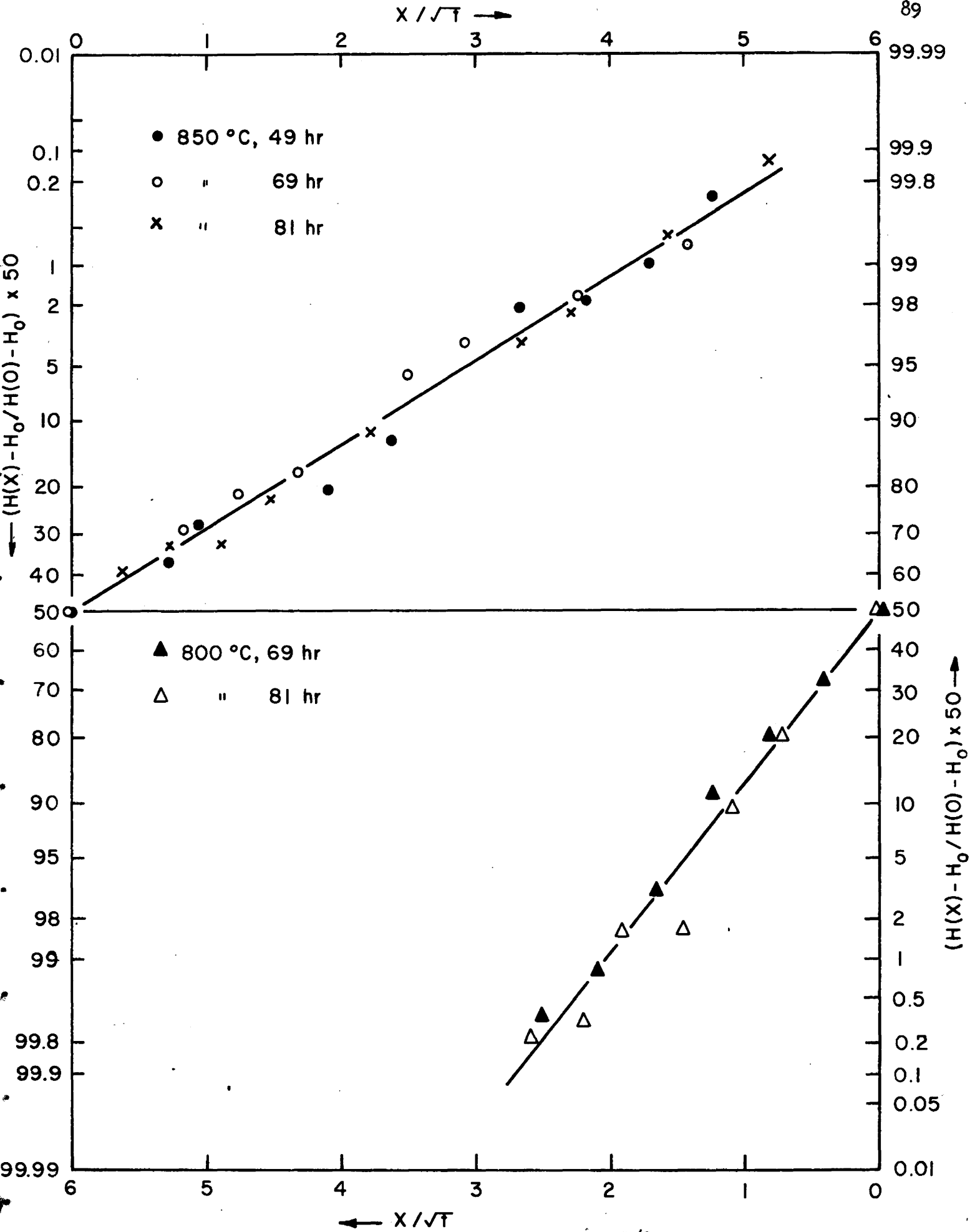


Fig. 33 Cumulative Normal Distribution of $x/t^{1/2}$; 800°C.

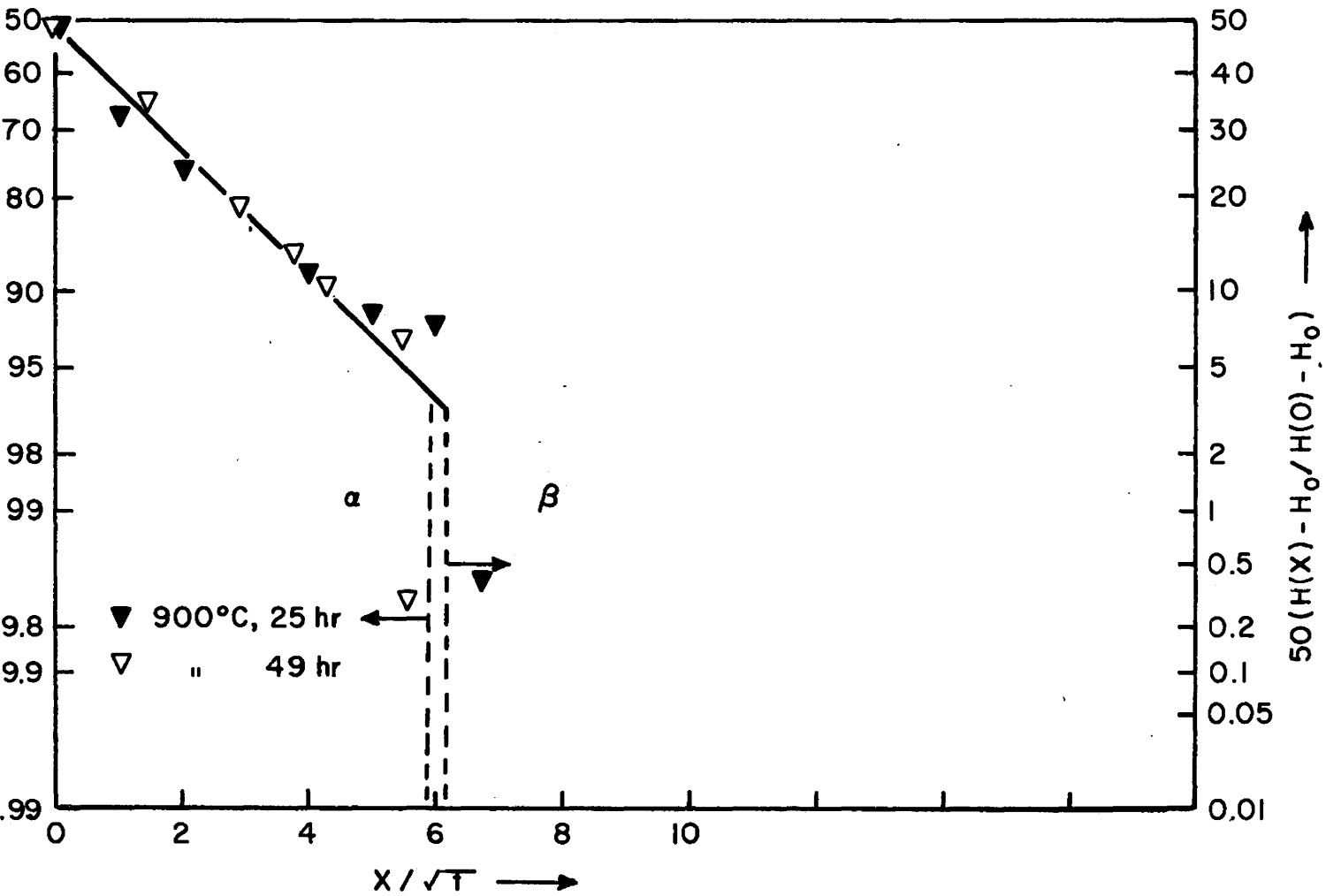
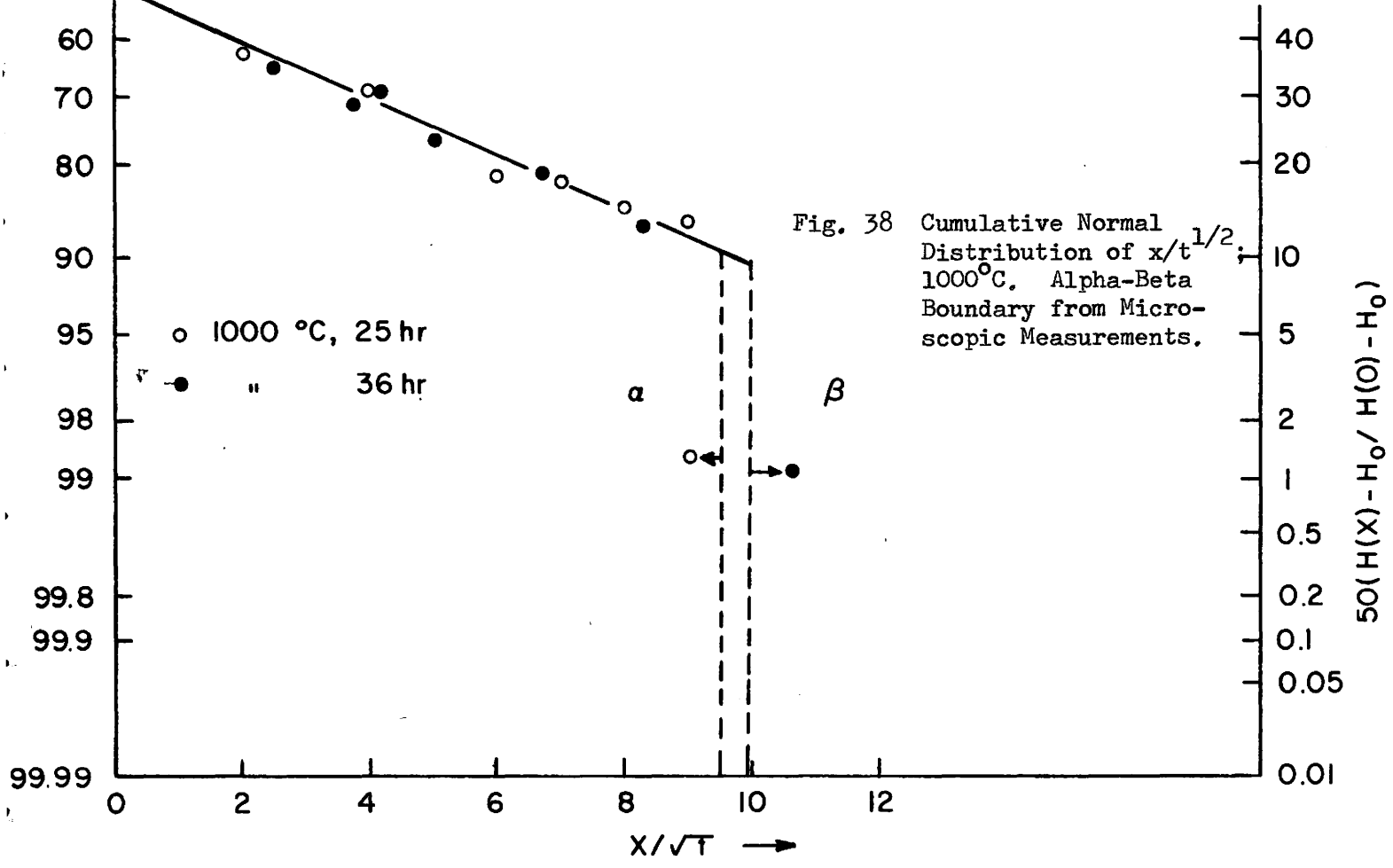
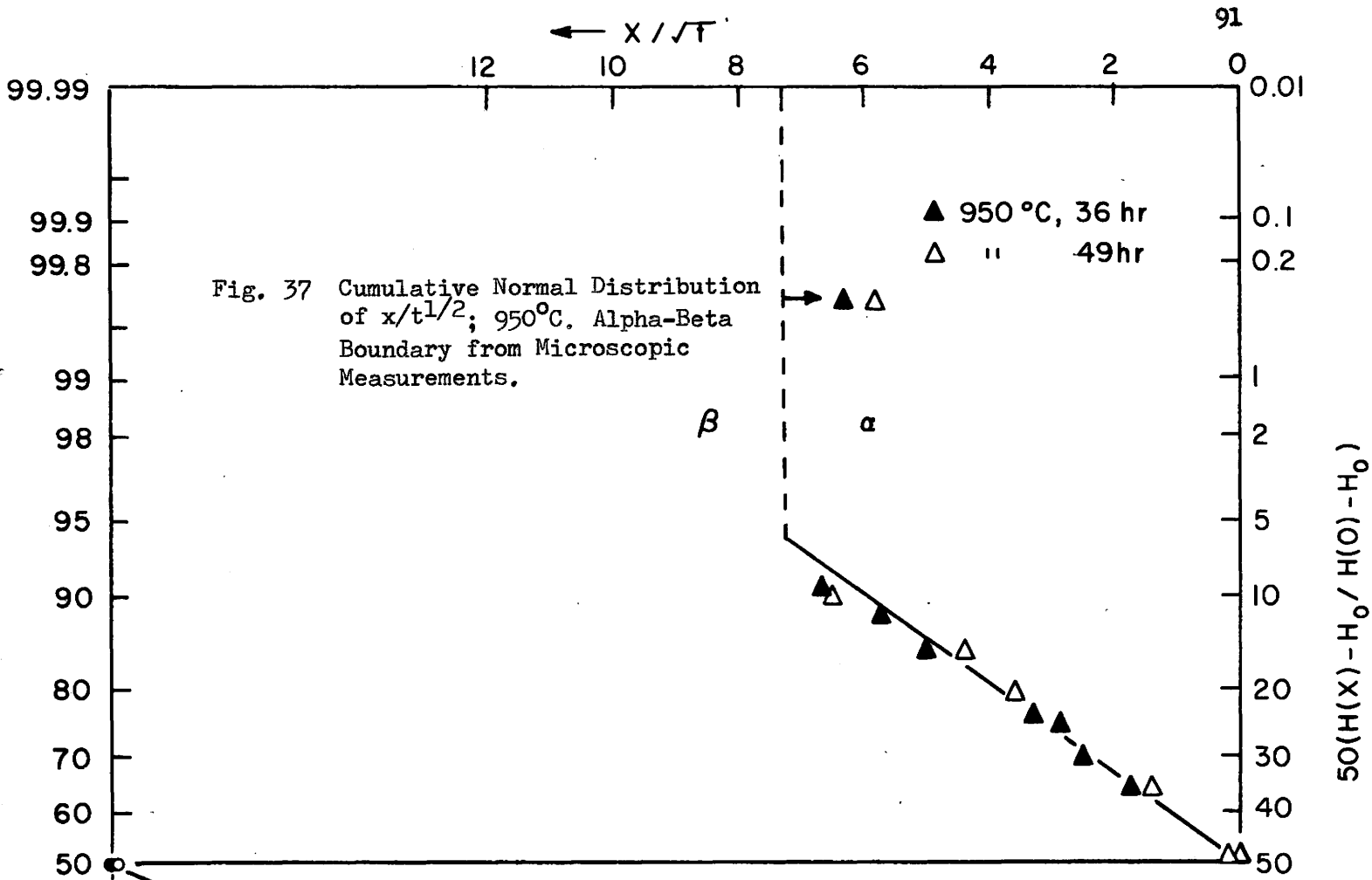


Fig. 35 Cumulative Normal Distribution of $x/t^{1/2}$; 900°C. Alpha-Beta Boundary from Microscopic Measurements.



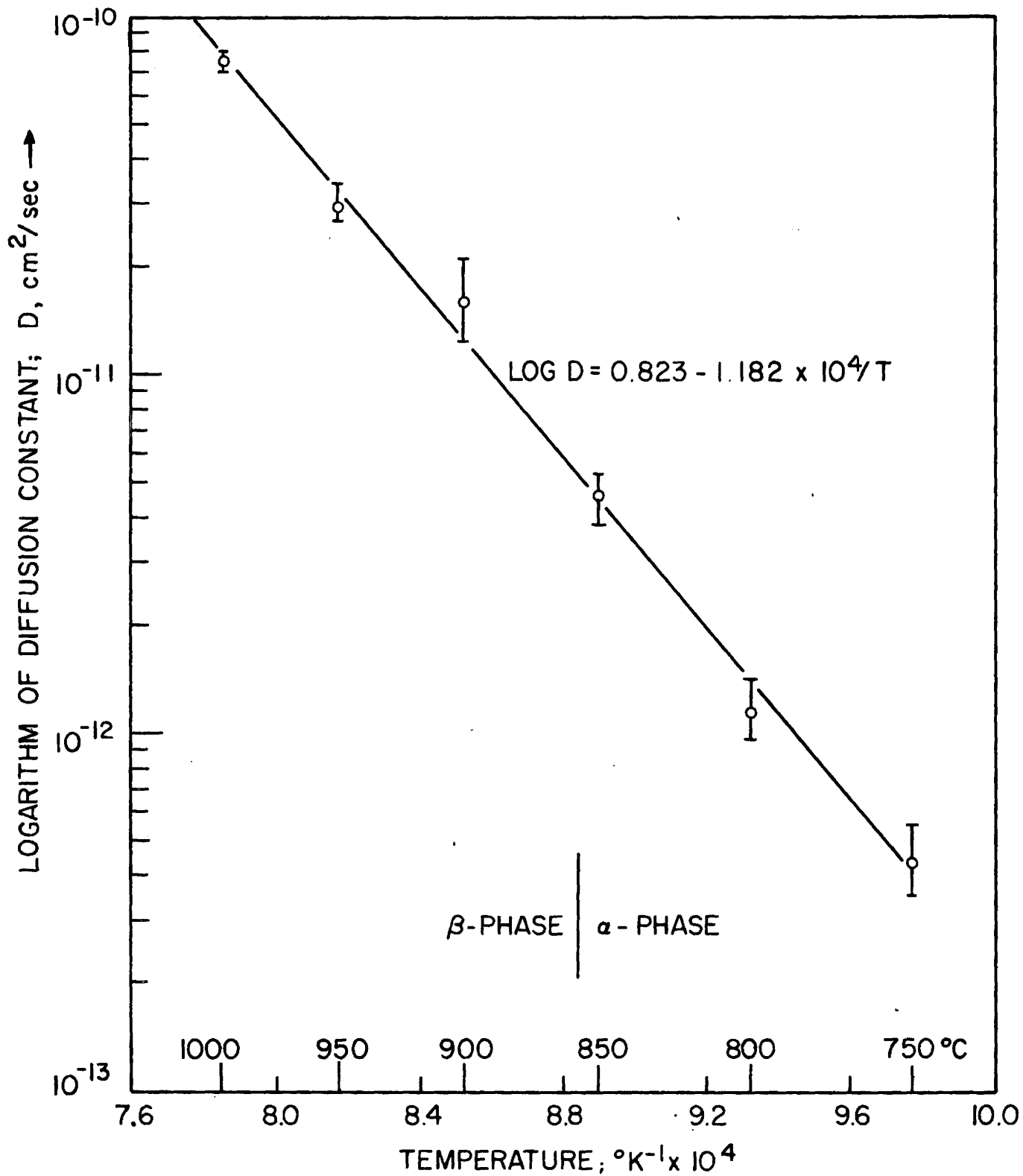


Fig. 39 Arrhenius Plot for Diffusion of Nitrogen in Alpha-Zirconium

film formed. This is in agreement with observations of DRAVNIIEKS⁽⁴⁴⁾ and MALLETT et al.⁽⁴⁵⁾. However, ELINSON and PETROV⁽⁷⁶⁾ report that the scale on zirconium is composed of the following nitrates: $ZrO(NO_3)_2 \cdot 2H_2O$, $Zr_2O_3(NO_3)_2 \cdot 5H_2O$ and $Zr(NO_3)_4 \cdot 5H_2O$ when the metal is exposed to nitrogen atmospheres. The contents of oxidizing impurities in the atmospheres were not reported.

X-ray analyses illustrated by the powder pattern in Fig. 40 shows that the yellow-film formed upon heating zirconium in nitrogen is ZrN (f.c.c.; $a_0 = 4.56\text{\AA}$) thus verifying the a priori assumption. Some of the data resulting from structure determinations are given in Table 12 of the appendix. Accordingly, the results reported by ELINSON and PETROV for formation of nitrates upon scaling of zirconium in nitrogen atmospheres must be associated with the unknown contents of oxidizing impurities.

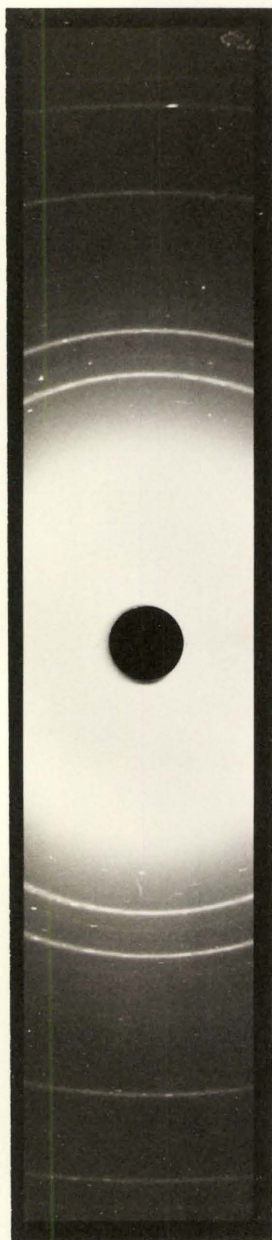


Fig. 40 X-Ray powder patterns of Zirconium Nitride. Nickel filtered Cu radiation. Straumanis method; Camera dia. 10.4 cm. Sample nitrated for 72 hr. at 950°C.

CHAPTER VII

Reaction of Zirconium with Gas Atmospheres. Results

7.1 Nitrogen-Oxygen Atmospheres, 850°C:

The combined presence of oxygen and nitrogen gave weight gain vs. time curves as shown in Figs. 41a,b , for several atmospheres. The run in air has been included for comparison. During isothermal runs in nitrogen-oxygen environments or in air, zirconium followed approximately a parabolic rate until time was reached after which a very rapid rate set in. Hereafter the point of change of rates will be called the "breakaway" or "transition" point.

Since runs in pure oxygen and pure nitrogen exhibited no increase in the scaling rate during exposures of 100 hours, these experiments established that the simultaneous presence of the two gases caused breakaway, even if present in small amounts. Also, it is observed that small additions of either gas increase the scaling rate constant, (approx. k_p), when compared with the values of k_p 's for reaction in pure oxygen or nitrogen. The dashed lines indicate approximately the weight changes accompanying the post-transition period. To fix accurately the breakaway point would require continuous self-recording equipment. The numerical equations for the parabolic range of curves represented in Fig. 41a,b are summarized in Table 13 of the appendix.

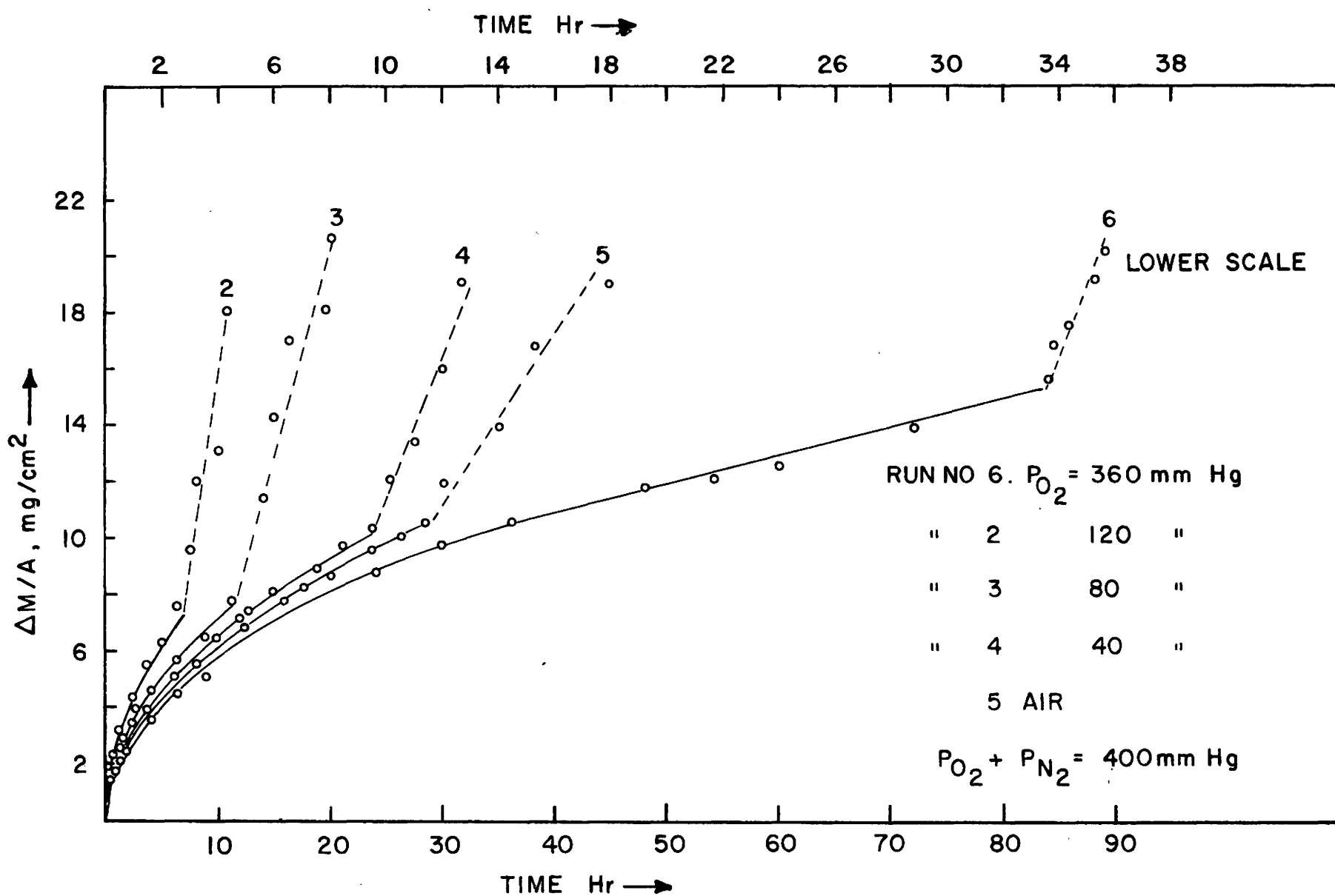


Fig. 4la. Reaction Rates of Zirconium in Oxygen-Nitrogen Atmospheres at 850°C.

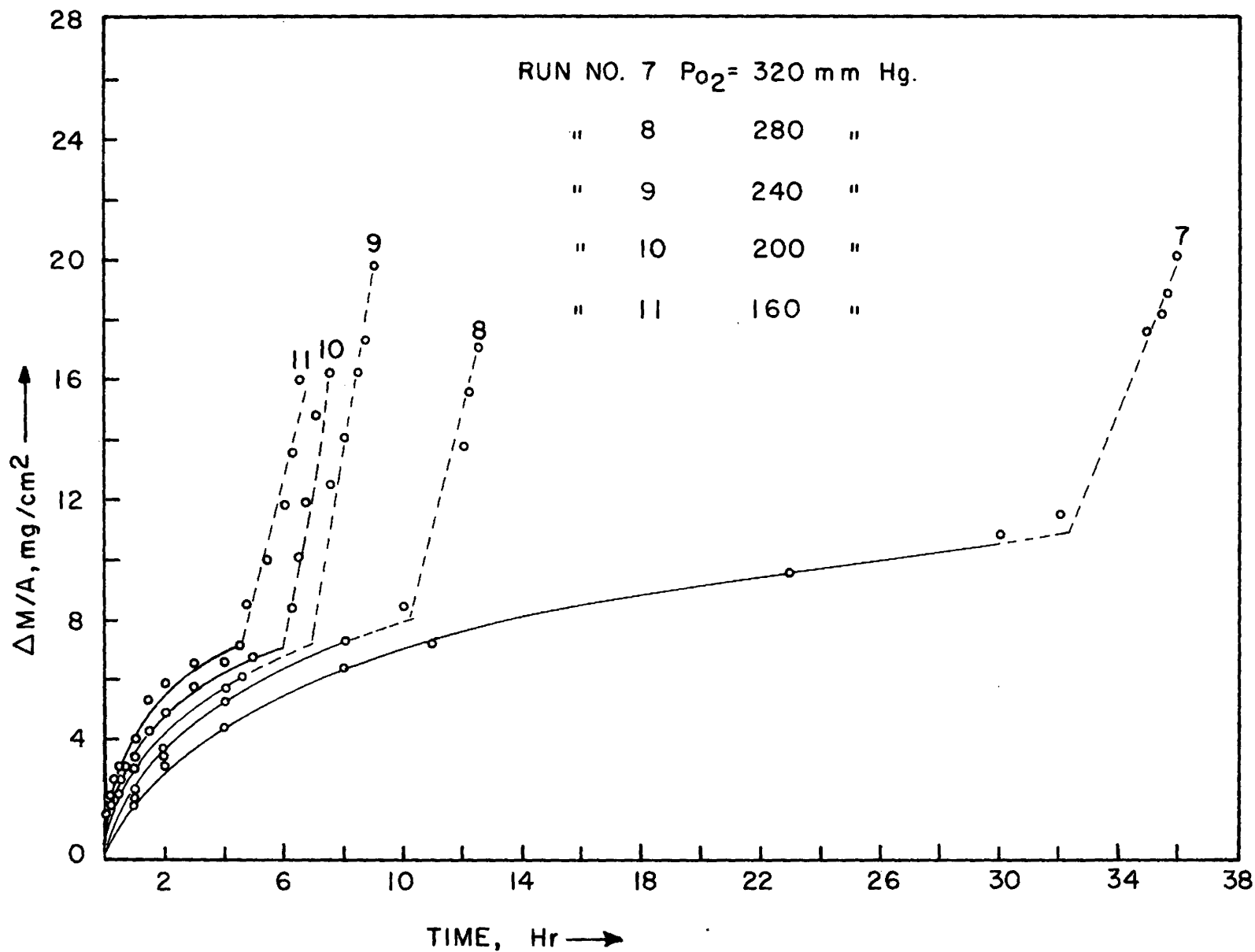


Fig. 4lb. Reaction Rates of Zirconium in Oxygen-Nitrogen Atmospheres at 850°C.

The times at which the increase in scaling rate occurred have been plotted as a function of nitrogen mole fraction in Fig. 42 . The strong dependence of atmosphere composition on the deviation time is readily apparent particularly at low concentrations of either gas where the time required for the upswing increased appreciably.

It will be noted that the deviation times for air and the oxygen-nitrogen atmosphere do not coincide; the breakaway point in air occurs after longer time. The reason for this behaviour is not clear. The fact that the oxygen-nitrogen atmosphere consisted of pure, dry gases as contrasted to air containing moisture does not afford an explanation for the difference in time deviation to the transition point. Moisture has been reported to accelerate the scaling rate of zirconium in air, by HAYES and ROBERSON⁽⁷⁷⁾.

Scaling in atmospheres of various oxygen-nitrogen compositions produced microstructures essentially similar to those observed in air. A series of typical structures obtained for specimens past the onset of the rapid scaling rate is shown in Fig. 43 . An example of the surface appearance is provided by Fig. 43a , where both white and gray oxides coexist. The microstructures reveal three distinct regions: 1. the alpha-zirconium core, 2. a fine filigree of a yellow phase close or at the scale-metal interface, and 3. the scale. Before the appearance of the white scale, the scale was gray and compact. However, after the advent of the white scale a number of fissures were observed almost parallel to the scaling surface.

It is evident from these photographs (especially Fig. 43c) that both white and gray scale have the same colour when viewed under a microscope with

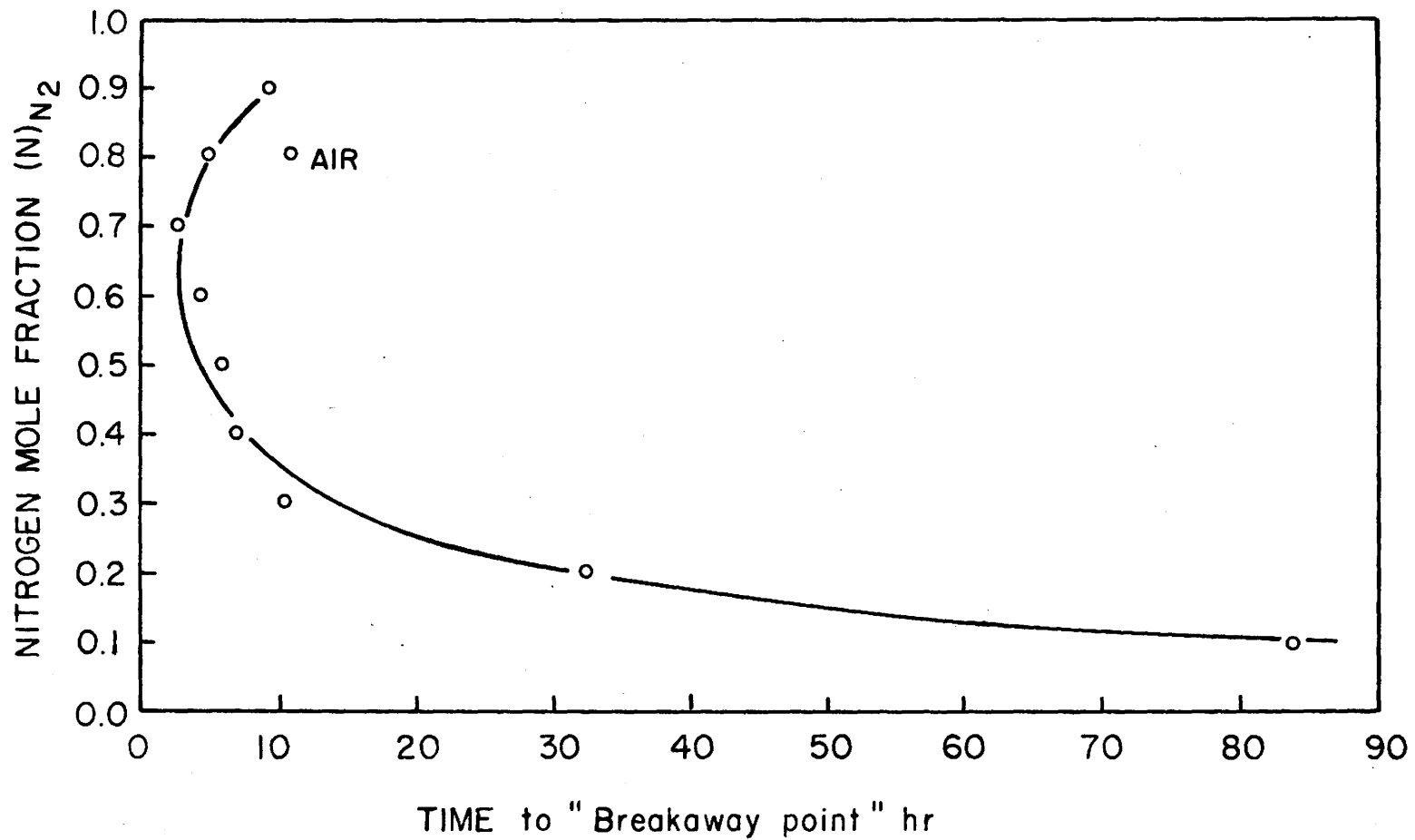


Fig. 42 Time to "Breakaway Point" as a Function of Nitrogen Mole Fraction $(N)_{N_2}$; at 850°C.

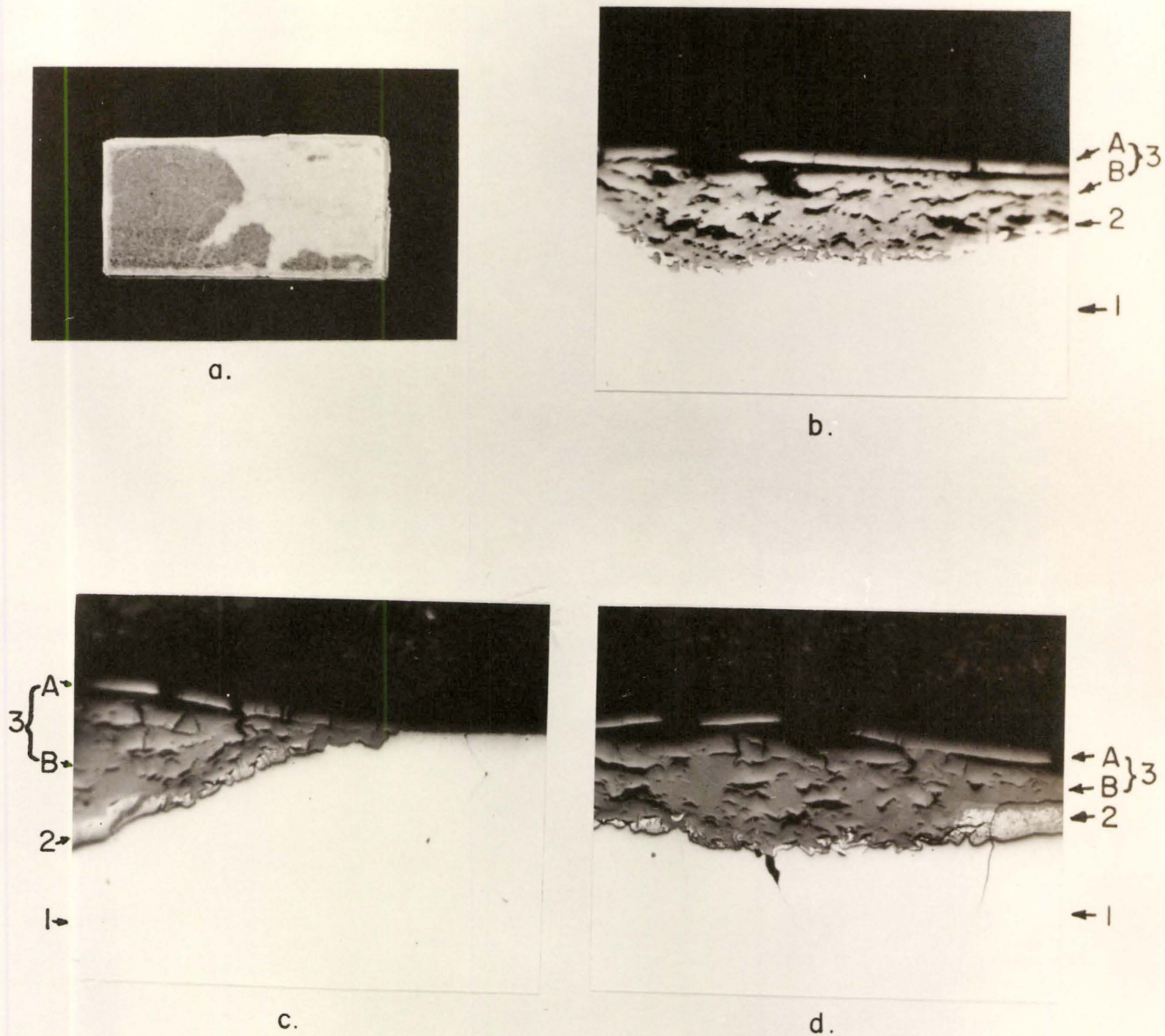


Fig. 43 Microstructures of Scale and Zirconium Metal, after cooling from 850°C .
 a. Topography, scaled in oxygen-nitrogen atmosphere. 3x.
 b. Cross-section, scaled in oxygen-nitrogen atmosphere. 250x. Heavily scaled section.
 c. Scaled in air, 250x.
 d. Scaled in air, 250x. Quenched in liquid nitrogen.
 (1) Alpha-Zirconium Solid Solution
 (2) Yellow phase filigree
 (3) Scale; A-white, B-gray

bright light illumination. Due to multiple reflection, there is a difference in colours under polarized light. The white scale is cracked. These cracks are perpendicular to the scaling surface and terminate at the junction between the gray and white scales as shown in Fig. 43b,c .

An attempt was made to identify the yellow phase at the metal-scale interface. Powder filed from selected areas of samples exhibiting the presence of this phase was analysed by X-ray techniques. The only diffraction lines found were those of zirconium dioxide. To investigate the solubility of nitrogen in zirconium dioxide, 11.12 gm of this oxide from Fisher Scientific Co. Ltd. was reacted with nitrogen at 850°C for 66 hrs. in a static atmosphere. The weight loss was about 30 µg and the colour of zirconium dioxide changed from white to grayish.

7.2 Water Vapour-Oxygen Atmospheres:

To investigate the influence of water as a gaseous impurity on the breakaway behaviour, several specimens were oxidized at 950°C in oxygen contaminated with water vapour from a source maintained at 25°C. The vapour pressure of water at this temperature is 23.8 mm. Hg. The extremely rapid reaction rate is shown by the kinetic data reported in curve 2, Fig. 44 . For comparison curve 1 (one of seven runs) shows the oxidation kinetics for specimens reacted in pure oxygen, which followed a parabolic rate equation for periods up to 96 hrs. Since the reaction rate was extremely rapid with this amount of water vapour at 950°C, additional experiments were performed at 850°C. A specimen was oxidized for 50 hr. in oxygen and water vapour was

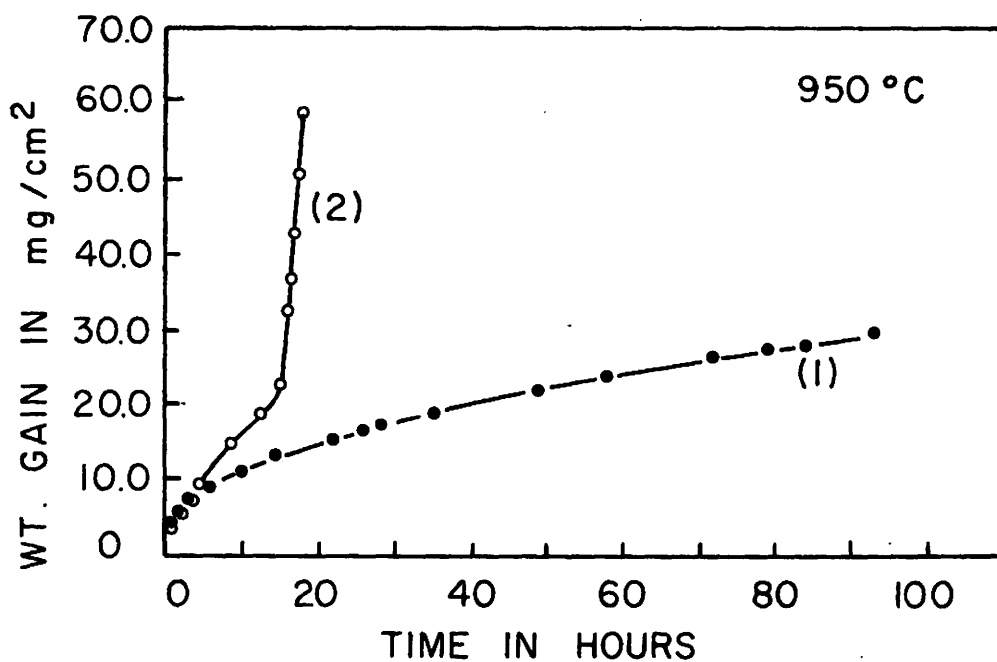


Fig. 44 Oxidation of Zirconium in Oxygen-Water Vapor Atmospheres

Curve (1): specimen thickness 2.23 mm, pure oxygen

Curve (2): specimen thickness 2.21 mm and oxygen contaminated with water at pressure of 23.8 mm Hg

then admitted to the reaction tube from a source maintained at 5°C . The vapour pressure of water at this temperature is 6.5 mm. Hg. The rate of reaction is given by curve 2 in Fig. 45 . The breakaway occurred after 80 hr. Again, curve 1 represents the kinetic behaviour for zirconium oxidized in pure oxygen.

Metallographic examinations revealed that massive amounts of porous oxide were formed due to more pronounced deviations from parabolic behaviour when specimens were exposed in oxygen atmospheres containing water vapour. This is demonstrated by Fig. 46 . Fig. 46a is a cross section of a specimen which was covered with areas of thick white oxide scale. Microscopic observations disclosed also that, in some places fingers of oxide penetrated into the metal, Fig. 46b ; whilst in others the oxide scale penetration was in the form shown in Fig. 46c . There was no evidence for presence of an additional hydride phase in the scale or at the oxide/metal interface. The two types of porous scales distinguished from these experiments, were similar to growths reported by PEMSLER⁽⁷⁸⁾. In the first case cracks in the oxide and metal essentially perpendicular to the surface resulted in the formation of oxide fingers. On the other hand, cracks essentially parallel to the scale-metal interface caused the formation of the broader hemispherical penetration of oxide. It was impossible to determine for these latter growths, the role of water vapour in the reaction mechanism and whether the cracks were initiated in the oxide or metal. In specimens cooled from 850°C precipitated zirconium hydride needles were observed in the central regions of the samples, showing that hydrogen diffused into the

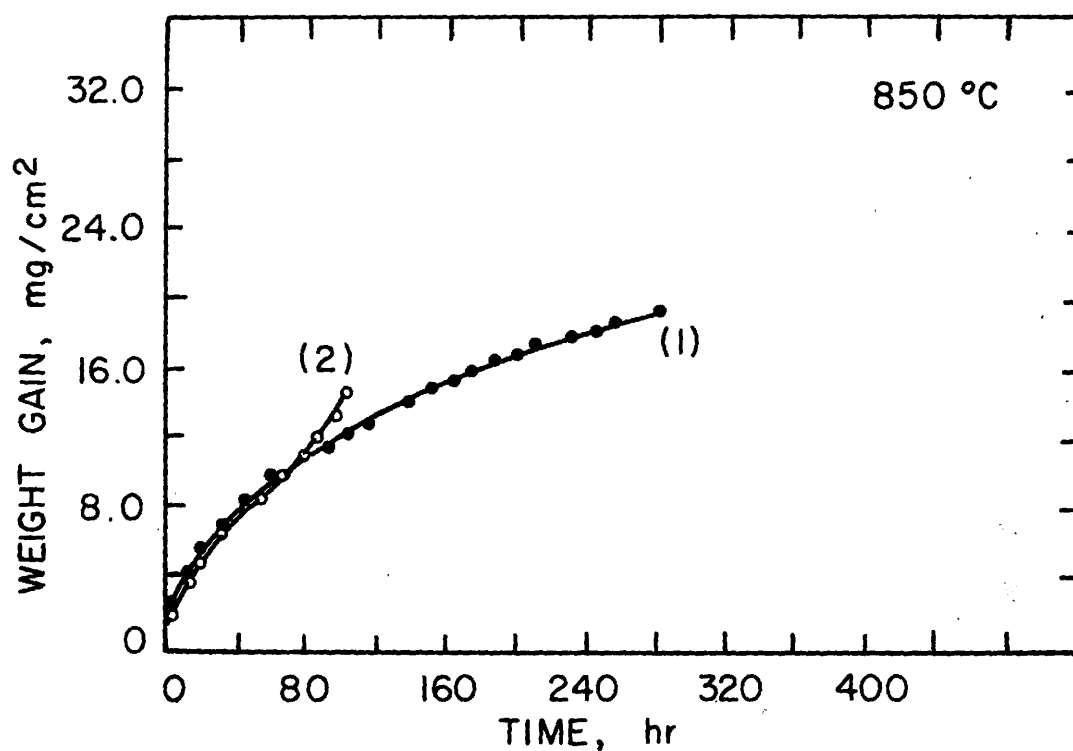
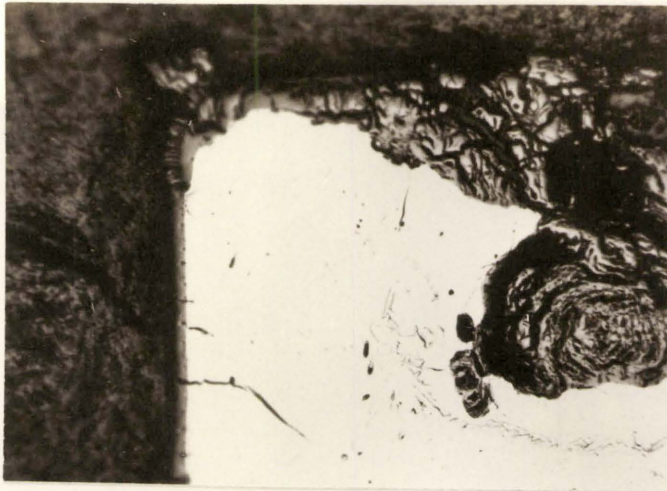


Fig. 45. Oxidation of Zirconium in Oxygen-Water Vapor Atmospheres

Curve (1): specimen thickness 2.14 mm, pure oxygen

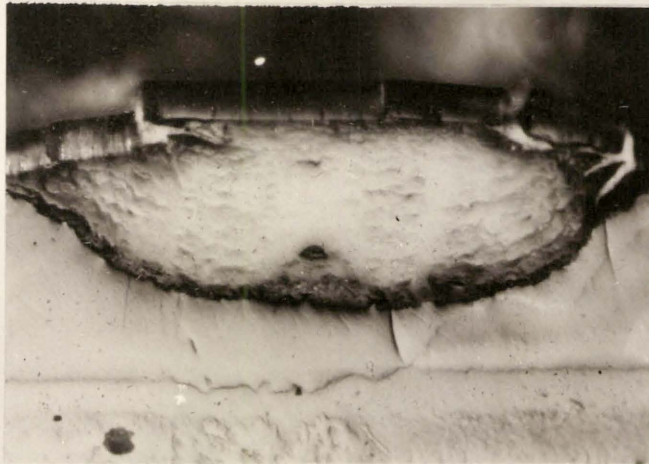
Curve (2): specimen thickness 2.00 mm and oxygen contaminated after exposure of 50 h with water vapor at pressure of 6.5 mm Hg



d.



b.



c.

Fig. 46 Metallography of Zirconium Specimens Oxidized in Oxygen-Water Vapor Atmospheres.

- a. Oxidized at 950°C , showing the massive oxide scale formed. Curve 2 of Fig. 44 (x40).
- b. Oxidized at 850°C , shows fingers of oxide penetrating the metal. Curve 2 of Fig. 45 (x150).
- c. Oxidized at 850°C , shows a defect produced in the oxygen rich surface layer. (x150, polarized light).

metal during oxidation in oxygen-water vapour mixtures. The observed zirconium hydride needles were similar in appearance to those reported by EVANS⁽⁶⁰⁾ for a Zircaloy-2 corroded in water at 300°C.

CHAPTER VIII

Discussion

8.1 Kinetics of Zirconium-Oxygen and Zirconium-Nitrogen Reactions:

8.1.1 Two-Phase Oxidation (850°C):

The volumetric determinations of the oxidation kinetics at 850°C obeyed a parabolic relationship for exposures extending to several hundred hours as shown in Figs. 5 and 6. It is possible to demonstrate that this behaviour is consistent with the diffusion model for two solid phases.

The measurements of oxide thickness were also consistent with the parabolic growth rate for exposures as long as 200 hrs. This agreement is shown in Fig. 15 where the present results in conjunction with those of other investigators have been plotted in form of a parabolic relationship. From here, it follows that the parabolic rate constant for oxide growth is:

$$2 \gamma_c \sqrt{D_{II}} = 0.645 \times 10^{-5} \quad \text{cm/sec.}^{1/2} \quad (64).$$

The densities of zirconium and zirconium dioxide are 6.5 and 5.83 g/cm³ respectively; and the concentrations of oxygen in zirconium dioxide and in the metal saturated with oxygen are 25.3 and 6.75 wt. % respectively. Consequently, the concentrations of oxygen at the oxide-metal interface are:

$C_{II}^I = 1.47$ and $C_I^{II} = 0.439$ gO./cm³. Substituting these values, together with the value of equation (64) into equation (30) one obtains:

$$(k_p)_{\text{oxide}} = 0.666 \times 10^{-5} \quad \text{gO./cm}^2 \text{sec}^{1/2} \quad (65).$$

The parabolic constant for oxygen solution in the metal can also be evaluated. Taking the average value for diffusivity of oxygen in alpha-zirconium from four investigators^(33,34,35,36) as $D_I = (7.9 \pm 3.5) \times 10^{-10} \text{ cm}^2/\text{sec}$, B_I can be calculated from equation (27) and is:

$$B_I = 0.439 - 9.1 \times 10^{-4}/1 - \text{erf } 0.114 = 0.503 \quad (66)$$

where: $9.1 \times 10^{-4} \text{ gO/cm}^3$ is the initial oxygen concentration, C_0 , of the as-received metal. Consequently, we can evaluate from equation (31):

$$(k_p)_{\text{metal}} = (1.47 \pm 0.2) \times 10^{-5} \text{ gO/cm}^2 \text{ sec}^{1/2} \quad (67)$$

The values of equations (65) and (67) may be substituted into equation (32) to give the total uptake of oxygen:

$$\left(\frac{\Delta m}{A}\right)_{\text{total}} = (2.14 \pm 0.3) \times 10^{-5} \cdot t^{1/2} \text{ gO/cm}^2 \quad (68)$$

As illustrated in Table 2 this value is in good agreement with the experimental evaluation of the parabolic rate constant at 850°C :

$$k_p = (2.02 \pm 0.1) \times 10^{-5} \text{ gO/cm}^2 \text{ sec}^{1/2}$$

Another way of calculating the total oxygen uptake is by means of the integral model. Here, the value of $(k_p)_{\text{oxide}}$ remains the same as before by virtue of equation (36). For $(k_p)_{\text{metal}}$ we have from equation (37):

$$(k_p)_{\text{metal}} = (1.57 \pm 0.1) \times 10^{-5} \text{ gO/cm}^2 \text{ sec}^{1/2} \quad (69)$$

and combining it with equation (65):

$$\left(\frac{\Delta m}{A}\right)_{\text{total}} = (2.24 \pm 0.2) \times 10^{-5} \cdot t^{1/2} \text{ gO/cm}^2 \quad (70).$$

Again, this is in fair agreement with the experimental data.

We may therefore conclude that the oxidation kinetics of zirconium at 850°C for exposures of several hundred hours may be correlated with the diffusion model for growth of the oxide scale and concurrent solution of oxygen in the metal. Oxygen dissolution in zirconium accounts for a large portion of oxygen consumed during the oxidation process. From the ratio of equations (67) or (69) to equations (68) or (70) respectively, the fraction of 68.6 - 70.0% was calculated for oxygen dissolved in the metal.

8.1.2 Three-Phase Oxidation (950°C):

The uptake of oxygen per unit area vs. time obeyed a parabolic relationship for exposures up to 100 hr at 950°C as shown in Figs. 12 and 13 .

There are sufficient data for the diffusivities of oxygen in the alpha and beta phases of zirconium and for oxygen saturation limits at the interfaces to allow us to evaluate by means of equations (50) and (57) the overall parabolic oxidation constant from the known growth rates of the oxide and alpha phases. The diffusivity of oxygen in alpha-zirconium at the temperature concerned has been reported by PEMSLER⁽³⁶⁾, DAVIS et al⁽⁷⁹⁾, and by KEARNS and CHIRICOS⁽³⁵⁾. The average value of these three investigations, $D_I = (4.5 \pm 1.8) \times 10^{-9} \text{ cm}^2/\text{sec}$, will be employed in this calculation. For the value of oxygen diffusivity in beta-zirconium we shall use $D_o = (4.2 \pm 2.6) \times 10^{-7} \text{ cm}^2/\text{sec}$, the only reported

value for diffusivity of oxygen in the beta phase of Zircaloy-2, by MALLETT et al. (37).

The density of beta-zirconium can be calculated from the lattice parameter of the b.c.c. structure by means of equation:

$$d = 2M/N_A a^3 = 6.35 \text{ g/cm}^3 \quad (71)$$

where:

d - density of beta-zirconium

M - molecular weight

N_A - Avogadro number

$a = 3.62 \text{ \AA}$ - lattice parameter of beta-zirconium (46)

Taking the concentrations of oxygen at appropriate interfaces from the oxygen-zirconium equilibrium phase diagram by GEBHARDT et al. (80) as 1.3 and 0.18 wt.% we can evaluate $C_I^I = 0.0554$ and $C_o^{II} = 0.0114 \text{ gO/cm}^3$.

As a first consideration the total oxygen uptake will be evaluated from expressions arising from the differential model, viz. section 3.3.

For oxide growth, equation (52):

$$(k_p)_{\text{oxide}} = (0.582 \pm 0.06) \times 10^{-5} \text{ gO/cm}^2 \text{ sec}^{1/2} \quad (72),$$

where:

$2\gamma_\epsilon \sqrt{D_{II}} = 0.57 \times 10^{-5} \text{ cm/sec}^{1/2}$ from plot in Fig. 18 and C_{II}^I and C_I^{II} equal 1.45 and 0.439 gO/cm^3 respectively, from HANSEN (57).

By means of equation (38), for the condition $x = \xi$, the constant

B_I is:

$$B_I = 0.438/1 - \text{erf} (0.285/6.71) = 0.460 \quad (73).$$

In order to evaluate the parabolic rate constant, $(k_p)_{\alpha}$, we require the value of $\gamma_{\Psi} \sqrt{D_I}$. This can be obtained from the slope-intercept equation from Fig. 18:

$$2\gamma_{\Psi} \sqrt{D_I} = 17.46 \times 10^{-5} \text{ cm/sec}^{1/2} \quad (74).$$

Consequently, the parabolic rate of oxygen dissolution in the alpha-zirconium phase in terms of equation (53) is:

$$(k_p)_{\alpha} = (3.61 \pm 1.32) \times 10^{-5} \text{ gO/cm}^2 \text{ sec}^{1/2} \quad (75)$$

where the value of $(\gamma_{\Psi})^2 = 1.696$ as obtained from equation (74) has been employed.

Finally, we calculate the value of B_o , from equation (39) for

$x = \Psi$,

$$B_o = 0.0105 / 1 - \text{erf}(8.73/64.8) = 0.0124 \quad (76).$$

For the rate of oxygen dissolution in beta-zirconium from equation (54) one obtains:

$$(k_p)_{\beta} = (0.89 \pm 0.59) \times 10^{-5} \text{ gO/cm}^2 \text{ sec}^{1/2} \quad (77).$$

Therefore, the total oxygen uptake during oxidation of zirconium at 950°C from equation (51) is:

$$\left(\frac{\Delta m}{A}\right)_{\text{total}} = (5.08 \pm 2.0) \times 10^{-5} \cdot t^{1/2} \text{ gO/cm}^2 \quad (78).$$

This value is to be compared with the experimental value of:

$$\left(\frac{\Delta m}{A}\right)_{\text{expt}} = (4.7 \pm 0.2) \times 10^{-5} \cdot t^{1/2} \text{ gO/cm}^2 \quad (79)$$

taken as an average of seven determinations; see Table 2 in the appendix. Within the accuracies of the determinations, the evaluations are in agreement and offer support for the interpretation of the oxidation kinetics by the assumed diffusion model. It should be remembered that the employed value for diffusivity of oxygen in beta-zirconium, D_o , was that given for beta-Zircaloy-2.

As a second consideration, the total uptake of oxygen will be evaluated in terms of equations arising from the integral model, section 3.4. By virtue of equation (58) the value for $(k_p)_{\text{oxide}}$ remains the same as that given above. Similarly, the constants B_I and B_o remain unchanged. For $(k_p)_{\text{alpha}}$ we have from equation (59):

$$\left(\frac{\Delta m}{A \sqrt{t}}\right)_{\text{alpha}} = (k_p)_{\text{alpha}} = (3.16 \pm 0.65) \times 10^{-5} \text{ gO/cm}^2 \text{ sec}^{1/2} \quad (80)$$

and from equation (60):

$$\left(\frac{\Delta m}{A \sqrt{t}}\right)_{\text{beta}} = (k_p)_{\text{beta}} = (0.87 \pm 0.66) \times 10^{-5} \text{ gO/cm}^2 \text{ sec}^{1/2} \quad (81)$$

Combining equations (72), (80) and (81) one obtains for the total amount of oxygen:

$$\left(\frac{\Delta m}{A}\right)_{\text{total}} = (4.62 \pm 0.2) \times 10^{-5} t^{1/2} \text{ gO/cm}^2 \quad (82)$$

which is in good agreement with the experimental data.

It is interesting to note that:

$$\left[\left(\frac{\Delta m}{A}\right)_{\text{alpha}} + \left(\frac{\Delta m}{A}\right)_{\text{beta}} \right] / \left(\frac{\Delta m}{A}\right)_{\text{total}} = (3.16 + 0.87) / 4.62 = 0.87 \quad (83)$$

Consequently, oxygen solution in the metal accounted for the larger portion of consumed oxygen, 68% of it being confined to stabilization and growth of the alpha solid solution layer. Since the oxygen distribution among the oxide, alpha and beta phases is in the ratio 12.6: 68.5: 18.9, equation (79) may be employed to calculate the weight, W , of zirconium dioxide formed per unit area:

$$\left(\frac{W}{A}\right)_{\text{ZrO}_2} = (2.28 \pm 0.1) \times 10^{-5} t^{1/2} \text{ gZrO}_2/\text{cm}^2 \quad (84)$$

with the assumption that stoichiometric oxide is formed only.

Although diffusion accounts for the oxidation kinetics, several anomalies were evident which indicate that the diffusion model only provides a partial understanding of the reaction mechanism. The ratio of the thicknesses of the diffusion layers according to this model should remain constant independent of time. As illustrated by the plot in Fig. 19, this restriction is valid for long exposures, but during the initial period of oxidation the oxide scale is thicker than predicted. The factors accounting for this behaviour are not obvious as, also, those leading to the formation of small voids at the metal-oxide interface, as shown in Fig. 16.

As a closing remark to this section it should be indicated that the gravimetric measurements from Fig. 14 give:

$$\left(\frac{\Delta m}{A}\right)_w = (4.43 \pm 0.27) \times 10^{-5} t^{1/2} \text{ gO/cm}^2 \quad (85).$$

Within the experimental precision, this value shows good agreement with the value from volumetric measurements, viz. equation (79).

A direct comparison of the calculated values to the experimental determinations is recorded in the following table:

TABLE I
Comparison of Calculated and Experimental Values of k_p 's
for Zirconium-Oxygen Reaction.

| Temp. °C | Method of Determination | $(k_p)_{\text{total}}$ gO/cm ² sec ^{1/2} | $\frac{(k_p)_{\text{expt.}}}{(k_p)_{\text{calculated}}}$ |
|-------------|--------------------------------|---|--|
| 950 | Experimental, - volumetric. | $(4.7 \pm 0.2) \times 10^{-5}$ | - |
| | Eqn. (59) | $(4.62 \pm 0.2) \times 10^{-5}$ | 1.02 |
| | Eqn. (50) | $(5.08 \pm 2.0) \times 10^{-5}$ | 0.93 |
| 850 | Experimental, - volumetric | $(2.02 \pm 0.1) \times 10^{-5}$ | - |
| | Eqn. (35) | $(2.24 \pm 0.2) \times 10^{-5}$ | 0.90 |
| | Eqn. (29) | $(2.14 \pm 0.3) \times 10^{-5}$ | 0.94 |

In a recent investigation, PEMSLER⁽⁸¹⁾ oxidized zirconium spheres of 1.74 cm diameter to suppress the effect of edges on oxidation kinetics. By using calculations similar to those presented here he was able to show that oxygen solution in the metal at 840°, 910° and 975°C complies with the diffusion controlled dissolution. Also, the rates of growths of oxide thicknesses at 840° and 910°C conformed to the parabolic relationship after initial periods of more rapid growths. A remarkable deviation from this relationship was obtained at 975°C. This discrepancy was explained in terms of the crystallographic change of zirconium dioxide from a monoclinic to tetragonal structure as already alluded to in section 5.1.

8.1.3 Zirconium-Nitrogen Reaction (750° - 1000°C):

The calculations for the zirconium-nitrogen reaction follow the same pattern as already discussed for the zirconium-oxygen system and therefore there is no need to duplicate them. The final results obtained and the intermediate values involved are given here in a tabulated form for the convenience of checking. We commence with the necessary values of nitrogen concentrations at the appropriate interfaces and in the metal. The C's values correspond to the designations given by the diffusion model in Fig. 1 .

TABLE II

Nitrogen Concentrations Relevant to the Diffusion Models.

| Temp., °C | Nitrogen Concentration | Nitrogen Concentration gN/cm ³ | Reference |
|-----------|---|--|-------------------------------------|
| 1000 | $C_{II}^I = 48 \text{ at } \% = 12.42 \text{ wt. } \%$ | $C_{II}^I = 0.880$ | HANSEN ⁽⁵⁷⁾ |
| | $C_I^{II} = 23 \text{ at } \% = 4.38 \text{ wt. } \%$ | $C_I^{II} = 0.285$ | " |
| | $C_I^I = 1.0 \text{ wt. } \%$ | $C_I^I = 0.065$ | DOMAGALA et al ⁽⁸²⁾ |
| | $C_o^{II} = 0.0714 \text{ wt. } \%$ | $C_o^{II} = 0.00453$ | " |
| | $C_o = 0.0001 \text{ wt. } \%$ | $C_o = 0.635 \times 10^{-5}$ | Analysis - see Table 1, appendix |
| 950 | $C_{II}^I = 48.25 \text{ at } \% = 12.57 \text{ wt. } \%$ | $C_{II}^I = 0.89$ | HANSEN ⁽⁵⁷⁾ |
| | $C_I^{II} = 22.75 \text{ at } \% = 4.32 \text{ wt. } \%$ | $C_I^{II} = 0.281$ | " |
| | $C_I^I = 0.8 \text{ wt. } \%$ | $C_I^I = 0.052$ | DOMAGALA et al ⁽⁸²⁾ |

TABLE II (Cont'd)

| Temp. °C | Nitrogen Concentration | Nitrogen concentration gN/cm ³ | Reference |
|----------|--|--|---------------------|
| | $C_{\circ}^{II} = 0.05 \text{ wt. } \%$ | $C_{\circ}^{II} = 0.00318$ | DOMAGALA et al (82) |
| | $C_{\circ} = \text{as above}$ | $C_{\circ} = \text{as above}$ | Analysis |
| 900 | $C_{II}^I = 48.75 \text{ at } \% = 12.76 \text{ wt } \%$ | $C_{II}^I = 0.905$ | HANSEN (57) |
| | $C_I^{II} = 22.5 \text{ at } \% = 4.26 \text{ wt } \%$ | $C_I^{II} = 0.277$ | " |
| | $C_I^I = 0.40 \text{ wt } \%$ | $C_I^I = 0.026$ | DOMAGALA et al (82) |
| | $C_{\circ}^{II} = 0.02 \text{ wt } \%$ | $C_{\circ}^{II} = 0.00127$ | " |
| | $C_{\circ} = \text{as above}$ | $C_{\circ} = \text{as above}$ | Analysis |
| 850 | $C_{II}^I = 49.0 \text{ at } \% = 12.85 \text{ wt } \%$ | $C_{II}^I = 0.91$ | HANSEN (57) |
| | $C_I^{II} = 22.25 \text{ at } \% = 4.21 \text{ wt } \%$ | $C_I^{II} = 0.274$ | " |
| | $C_{\circ} = 0.0001 \text{ wt } \%$ | $C_{\circ} = 0.65 \times 10^{-5}$ | Analysis |
| 800 | $C_{II}^I = 49.25 \text{ at } \% = 13.0 \text{ wt } \%$ | $C_{II}^I = 0.92$ | HANSEN (57) |
| | $C_I^{II} = 22.0 \text{ at } \% = 4.15 \text{ wt } \%$ | $C_I^{II} = 0.27$ | " |
| | $C_{\circ} = \text{as above}$ | $C_{\circ} = \text{as above}$ | Analysis |
| 750 | $C_{II}^I = 49.5 \text{ at } \% = 13.5 \text{ wt } \%$ | $C_{II}^I = 0.956$ | HANSEN (57) |
| | $C_I^{II} = 21.75 \text{ at } \% = 4.08 \text{ wt } \%$ | $C_I^{II} = 0.268$ | " |
| | $C_{\circ} = \text{as above}$ | $C_{\circ} = \text{as above}$ | Analysis |

NOTE: All values calculated with the aid of computer-expanded erf x (for x = 0.001 interval) and exp (-x) for x < 1 (at x = 0.001 interval)

TABLE III

Intermediate Values Obtained from the Diffusion Model for Zirconium-Nitrogen Reaction

| Temp. °C and Ref. | D_o cm ² /sec | $\gamma_{\psi} D_I$ cm/sec ^{1/2} | B_o | $(\gamma_{\psi})^2$ | γD_{II} | D_I cm/sec ^{1/2} | B_I |
|-------------------------|-------------------------------|--|-----------------------|---------------------|------------------------|--------------------------------|-----------|
| 1000 | 0.832×10^{-7} | 0.835×10^{-5} | 4.67×10^{-3} | 0.917 | 0.425×10^{-6} | 7.6×10^{-11} | 0.301 |
| Ref. | (45) or 2.6 | Fig. 25 | eqn. (39) | - | Fig. 24 | Fig. 39 or 6.4 | eqn. (38) |
| 950 | 0.5×10^{-7} | 0.588×10^{-5} | 3.26×10^{-3} | 1.05 | 0.33×10^{-6} | 3.28×10^{-11} | 0.301 |
| Ref. | (45) or 2.6 | Fig. 25 | eqn (39) | - | Fig. 24 | Fig. 39 or 6.4 | eqn. (38) |
| 900 | 0.284×10^{-7} | 0.5×10^{-5} | 1.31×10^{-3} | 1.97 | 0.233×10^{-6} | 1.27×10^{-11} | 0.299 |
| Ref. | (45) or 2.6 | Fig. 25 | eqn (39) | - | Fig. (24 | Fig. 39 or 6.4 | eqn. (38) |
| 850 | -- | -- | -- | -- | 0.175×10^{-6} | 4.6×10^{-12} | 0.302 |
| Ref. | -- | -- | -- | -- | Fig. 24 | Fig. 39 or 6.4 | eqn. (27) |
| 800 | -- | -- | -- | -- | 0.10×10^{-6} | 1.39×10^{-12} | 0.298 |
| Ref. | -- | -- | -- | -- | Fig. 24 | Fig. 39 or 6.4 | eqn. (27) |
| 750 | -- | -- | -- | -- | 0.08×10^{-6} | 0.42×10^{-12} | 0.272 |
| Ref. | -- | -- | -- | -- | Fig. 24 | Fig. 39 or 6.4 | eqn. (27) |

In the above summary the following values have been used for conversion of N_2 wt % into gN/cm^3 :

7.09 g/cm^3 - density of ZrN, Handbook of Chemistry and Physics⁽⁸³⁾.

6.5 g/cm^3 - density of alpha-zirconium⁽⁸⁴⁾

6.35 g/cm^3 - density of beta-zirconium, from X-ray data.

The reported intermediate values (Table III) at different temperatures have been obtained from the differential model and from the experimental evidence given in Chapter VI.

Having obtained all necessary data we can evaluate the parabolic constants for the nitride, alpha-zirconium and beta-zirconium and compare them with the experimentally determined value of the total parabolic rate constant. Such comparison is made below in Table IV and includes values calculated from both the differential and integral models discussed in Chapter III.

TABLE IV

Comparison of Calculated and Experimental Values of

k_p 's for Zirconium-Nitrogen Reaction.

| Temp. °C | Eqn. | $(k_p)_{ZrN}$ $gN/cm^2 sec^{1/2}$ | $(k_p)_{Zr-alpha}$ $gN/cm^2 sec^{1/2}$ | $(k_p)_{Zr-beta}$ $gN/cm^2 sec^{1/2}$ | $(k_p)_{total}$ calculated | $(k_p)_{total}$ experim- ental |
|-------------|------|--------------------------------------|---|--|-------------------------------|--------------------------------------|
| 1000 | 51 | 0.506×10^{-6} | 2.78×10^{-6} | 1.51×10^{-6} | 4.796×10^{-6} | 4.24×10^{-6} |
| | 55 | idem | 2.586×10^{-6} | 1.515×10^{-6} | 4.607×10^{-6} | from Fig. 22 |

TABLE IV (cont'd)

| Temp. °C. | Eqn. | $(k_p)_{\text{ZrN}}$ gN/cm ² sec ^{1/2} | $(k_p)_{\text{Zr-alpha}}$ gN/cm ² sec ^{1/2} | $(k_p)_{\text{Zr-beta}}$ gN/cm ² sec ^{1/2} | (k_p) total calculated | (k_p) total experimental |
|--------------|------|---|--|---|-----------------------------|---|
| 950 | 51 | 0.412×10^{-6} | 1.836×10^{-6} | 0.825×10^{-6} | 3.073×10^{-6} | 2.73×10^{-6} from Fig. 22 |
| | 55 | idem | 1.643×10^{-6} | 0.823×10^{-6} | 2.878×10^{-6} | |
| 900 | 51 | 0.293×10^{-6} | 1.28×10^{-6} | 0.249×10^{-6} | 1.822×10^{-6} | 1.65×10^{-6} from Fig. 22 |
| | 55 | idem | 1.151×10^{-6} | 0.249×10^{-6} | 1.696×10^{-6} | |
| 850 | 29 | 0.222×10^{-6} | 0.730×10^{-6} | -- | 0.952×10^{-6} | 0.846×10^{-6} from Fig. 22 |
| | 33 | idem | 0.728×10^{-6} | -- | 0.95×10^{-6} | |
| 700 | 29 | 0.13×10^{-6} | 0.393×10^{-6} | -- | 0.523×10^{-6} | 0.427×10^{-6} from Fig. 22 |
| | 33 | idem | 0.394×10^{-6} | -- | 0.524×10^{-6} | |
| 750 | 29 | 0.11×10^{-6} | 0.197×10^{-6} | -- | 0.307×10^{-6} | 0.29×10^{-6} from Fig. 22 |
| | 33 | idem | 0.202×10^{-6} | -- | 0.313×10^{-6} | |

Considering the errors arising from boundary concentrations (phase diagram) and those inherent to the values of D's, we conclude that the agreement between the calculations based on diffusion parameters and the data obtained from kinetics experiments is good.

Within the experimental exposure periods employed in this investigation the ratio of the thickness of alpha-phase to the thickness of zirconium nitride remains constant as required by equation (61). This has been indicated in Fig. 25. As a result of experimental precision the straight lines at 950° and 1000°C overlap and for this reason they have been drawn dashed.

8.2 Metallography and X-ray Analyses:

The present metallographic examinations imply that the transformation of compact gray oxide into white oxide for zirconium samples reacted in atmospheres containing oxygen may take place within the oxide phase, viz. Fig. 20c,e,f , and that formation of a duplex scale, Fig. 20d , consisting of gray and white oxides with a well defined boundary between them may be regarded as a specific case. X-ray powder patterns of gray and white zirconium dioxide showed no essential differences, both oxides were monoclinic with approximately the same lattice spacings. Furthermore, the initial white oxide formed does not necessarily have to be porous and to give rise to a marked deviation from parabolic oxidation kinetics, viz. Figs. 10 and 11 .

The presence of perpendicular cracks in the oxide is evident from both Figs. 16 and 20d . The genesis of them can be attributed to the oxidation process at the elevated temperature and it is unlikely that they formed during cooling to room temperature. This is evidenced by the formation of white oxide within the cracks as shown in Fig. 20d . However, we cannot conclude unequivocally from the present evidence whether these cracks originate in the oxide, at the metal-oxide or oxide-oxygen interfaces.

No exact explanation may be made of the voids present in the gray oxide formed on zirconium in oxygen atmospheres as shown in Fig. 16 . The voids appear to originate at the metal-oxide interface and become embedded in the scale as oxidation continues. In general all voids were located at approx. the same depth beneath the oxide surface and the number of voids produced in any specimen was insufficient to affect the parabolic kinetic data.

We cannot advance a specific mechanism accounting for the formation of voids. It is the author's opinion that these pores are associated with the Kirkendall effect⁽⁸⁵⁾ and are presumably formed by the condensation of excess oxygen vacancies. Oxygen vacancies are formed at the metal-oxide interface by the formation of oxide from the metal and, also, by removal of oxygen from the oxide and its solubility in the metal. Although the degree of supersaturation of vacancies is low and the probability that few of them will condense to form a void is small, they will nevertheless tend to collect into macroscopic pores because by doing so total elastic energy of the stress system is being decreased. This elastic stress of the system around the advancing boundary may be brought about by the occurrence of volume changes associated with the diffusion process.

Similar formations of pores have been found in 50/50 Au-Ag diffusion couples by SEITH⁽⁸⁶⁾ and by MALLETT and ALBRECHT⁽⁸⁷⁾ in Zr-2.5 wt % Sn and Zr - 1.5 wt % Sn alloys. Most recently, PEMSLER⁽⁸¹⁾ confirmed the formation of voids during oxidation of zirconium in the temperature range 975°C to 1100°C; however, the oxide formed on samples exposed at 910° and 840°C was quite similar and did not exhibit the formations of voids.

Microscopic examinations of the zirconium nitride-zirconium interfaces did not disclose voids similar to those for zirconium-oxygen system, even at magnifications of 1000X with the immersion objective. The interface appeared to be smooth and flat as illustrated in Fig. 26b .

Scaling in oxygen-nitrogen atmospheres produced microstructures similar to those observed in air. As shown in Fig. 43 the scale thickness becomes

non-uniform indicating a strong localized attack. An interesting feature observed in these samples was the presence of thin filigrees at the metal-metal scale interface. This phase was observed only in places where the localized attack was pronounced; where the scale was compact and uniform this phase could not be distinguished viz. Fig. 43c .

In the present investigation it was not possible by X-ray analyses to identify the phase composing these filigrees. It was shown also that zirconium dioxide does not react with nitrogen at 850°C to form a oxy - nitride compound. Although it may not be definitely concluded, the author is of the opinion from the metallographic evidence that this phase is zirconium nitride.

The possibility that this phase was stable at the reaction temperature or had decomposed from solid solution during cooling to room temperature was investigated by examining the structure of the specimen quenched in liquid nitrogen from the reaction temperature. The filigrees were still present, viz. Fig. 43d , suggesting that they formed and were stable at the scaling temperature. Since the mutual diffusivities of nitrogen in zirconium dioxide and of oxygen in zirconium nitride are not known it is impossible to establish definitely whether this phase is the cause or the effect of localized scaling. The author is inclined to believe in the first alternative.

The cross-sections of zirconium samples scaled in oxygen-water vapor atmospheres exhibited localized structural defects as shown in Fig. 46 . Fingers of oxide penetrating into the metal substrate were commonly observed.

Because of their large size it is difficult to associate their formation with the grain boundaries of the metal. Wherever these defects formed the outer scale was severely damaged indicating that low resistance paths for the diffusion of reactions species was necessary for penetration into the metal. These low resistance paths could possibly be associated with cracks in both the scale and metal.

8.3 The "Breakaway" Phenomenon:

The definition of this expression has been given in Chapter 7.1. From the review of literature^(18,88,89,90,91) and from the obtained oxidation and scaling kinetic data shown in Figs. 6; 7; 9; 41a,b; 44; 45 it is evident that a transition from a relatively slow parabolic reaction rate to a somewhat faster relationship exists and that oxidation time is not the only factor which governs this phenomenon.

Some investigators e.g. KOFSTAD and OESTHAGEN⁽⁸⁹⁾ and COX⁽⁹¹⁾ express the post-transition oxidation rate by a linear relationship and attribute the increased oxidation rate to the formation of white oxide scale. This explanation is only partially consistent with the present experimental observations. A comparison of data from Fig. 9 (which corresponds to the surface appearance of samples displayed in the upper row of Fig. 8) with the oxidation kinetics given by Fig. 7,10,11 (for samples shown in the middle row of Fig. 8) leads to the conclusion that the post-transition period cannot be expressed by a simple linear relationship unless oxidation is very rapid. Moreover, for such a case there is no satisfactory evidence for a single breakaway point.

Nevertheless, it follows from the present investigation that the formation of white oxide may give rise to increased oxidation rates. Confirmation of this can be found by comparing the oxidation data of Figs. 10, 11 with the metallography of the oxides in Fig. 20c, d, e . Having concluded that the deviation from parabolic oxidation may be detected by the presence of white oxide, the differences are examined between the gray and white oxides.

The viewpoint is adopted that the gray oxide represents hypo-stoichiometric, thermodynamically unstable form which with time transforms towards the stoichiometric, thermodynamically stable composition of ZrO_2 . The color of oxide changes simultaneously. The transformation takes place irrespective of the physical state and shape of the metal. Certain factors, however, may accelerate the transformation rate of gray oxide into white oxide.

8.3.1 Effect of Stress:

Since the volume of oxide is larger than the volume of consumed metal the oxide could be under large lateral stress. Some form of mechanical breakdown of the oxide layer can be expected and the purely diffusion controlled oxidation kinetics become violated. The mechanical breakdown assumes a form of shear-cracking where cohesion is weak, giving rise to low resistance paths. Such a breakdown of the oxide scale is demonstrated by Figs. 16, 43, 46 . Where the adhesion is weak and cohesion strong one can expect separation of the oxide from a metal substrate. Confirming evidence of such a case was shown by the occurrence of voids at the metal-oxide interface, viz. Fig. 16. Obviously, both mechanisms for crack formation can cooperate concurrently.

It is also possible that cracking of both oxide and metal occurs. Oxygen enrichment in the metal beneath the oxide scale may enhance the cracking of the metal due to its embrittlement. This viewpoint has been advanced by LEHR and DEBUIGNE⁽⁹²⁾ and by O'DRISCOLL et al⁽⁹³⁾. This type of cracking could account for areas of localized rapid oxidation and breakaway. Possible example of this behaviour is shown in Fig. 46a .

8.3.2 Sample Thickness:

Inspection of the oxidation curves of Fig. 6 and Fig. 7 shows that there is a relationship between the time interval to the breakaway point and the thicknesses of the specimens. Breakaway occurred at shorter times with thinner specimens. The data were reproducible only in the parabolic range; in the post-transition period the deviations were irregular indicating localized oxidation. Here again an unequivocal explanation cannot be presented for this behaviour.

The shorter time to the breakaway point for thinner samples could be associated with the factor that the sample ceases to be a semi-infinite plate for oxygen diffusion from a planar source. When the oxygen gradients from opposite faces meet, the concentration of oxygen in the middle of the sample increases. The oxygen gradient becomes less steep as oxidation continues and less oxygen is taken up by the metal. Because the oxide scale is in a non-stoichiometric condition at its outer interface, more oxygen may become available for the transformation of gray to white oxide. The fact that PEMSLER'S⁽⁸¹⁾

data for oxidation of zirconium spheres of 1.74 cm in diameter at 840°C for 600 hrs do not indicate the transition point is compatible with the given interpretation.

8.3.3 Influence of Atmospheres:

As illustrated by Figs. 41a, b the weight change as a function of time obeys to a first approximation the parabolic relationship in the pretransition region for samples reacted in oxygen atmospheres containing nitrogen and water vapor. The onset of breakaway oxidation was associated with the transformation of gray to white oxide.

The scaling rate of zirconium reacted at 850°C in oxygen-nitrogen atmospheres (starting with 10% nitrogen) was higher than in pure oxygen or nitrogen. Increasing the ratio of nitrogen to oxygen the scaling rate increased up to the nitrogen mole fraction of 0.7 and decreased thereafter. The initial increase in scaling rate can be explained in terms of the defect equation for zirconium dioxide i.e. at the oxygen-oxide interface:



where: $\square O^{2-}$ represents an oxygen ion vacancy in the oxide lattice, O_{ℓ}^{2-} is an oxygen ion in the oxide lattice and e^- is an electron.

The replacement of oxygen atoms in the oxide lattice by nitrogen atoms is at a ratio 2/3, that is $2N^{3-}$ will replace $3O_{\ell}^{2-}$. Therefore in a n-type oxide the presence of nitrogen would increase the number of vacant oxygen sites and consequently the oxidation rate would increase also. A tentative mathematical proof is given as Problem 2 in the appendix.

The decreasing scaling rates for nitrogen mole fractions in excess of 0.7 as well as the variation in time to the breakaway point as a function of nitrogen content in the atmosphere could not be easily explained.

The reaction of zirconium in oxygen-water vapour atmospheres complies with the parabolic scaling kinetics for exposures up to 5 hr at 950°C and to 80 hr at 850°C. The parabolic oxidation is followed by a breakaway point and much faster scaling. This has been illustrated by curves 2 in Figs. 44 and 45. Oxidation curves for zirconium reacted in pure oxygen have been incorporated for comparison. The initial period of scaling, curves 2, is about the same as for reaction in oxygen, curves 1. WESTERMAN⁽⁹⁴⁾ found for zirconium reacted in water vapor at 800°C and for 20 hr that the scaling rates were about the same as in oxygen.

Apparently solubility of hydrogen in the non-stoichiometric gray oxide in the early stages of oxidation does not markedly influence the defect structure of this oxide and the diffusion rate of oxygen through the initially formed scale.

DOUGLASS⁽⁹⁵⁾ investigated the effect of alloying elements on the post-transition oxidation rates of zirconium tested in steam at 400°C. It was found that both tin and niobium increase the post-transition corrosion rates, and that no suitable mechanism accounting for the breakaway could be advanced. Similarly, the present investigation indicates that for zirconium oxidized in oxygen atmospheres containing nitrogen or water vapor we cannot offer a unique and simple explanation for the breakaway phenomenon.

CHAPTER IX

Conclusions.

- i. The oxidation of zirconium at 850° and 950°C and the reaction of zirconium with nitrogen in the range of 750° to 1000°C obey a parabolic relationship.
- ii. The nitriding and oxidation kinetics are consistent with the theoretical evaluations based on the diffusion models.
- iii. The diffusivity of nitrogen in alpha-zirconium in the temperature range of 750° to 1000°C is:

$$D = 0.15 \exp (-54100 / RT).$$

This value was obtained from traverse microhardness measurements of nitrated zirconium samples.

- iv. The parabolic oxidation kinetics of zirconium are followed by deviations towards more rapid oxidation rates. These deviations could be attributed to the stoichiometry of the oxide, cracking of the scale and to the geometry of the specimens. The smaller the thickness of a plate specimen the shorter is the time to the breakaway point.
- v. Nitrogen-oxygen mixtures enhance the scaling rate of zirconium at 850°C and decrease the time interval to the breakaway points when compared with the influence of pure oxygen. The reaction of zirconium with oxygen-water

vapour atmospheres at 850° and 950°C conforms to parabolic scaling kinetics and is followed by a more rapid rate after the breakaway point. The influence of these atmospheres on the transformation from non-stoichiometric grey oxide to white oxide remains undetermined.

CHAPTER X

Recommendation for Future Work

Our calculations based on the diffusion model were approximated by neglecting the variation in concentrations of oxygen and nitrogen within the oxide and nitride phases, because the diffusivities of oxygen in non-stoichiometric zirconium oxide and of nitrogen in zirconium nitride are not known. It should be possible to evaluate these diffusivities and the values for γ_i 's from the kinetic data and the known diffusivities of these species in the respective alpha-zirconium phases.

Since the volume ratio of nitride formed to zirconium metal consumed is close to one, it would be easier to develop a mathematical treatment for the zirconium-nitrogen system first. For zirconium-oxygen system this ratio is about 1.52 and one would have to consider a moving boundary problem which takes into account the difference arising from the excess of zirconium oxide formed. The method derived by CARSLAW and JAEGER⁽⁹⁶⁾ could be helpful here. The concentration of oxygen in zirconium dioxide at the oxide/oxygen interface could be taken as that corresponding to the stoichiometric ZrO_2 . The value of $D_{O_2 \rightarrow ZrO_{2-x}}$ obtained in this way could be compared with the value of $D_{O_2 \rightarrow ZrO_2}$ determined from the experimental work under progress in this laboratory. The difference between these two separately determined values could be explained in terms of concentration dependence of the diffusion coefficient.

APPENDIX

PROBLEM 1

Consider first the simpler case; show the identity of equation (54) and (60) i.e.

$$2 B_0 \sqrt{D_0/\pi} \exp - \gamma_\psi^2 \cdot D_I/D_0 = 2 B_0 \sqrt{D_0} \operatorname{ierfc} \gamma_\psi \sqrt{D_I/D_0} + 2(C_0^{II} - C_0) \gamma_\psi \sqrt{D_I} \quad (1)$$

Since by definition:

$$\operatorname{ierfc} x = \frac{1}{\sqrt{\pi}} \exp(-x^2) - \operatorname{erfc} x$$

The R.H. side of equation (1) transforms to:

$$2 B_0 \sqrt{D_0/\pi} \exp - \gamma_\psi^2 \cdot D_I/D_0 - 2 B_0 \gamma_\psi \sqrt{D_I} \operatorname{erfc} \gamma_\psi \sqrt{D_I/D_0} + 2(C_0^{II} - C_0) \gamma_\psi \sqrt{D_I} \quad (2)$$

Reducing the appropriate terms leaves:

$$C_0^{II} = C_0 + B_0 (1 - \operatorname{erf} \psi/2 \sqrt{D_0 t}) \equiv C_0^{II} \quad (3)$$

which is a solution of Fick's second law for $x = \psi$. For reference see JOST⁽⁵⁸⁾. Equation (3) shows that the two terms for k_p 's for the beta phase are identical.

Similarly, we can show the identity of equation (53) and (59) i.e.

$$\begin{aligned} 2(C_I^I - C_0^{II}) \gamma_\psi \sqrt{D_I} + 2 B_I \sqrt{D_I/\pi} (\exp - \gamma_\epsilon^2 \cdot D_{II}/D_I - \exp - \gamma_\psi^2) = \\ = 2 B_I \sqrt{D_I} (\operatorname{ierfc} \gamma_\epsilon \sqrt{D_{II}/D_I} - \operatorname{ierfc} \gamma_\psi) + 2(C_I^{II} - C_0) \gamma_\epsilon \sqrt{D_{II}} - 2(C_0^{II} - C_0) \gamma_\psi \sqrt{D_I} \end{aligned} \quad (4)$$

which when applying the $\operatorname{ierfc} x$ definition given above, reduces to:

$$2 C_I^I \gamma_\Psi \sqrt{D_I} = 2B_I \gamma_\Psi \sqrt{D_I} \operatorname{erfc} \gamma_\Psi - 2B_I \gamma_\xi \sqrt{D_{II}} \operatorname{erfc} \gamma_\xi \sqrt{D_{II}/D_I} + 2(C_I^{II} - C_o) \gamma_\xi \sqrt{D_{II}} + 2 C_o \gamma_\Psi \sqrt{D_I} \quad (5).$$

From here it follows that:

$$C_I^I = C_o + B_I (1 - \operatorname{erf} \Psi / 2 \sqrt{D_I t}) \cong C_I^I \text{ for } x = \Psi \quad (6)$$

and

$$C_I^{II} = C_o + B_I (1 - \operatorname{erf} \xi / 2 \sqrt{D_I t}) \cong C_I^{II} \text{ for } x = \xi \quad (7).$$

Hence we have proved that, not only the expressions of k_p 's for the beta-phase derived from the three-phase analytical and integral model are identical, but also that this identity must hold for the parabolic rate constants obtained from the two-phase models, viz. equations (31) and (37) in the text.

TABLE 1Impurity Contents of Zirconium

| Elements | Analyses* (ppm) |
|------------|-----------------|
| Al, Cu, Ti | 25 |
| Mg, Mn, Sn | 10 |
| Co, Pb, V | 5 |
| C | 30 |
| H | 2.2 |
| Fe | 210 |
| Hf | 60 |
| O | 140 |
| N, Ni | 1.0 |
| Cd | 0.3 |
| Si | 85 |
| W | 25 |
| Zn | 50 |

* After: AECL, Chalk River, Ont.

TABLE 2

Experimental Test Conditions

| Run | Fig. | Temp. °C | Original Vacuum mm Hg. | Leak Rate mm Hg/min | (k _p) expt. gO/cm ² sec ^{1/2} | Remarks |
|-------|------|-------------|------------------------------|-------------------------|---|--|
| II | 5 | 850 | 4 x 10 ⁻⁶ | 0.25 x 10 ⁻⁵ | 2.03 x 10 ⁻⁵ | - |
| III | 6 | 850 | 3 x 10 ⁻⁵ | 0.13 x 10 ⁻⁵ | 2.08 x 10 ⁻⁵ | k _p -for parabolic relation only |
| VI | 6 | 850 | 5 x 10 ⁻⁵ | - | 1.96 x 10 ⁻⁵ | ditto |
| IV | 7 | 850 | 2 x 10 ⁻⁵ | 1.5 x 10 ⁻⁵ | - | sample thickness 1/2 of Run, II, III VI. |
| V | 7 | 850 | 3 x 10 ⁻⁵ | - | - | ditto |
| VII | 9 | 950 | 5 x 10 ⁻⁴ | 2.2 x 10 ⁻⁵ | - | - |
| X | 9 | 950 | 4 x 10 ⁻⁴ | - | - | - |
| XI | 10 | 950 | 7 x 10 ⁻⁵ | 2.5 x 10 ⁻⁵ | ~ 7.67 x 10 ⁻⁵ | $\frac{\Delta m}{A} \approx 0.4 + 4.6 \sqrt{t}$ |
| XII | 11 | 950 | 5 x 10 ⁻⁵ | 2.4 x 10 ⁻⁵ | ~ 7.58 x 10 ⁻⁵ | $\frac{\Delta m}{A} \approx 0.2 + 4.55 \sqrt{t}$ |
| XIII | 10 | 950 | 3 x 10 ⁻⁵ | - | ~ 5.78 x 10 ⁻⁵ | $\frac{\Delta m}{A} \approx 0.4 + 3.46 \sqrt{t}$ |
| XIV | 12 | 950 | 5 x 10 ⁻⁶ | 1.8 x 10 ⁻⁵ | 4.76 x 10 ⁻⁵ | $\frac{\Delta m}{A} = 2.5 + 2.85 \sqrt{t}$ |
| XVI | 12 | 950 | 5 x 10 ⁻⁶ | - | 4.62 x 10 ⁻⁵ | $\frac{\Delta m}{A} = 2.06 + 2.77 \sqrt{t}$ |
| XVIII | 12 | 950 | 2 x 10 ⁻⁶ | - | 4.77 x 10 ⁻⁵ | $\frac{\Delta m}{A} = 3.19 + 2.86 \sqrt{t}$ |
| XV | 13 | 950 | 5 x 10 ⁻⁶ | - | 4.6 x 10 ⁻⁵ | $\frac{\Delta m}{A} = 2.31 + 2.76 \sqrt{t}$ |
| VIII | 13 | 950 | 3 x 10 ⁻⁶ | 1.9 x 10 ⁻⁵ | 4.7 x 10 ⁻⁵ | $\frac{\Delta m}{A} = 1.46 + 2.82 \sqrt{t}$ |
| XVII | 13 | 950 | 5 x 10 ⁻⁶ | - | 4.65 x 10 ⁻⁵ | $\frac{\Delta m}{A} = 2.35 + 2.79 \sqrt{t}$ |
| IX | 13 | 950 | 2 x 10 ⁻⁶ | 1.5 x 10 ⁻⁵ | 4.92 x 10 ⁻⁵ | $\frac{\Delta m}{A} = 1.56 + 2.95 \sqrt{t}$ |

NOTE:

For values of curve equations time, t , has been given in hrs,
and $\Delta m/A$ in mg. of oxygen per cm.²

TABLE 3Weight Measurements (950°C)

| RUN | TIME hrs | Weight in mg | | | Area (A) cm ² | $\left(\frac{\Delta m}{A}\right)_w$ |
|-------|-------------|---------------------|--------------------|-------------------------------------|-----------------------------|-------------------------------------|
| | | Before Oxidation | After Oxidation | Gain (Δm) _w | | |
| XV | 16 1/2 | 2983.2 | 3071.3 | 88.1 | 5.866 | 15.03 |
| XIV | 25 | 2967.4 | 3074.6 | 107.2 | 5.989 | 17.9 |
| VIII | 42 | 2884.0 | 2998.4 | 114.4 | 5.480 | 20.87 |
| IX | 59 | 2891.0 | 3018.7 | 127.7 | 5.280 | 24.15 |
| XVIII | 76 | 3213.5 | 3374.9 | 161.4 | 5.892 | 27.4 |
| XVII | 93 | 2645.2 | 3850.0 | 204.8 | 6.765 | 30.3 |

NOTE:

Index (w) means: gravimetric determination.

TABLE 4

Microscopic Measurements (950°C)

| RUN | TIME hrs | THICKNESS OF GRAY OXIDE μ | THICK. OF METAL, mm | | RATIO 4:3 |
|-------|-------------|------------------------------------|---------------------|---------|--------------|
| | | | α-phase | β-phase | |
| 1 | 2 | 3 | 4 | 5 | 6 |
| XVI | 8 | 23.5 ± 2.5 | 0.982±0.030 | 1.452 | 12.0±2.1 |
| XV | 16 1/2 | 27.9 ± 2.5 | 0.412±0.020 | 1.115 | 14.8±1.4 |
| XIV | 25 | 32.3 ± 2.0 | 0.567±0.028 | 0.900 | 17.5±2.0 |
| VIII | 42 | 34.6 ± 1.7 | 0.663±0.020 | 0.662 | 19.3±1.2 |
| IX | 59 | 38.0 ± 1.6 | 0.722±0.020 | 0.485 | 20.3±1.2 |
| XVIII | 76 | 43.7 ± 1.8 | 0.915±0.018 | 0.154 | 20.98±1.3 |
| XVII | 93 | 47.8 ± 1.8 | 1.018±0.020 | 0.089 | 21.3±1.1 |

NOTE:

- 1) Measurements given in columns 3 and 4 are averages of 20 values
- 2) Measurements in column 5 are averages of 10 values.

TABLE 5
Microscopic Measurements (850°C)

| Oxidation Time hrs. | Gray Oxide Thickness, microns | Reference |
|------------------------|----------------------------------|-------------------------------------|
| 6 | 10.0 ± 2.0 | HUSSEY and SMELTZER ⁽³³⁾ |
| 16 | 21.0 ± 2.0 | " " " |
| 24 | 23.0 ± 2.0 | " " " |
| 48 | 33.0 ± 2.0 | " " " |
| 6 | 15.0 ± 0.6 | DEBUIGNE and LEHR ⁽³⁴⁾ |
| 24 | 20.0 ± 0.6 | " " " |
| 174 | 54.8 | WALLWORK et al. ⁽⁷⁰⁾ |
| 96 | 40.0 | " " " |
| 200 | 59.0 | " " " |
| 250 | 65.0 | " " " |
| 16 | 19.9 ± 1.0 | Present investigation |
| 18 | 20.6 ± 2.0 | " " |
| 36 | 24.0 ± 2.0 | " " |
| 48 | 30.4 ± 1.6 | " " |
| 72 | 34.8 ± 1.6 | " " |
| 117 | 44.5 ± 1.6 | " " |

Equation of the line shown in Fig. 15 is:

$$\xi = 3.38 + 3.87 \sqrt{t}$$

TABLE 6

X-Ray Powder Data for Gray and White Zirconium Dioxide

Specimen: Zirconium dioxide, gray oxide Description: Oxidized in pure oxygen for 76 hr at 950°. Run XVIII

Radiation: Cu Filter: Ni λ: 1.542 Å KV: 28 mA: 14 Exposure Time: 26 hr.

θ: 88.02 mm Correction factor: 1.0045

| Line | S uncorr. ($S_1 - \theta_1$) (mm) | $\frac{S}{2}$ (θ) degrees (large camera) | sin θ | Data for ASTM powder file | |
|------|--|---|--------|---|----------------|
| | | | | d (Å) = $\frac{\lambda}{2 \sin \theta}$ | I intensity |
| 1 | 17.98 | 8.99 | 0.1562 | 4.926 | F |
| 2 | 24.78 | 12.39 | 0.1245 | 3.594 | M |
| 3 | 28.58 | 14.29 | 0.2469 | 3.122 | V.S. |
| 4 | 32.08 | 16.04 | 0.2763 | 2.790 | V.S. |
| 5 | 34.88 | 17.44 | 0.2997 | 2.572 | S. |
| 6 | 35.88 | 17.94 | 0.3080 | 2.530 | M. |
| 7 | 39.48 | 19.74 | 0.3378 | 2.282 | F |
| 8 | 41.88 | 20.94 | 0.3574 | 2.157 | F |
| 9 | 46.18 | 23.09 | 0.3921 | 1.966 | F |
| 10 | 50.28 | 25.14 | 0.4249 | 1.814 | F |
| 11 | 51.18 | 25.59 | 0.4319 | 1.785 | M |
| 12 | 55.18 | 27.59 | 0.4361 | 1.665 | F |
| 13 | 56.58 | 28.29 | 0.4739 | 1.627 | F |
| 14 | 58.58 | 29.29 | 0.4892 | 1.576 | W |

TABLE 6 cont'd

Specimen: Zirconium dioxide, white oxide

Description: Oxidized in pure oxygen for 12 hr at 950°. Run VII

 $\theta = 87.78$

Correction factor: 1.004

| Line | S uncorr. ($S_1 - \theta_1$) (mm) | $\frac{S}{2}$ (θ) degrees (large camera) | sin θ | Data for ASTM powder file | |
|------|--|--|--------------|------------------------------|----------------|
| | | | | d (\AA) | I intensity |
| 1 | 17.75 | 8.875 | 0.1543 | 4.997 | M |
| 2 | 24.98 | 12.49 | 0.2163 | 3.564 | S |
| 3 | 28.99 | 14.495 | 0.2504 | 3.079 | V.S. |
| 4 | 32.31 | 16.155 | 0.2782 | 2.771 | V.S. |
| 5 | 35.42 | 17.71 | 0.3042 | 2.535 | S |
| 6 | 36.08 | 18.04 | 0.3097 | 2.489 | M |
| 7 | 39.74 | 19.87 | 0.3399 | 2.268 | F |
| 8 | 41.64 | 20.82 | 0.3554 | 2.169 | M |
| 9 | 42.65 | 21.32 | 0.3636 | 2.120 | M |
| 10 | 46.47 | 23.23 | 0.3944 | 1.955 | M |
| 11 | 47.07 | 23.53 | 0.3992 | 1.931 | S |
| 12 | 50.48 | 25.24 | 0.4264 | 1.808 | F |
| 13 | 51.69 | 25.85 | 0.4360 | 1.768 | M |
| 14. | 55.50 | 27.75 | 0.4656 | 1.656 | M |

F-Fair, V.S. - Very Strong, M - medium, S - strong, W - Weak; d-doublet

TABLE 7

Line Equations for Zirconium-Nitrogen Reaction

| Temperature °K. | Line Equations | |
|--------------------|--|--|
| | Gravimetric Technique | Volumetric Technique |
| 1023 | $\Delta m/A = -0.022 + 0.174 \sqrt{t}$ | - |
| 1073 | $\Delta m/A = 0.025 + 0.0286 \sqrt{t}$ | - |
| 1123 | $\Delta m/A = 0.038 + 0.0507 \sqrt{t}$ | $\Delta m/A = 0.014 + 0.051 \sqrt{t}$ |
| 1173 | $\Delta m/A = 0.027 + 0.099 \sqrt{t}$ | - |
| 1223 | $\Delta m/A = 0.021 + 0.158 \sqrt{t}$ | $\Delta m/A = -0.01 + 0.158 \sqrt{t}$ $\Delta m/A = 0.02 + 0.152 \sqrt{t}$ $\Delta m/A = -0.01 + 0.136 \sqrt{t}$ |
| 1273 | $\Delta m/A = 0.001 + 0.254 \sqrt{t}$ | - |

TABLE 8

Weight Measurement (750°- 1000°C)

| Temp. °C | Test time hrs | Weight-Gain ΔW , mg | Area A, cm ² | $\left(\frac{\Delta W}{A}\right)_w$ | $\left(\frac{\Delta W}{A}\right)_v$, mg/cm ² |
|-------------|------------------|--------------------------------|----------------------------|-------------------------------------|--|
| 1000 | 9 | 2.280 | 2.964 | 0.768 | |
| | 25 | 3.32 | 2.637 | 1.261 | |
| | 36 | 3.42 | 2.237 | 1.530 | |
| 950 | 25 | 1.86 | 2.217 | 0.842 | |
| | 36 | 2.18 | 2.234 | 0.976 | |
| | 49 | 2.58 | 2.158 | 1.196 | |
| | 48 | 2.34 | 2.412 | 0.97 | 0.95 |
| | 72 | 3.21 | 2.264 | 1.40 | 1.38 and 1.35 |
| 900 | 25 | 1.61 | 3.084 | 0.522 | |
| | 49 | 2.06 | 1.705 | 0.720 | |
| | 81 | 1.97 | 2.142 | 0.918 | |
| 850 | 25 | 0.75 | 2.425 | 0.295 | |
| | 36 | 0.85 | 2.452 | 0.346 | |
| | 49 | 0.81 | 2.193 | 0.369 | |
| | 64 | 1.06 | 2.303 | 0.460 | |
| | 71 | 0.91 | 2.186 | 0.417 | 0.426 |
| | 81 | 1.29 | 2.422 | 0.535 | |
| 800 | 36 | 0.79 | 3.929 | 0.206 | |
| | 64 | 1.00 | 4.082 | 0.245 | |
| | 81 | 1.11 | 4.164 | 0.267 | |
| | 100 | 1.44 | 4.064 | 0.322 | |

Cont'd

TABLE 8 Cont'd

| Temp. °C. | Test time hrs | Weight-Gain ΔW , mg | Area A , cm^2 | $(\frac{\Delta W}{A})_w$ | $(\frac{\Delta W}{A})_v$, mg/cm^2 |
|--------------|------------------|--------------------------------|-----------------------------|--------------------------|--|
| 750 | 49 | 0.38 | 3.888 | 0.098 | |
| | 102 | 0.65 | 3.901 | 0.166 | |
| | 144 | 0.70 | 4.048 | 0.173 | |
| | 169 | 0.82 | 4.091 | 0.206 | |

- Legend; 1. subscripts (w) and (v) - denote static-gravimetric and volumetric measurements.
2. Measurement of area has been based on average of three readings across the diagonals.

TABLE 9

Microscopic Measurements (750° - 1000°C)

| Temp. °C | Time hrs | Thick. of Nitride μ | Thick. of Alpha- Phase μ | Ratio of thick. of alpha phase to thick. of nitride |
|-------------|-------------|------------------------|-----------------------------|---|
| 1000 | 9 | 1.9 ± 0.3 | 31.1 ± 2.0 | 16.4 ± 1.2 |
| | 25 | 3.0 ± 0.2 | 47.5 ± 1.5 | 15.8 ± 0.7 |
| | 36 | 3.5 ± 0.5 | 59.9 ± 2.2 | 17.1 ± 1.6 |
| 950 | 25 | 2.01 ± 0.45 | 34.7 ± 2.2 | 17.3 ± 2.4 |
| | 36 | 2.62 ± 0.26 | 43.6 ± 1.5 | 16.6 ± 1.0 |
| | 48 | 3.04 ± 0.20 | 50.75 ± 2.5 | 16.7 ± 0.3 |
| | 49 | 3.14 ± 0.26 | 51.05 ± 2.2 | 16.2 ± 0.7 |
| | 72 | 3.4 ± 0.20 | 58.25 ± 1.7 | 17.1 ± 0.5 |
| 900 | 25 | 1.6 ± 0.17 | 30.5 ± 2.5 | 19.0 ± 1.1 |
| | 49 | 2.15 ± 0.30 | 41.05 ± 1.7 | 19.0 ± 0.8 |
| | 81 | 2.70 ± 0.26 | 53.25 ± 2.2 | 19.7 ± 1.2 |
| 850 | 25 | 1.20 ± 0.15 | | |
| | 36 | 1.30 ± 0.12 | | |
| | 49 | 1.42 ± 0.20 | | |
| | 64 | 1.80 ± 0.12 | | |
| | 71 | 1.85 ± 0.12 | | |
| | 81 | 2.07 ± 0.15 | | |
| 800 | 36 | 1.05 ± 0.15 | | |
| | 64 | 1.20 ± 0.10 | | |
| | 81 | 1.30 ± 0.15 | | |
| | 100 | 1.62 ± 0.12 | | |
| 750 | 49 | 0.60 ± 0.15 | | |
| | 102 | 1.05 ± 0.25 | | |
| | 144 | 1.13 ± 0.20 | | |
| | 169 | 1.17 ± 0.22 | | |

NOTE: All values are averages of 10 measurements. Errors indicate the average of max. and min. deviation.

TABLE 10Line Equations for the Thicknesses of Zirconium-Nitride andAlpha-Phase as a Function of Time

| Temp. °K. | Thickness (η) of alpha-phase, μ | Thickness (ξ) of zirconium nitride, μ | Thickness (η) + (ξ) μ |
|--------------|---|--|---|
| 1023 | - | $\xi = -0.06 + 0.096 \sqrt{t}$ | - |
| 1073 | - | $\xi = 0.1 + 0.12 \sqrt{t}$ | - |
| 1123 | - | $\xi = 0.09 + 0.21 \sqrt{t}$ | - |
| 1173 | $\eta = 1.78 + 5.69 \sqrt{t}$ | $\xi = 0.19 + 0.28 \sqrt{t}$ | $(\xi + \eta) = 1.66 + 6.01 \sqrt{t}$ |
| 1228 | $\eta = 2.27 + 6.79 \sqrt{t}$ | $\xi = 0.12 + 0.407 \sqrt{t}$ | $(\xi + \eta) = 3.41 + 7.05 \sqrt{t}$ |
| 1273 | $\eta = 2.30 + 9.40 \sqrt{t}$ | $\xi = 0.29 + 0.51 \sqrt{t}$ | $(\xi + \eta) = 2.13 + 10.03 \sqrt{t}$ |

TABLE 11

Microhardness Measurements and Diffusion Data

| Temp. and time °C | d; μ | x; μ | H(x); DPN kg/mm ² | $\frac{H(x)-H_0}{H(0)-H_0} = \frac{H(x)-145}{1665-145} \cdot 50$ | D; cm ² /sec |
|-------------------|------------------|----------|---------------------------------|--|--------------------------|
| 750°C 102 hr. | 34 1/2 | 0 | 1665=H(0) | 50 | - |
| | 52 | 3.3 | 930 | 25.8 | 3.52 x 10 ⁻¹³ |
| | 61 | 6.75 | 530 | 12.6 | 4.76 |
| | 103 | 11.7 | 186 | 1.35 | 3.81 |
| | 112 | 16.7 | 157 | 0.4 | 5.37 |
| | 114 | 18.0 | 152 | 0.23 | 5.49 |
| | 118 | 26.6 | 142 | - | - |
| | 116 | 32.2 | 147 | - | - |
| | 118 | 36.6 | 142 | - | - |
| | 118 | 50.0 | 142 | - | - |
| | 116 | 60.0 | 147 | - | - |
| | 750°C 144 hr. | 34 1/2 | 0 | 1665=H(0) | 50 |
| 44 | | 3.3 | 1019 | 28.4 | 3.20 x 10 ⁻¹³ |
| 90 | | 10.0 | 244 | 3.25 | 2.81 |
| 89 | | 12.0 | 249 | 3.42 | 4.16 |
| 93 | | 15.5 | 228 | 2.73 | 6.27 |
| 107 | | 18.0 | 172 | 0.89 | 5.57 |
| 115 | | 20.0 | 149 | 0.13 | 4.30 |
| 118 | | 21.6 | 142 | - | - |
| 118 | | 23.4 | 142 | - | - |
| 116 | | 26.6 | 147 | - | - |
| 117 | | 33.0 | 144 | - | - |
| 118 | | 36.5 | 142 | - | - |
| 117 | | 46.5 | 144 | - | - |
| 800°C 64 hr. | | 34 | 0 | 1706=H(0) | 50 |
| | 41 | 3.3 | 1174 | 33.0 | 1.21 x 10 ⁻¹² |
| | 50 | 6.75 | 789 | 20.6 | 1.47 |
| | 63 | 10.0 | 497 | 11.3 | 1.47 |
| | 87 | 13.3 | 261 | 3.2 | 1.20 |
| | 108 | 16.7 | 169 | 0.77 | 1.03 |
| | 112 | 20.0 | 157 | 0.38 | 1.22 |
| | 119 | 30.0 | 139 | - | - |
| | 118 | 36.5 | 142 | - | - |
| | 116 | 40.0 | 147 | - | - |
| | 116 | 46.5 | 147 | - | - |
| | 117 | 56.5 | 147 | - | - |

TABLE 11 (cont'd)

| | | | | | | |
|-----------------|-----------------|------|-----------|-----------|--------------------------|--------------------------|
| 800°C 81 hr. | 34 | 0 | 1706=H(0) | 50 | - | |
| | 50 | 6.7 | 789 | 20.6 | 1.15 x 10 ⁻¹² | |
| | 66 | 10.0 | 453 | 9.87 | 1.03 | |
| | 100 | 13.3 | 197 | 1.67 | 0.82 | |
| | 100 | 16.7 | 197 | 1.67 | 1.06 | |
| | 113 | 20.0 | 155 | 0.32 | 0.96 | |
| | 114 | 23.3 | 152 | 0.224 | 1.16 | |
| | 118 | 30.0 | 142 | - | - | |
| | 120 | 36.6 | 137 | - | - | |
| | 117 | 46.6 | 144 | - | - | |
| | 117 | 53.3 | 144 | - | - | |
| | 116 | 66.5 | 147 | - | - | |
| | 850°C 49 hr. | 34 | 0 | 1706=H(0) | 50 | - |
| | | 39 | 5.0 | 1297 | 36.9 | 6.35 x 10 ⁻¹² |
| 44 | | 6.7 | 1019 | 28.0 | 3.76 | |
| 50 | | 13.3 | 789 | 20.6 | 7.45 | |
| 60 | | 16.5 | 548 | 12.9 | 5.94 | |
| 97 | | 23.0 | 210 | 2.08 | 3.62 | |
| 98 | | 26.6 | 205 | 1.94 | 4.66 | |
| 106 | | 30.0 | 176 | 0.99 | 4.79 | |
| 113 | | 33.0 | 154 | 0.288 | 3.96 | |
| 117 | | 40.0 | 144 | - | - | |
| 115 | | 50.0 | 149 | - | - | |
| 117 | | 57.0 | 144 | - | - | |
| 117 | | 60.0 | 144 | - | - | |
| 118 | | 67.0 | 142 | - | - | |
| 117 | 86.5 | 144 | - | - | | |
| 850°C 64 hr. | 34 | 0 | 1706=H(0) | 50 | - | |
| | 43 | 6.7 | 1067 | 29.5 | 3.38 x 10 ⁻¹² | |
| | 49 | 10.0 | 822 | 21.6 | 3.54 | |
| | 53 | 13.3 | 702 | 17.85 | 4.93 | |
| | 78 | 20.0 | 324 | 5.75 | 3.48 | |
| | 88 | 23.4 | 254 | 3.49 | 3.59 | |
| | 98 | 30.0 | 205 | 1.94 | 4.54 | |
| | 109 | 36.5 | 166 | 0.672 | 4.48 | |
| | 118 | 46.5 | 142 | - | - | |
| | 115 | 56.5 | 149 | - | - | |
| | 119 | 60.0 | 139 | - | - | |
| | 117 | 66.6 | 144 | - | - | |
| | 117 | 80.0 | 144 | - | - | |

TABLE 11 (cont'd)

| | | | | | |
|--------|--------|-------|-----------|--|------------------------|
| 850°C | - | 0 | 1706=H(0) | 50 | - |
| 81 hr | 38 | 3.4 | 1366 | 39.2 | 2.63×10^{-12} |
| | 41 | 6.7 | 1174 | 33.0 | 3.96 |
| | 41 | 8.3 | 1174 | 33.0 | 6.10 |
| | 48 | 13.3 | 856 | 22.8 | 5.49 |
| | 62 | 20.0 | 513 | 11.8 | 4.97 |
| | 89 | 30.0 | 249 | 3.46 | 4.67 |
| | 96 | 33.25 | 214 | 2.21 | 4.67 |
| | 110 | 40.0 | 163 | 0.577 | 4.33 |
| | 115 | 46.5 | 149 | 0.125 | 4.08 |
| | 118 | 53.3 | 142 | - | - |
| | 116 | 56.5 | 147 | - | - |
| | 116 | 60.0 | 147 | - | - |
| | 117 | 73.5 | 144 | - | - |
| | 118 | 83.5 | 142 | - | - |
| 900°C | 34 | 0 | 1706=H(0) | 50 | - |
| 25 hr. | 41 | 5 | 1174 | 33.0 | 7.19×10^{-12} |
| | 47 | 10 | 893 | 24.0 | 11.1 |
| | 62 | 20 | 513 | 11.8 | 15.8 |
| | 70 | 25 | 402 | 8.25 | 18.0 |
| | 72 | 30 | 381 | 7.55 | 24.2 |
| | 96 | 40 | 214 | - | - |
| | 104 | 50 | 182 | - | - |
| | 110 | 70 | 163 | - | - |
| | 116 | 90 | 147 | - | - |
| | 117 | 140 | 144 | - | - |
| 900°C | 34 | 0 | 1706=H(0) | 50 | - |
| 49 hr. | 40 | 10 | 1233 | 34.8 | 1.88×10^{-11} |
| | 57 | 20 | 629 | 18.7 | 1.44 |
| | 59 | 25 | 566 | 13.5 | 1.45 |
| | 65 | 30 | 467 | 10.3 | 1.61 |
| | 74 | 40 | 351 | 6.6 | 2.00 |
| | 96 | 50 | 214 | - | - |
| | 105 | 60 | 179 | - | - |
| | 114 | 100 | 152 | - | - |
| | 116 | 130 | 147 | - | - |
| | 116 | 150 | 147 | - | - |
| | | | | $\frac{H(x) - 145}{1765 - 145} \cdot 50$ | |
| 950°C | 33 1/2 | 0 | 1765=H(0) | 50 | - |
| 36 hr. | 39 | 10 | 1297 | 35.6 | 2.86×10^{-11} |
| | 42 | 15 | 1118 | 30.0 | 3.16 |
| | 46 | 20 | 932 | 24.2 | 3.16 |

TABLE 11 (cont'd)

| | | | | | |
|--------|--------|------|-----------|------|--------------------------|
| | 55 | 30 | 652 | 15.6 | 3.40 |
| | 65 | 35 | 466 | 9.9 | 2.85 |
| | 98 | 50 | 205 | - | - |
| | 102 | 80 | 189 | - | - |
| | 109 | 100 | 166 | - | - |
| | 118 | 140 | 141 | - | - |
| 950°C | 33 1/2 | 0 | 1765=H(0) | 50 | - |
| 49 hr. | 39 | 10 | 1279 | 35.6 | 2.10 x 10 ⁻¹¹ |
| | 45 | 20 | 974 | 25.6 | 2.62 |
| | 49 | 25 | 822 | 20.8 | 2.68 |
| | 55 | 30 | 652 | 15.6 | 2.50 |
| | 61 | 40 | 530 | 12.4 | 3.27 |
| | 64 | 45 | 481 | 10.3 | 3.60 |
| | 97 | 60 | 209 | - | - |
| | 107 | 80 | 172 | - | - |
| | 108 | 90 | 169 | - | - |
| | 112 | 120 | 157 | - | - |
| | 117 | 150 | 144 | - | - |
| | 116 | 190 | 146 | - | - |
| 1000°C | 33 1/2 | 0 | 1765=H(0) | 50 | - |
| 25 hr. | 38 | 10 | 1366 | 37.7 | 5.7 x 10 ⁻¹¹ |
| | 44 | 20 | 1019 | 31.0 | 9.02 |
| | 51 | 30 | 759 | 18.9 | 6.48 |
| | 53 | 35 | 702 | 17.8 | 7.98 |
| | 56 | 40 | 629 | 14.9 | 8.24 |
| | 59 | 45 | 566 | 13.0 | 8.85 |
| | 98 | 60 | 205 | - | - |
| | 106 | 70 | 175 | - | - |
| | 109 | 90 | 166 | - | - |
| | 113 | 100 | 154 | - | - |
| | 116 | 140 | 146 | - | - |
| | 116 | 180 | 146 | - | - |
| 1000°C | 33 1/2 | 0 | 1765=H(0) | 50 | - |
| 36 hr. | 39 | 15 | 1297 | 35.6 | 6.37 x 10 ⁻¹¹ |
| | 43 | 22.5 | 1067 | 28.4 | 6.01 |
| | 44 | 25 | 1019 | 31.0 | 9.9 |
| | 47 | 30 | 893 | 23.0 | 6.4 |
| | 51 | 40 | 758 | 18.9 | 8.0 |
| | 59 | 50 | 566 | 13.0 | 7.62 |
| | 94 | 70 | 223 | - | - |
| | 101 | 100 | 190 | - | - |
| | 105 | 120 | 178 | - | - |
| | 112 | 150 | 157 | - | - |
| | 118 | 180 | 140 | - | - |
| | 117 | 200 | 144 | - | - |
| | 117 | 220 | 144 | - | - |

TABLE 12X-Ray Powder Data for Zirconium Nitride

Specimen: Zirconium Nitride Description: Zirconium reacted in pure nitrogen
for 72 hr. at 950°C. Run 5

Radiation: Cu Filter: Ni $\lambda = 1.542 \text{ \AA}$ KV: 28 mA: 20

Exposure Time: 24 hr. $\theta = 104.225$ Correction factor: 1.0025

| Line | S uncorr. ($S_1 - \theta_1$) (mm) | $\frac{S}{2}$ θ degrees (large camera) | sin θ | Data for ASTM powder file | |
|------|--|--|--------------|---------------------------|----------------|
| | | | | d (\AA) | I intensity |
| 1 | 34.65 | 17.368 | 0.2985 | 2.582 | S |
| 2 | 40.05 | 20.075 | 0.3432 | 2.246 | S |
| 3 | 57.8 | 28.972 | 0.4843 | 1.592 | S |
| 4 | 68.9 | 34.536 | 0.5669 | 1.360 | M |
| 5 | 72.45 | 36.316 | 0.5923 | 1.3017 | F |
| 6 | 81.78 | 42.997 | 0.6818 | 1.1308 | W |
| 7 | 95.58 | 47.909 | 0.7420 | 1.0391 | F |
| 8 | 98.98 | 49.613 | 0.7617 | 1.012 | F |
| 9 | 112.18 | 56.230 | 0.8318 | 0.927 | W |
| 10 | 122.78 | 56.530 | 0.8342 | 0.924 | W |

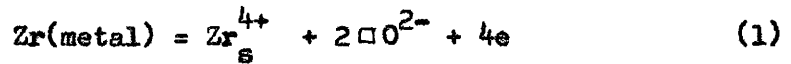
TABLE 13Line Equations for Reaction of Zirconium in Nitrogen-OxygenAtmospheres at 850°C.

$$P_{O_2} + P_{N_2} = 400 \text{ mm Hg}$$

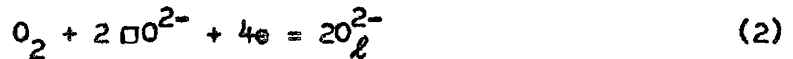
| P_{O_2} mm Hg | Line equation |
|----------------------|-------------------------------------|
| 40 | $\Delta m/A = 0.3, + 3.10 \sqrt{t}$ |
| 80 | $\Delta m/A = 0.1 + 3.84 \sqrt{t}$ |
| 120 | $\Delta m/A = 0.3 + 4.10 \sqrt{t}$ |
| 160 | $\Delta m/A = 1.0 + 3.05 \sqrt{t}$ |
| 200 | $\Delta m/A = 1.0 + 2.70 \sqrt{t}$ |
| 240 | $\Delta m/A = 0.7 + 2.45 \sqrt{t}$ |
| 280 | $\Delta m/A = 0.5 + 2.37 \sqrt{t}$ |
| 320 | $\Delta m/A = 0.1 + 2.24 \sqrt{t}$ |
| 360 | $\Delta m/A = 0.2 + 1.67 \sqrt{t}$ |
| Air at 400 mm Hg. | $\Delta m/A = 0.2 + 2.96 \sqrt{t}$ |

PROBLEM 2

The zirconium oxidation process can be pictured as occurring by the formation of an oxygen ion vacancy at the metal-oxide interface:



where: $\text{Zr}(\text{metal})$ represents a zirconium atom in the metal lattice and $\text{Zr}_{\text{S}}^{4+}$ is a Zr^{4+} ion on a lattice site in the oxide. In order for parabolic oxidation to proceed, O^{2-} and electrons must diffuse through the oxide to the oxygen-oxide interface where they are consumed in the reaction:



for which the equilibrium constant in terms of concentrations is:

$$k = 1/p_{\text{O}_2} \cdot (c_{\text{e}})^4 \cdot (c_{\text{O}^{2-}})^2 \quad (3).$$

Since, from mass action law:

$$(c_{\text{O}^{2-}}) = 1/2 (c_{\text{e}}) \quad (4),$$

we have

$$k = 1/16p_{\text{O}_2} \cdot (c_{\text{O}^{2-}})^6 \quad (5).$$

Assuming the ionic conductivity, $\sigma_{\text{O}^{2-}}$, to be a linear function of concentration of oxygen vacancies:

$$\sigma_{\text{O}^{2-}} = k_1 \cdot (p_{\text{O}_2})^{-1/6} \quad (6).$$

From the theory of parabolic scaling, equation 14, follows that generally oxidation of a n-type semiconductor increases as ionic conductivity increases, $k_p = f(\sigma_{\text{O}^{2-}})$.

If $2N^{3-}$ ions may replace $3O^{2-}$ ions in the zirconium oxide lattice, we have in terms of the electronic balance:

$$c_e = 2c_{\square O^{2-}} - c_{N^{3-}}^{O^{2-}} \quad (7),$$

where: $c_{N^{3-}}^{O^{2-}}$ means concentration of nitrogen in oxygen sites. From equation (3):

$$k' = 1/16 p_{O_2} \cdot \left(1 - \frac{c_{N^{3-}}^{O^{2-}}}{2c_{\square O^{2-}}}\right)^4 \cdot (c_{\square O^{2-}})^6 \quad (8)$$

for the equilibrium constant. Again assuming $G_{\square} = f(c_{\square O^{2-}})$ we have:

$$G_{\square}' = k_2 p_{O_2}^{-1/6} \cdot \left(1 - \frac{c_{N^{3-}}^{O^{2-}}}{2c_{\square O^{2-}}}\right)^{-2/3} \quad (9)$$

which can be compared with equation (6) if we assume that $k_1 \approx k_2$ for small enough concentrations of nitrogen. Then :

$$\frac{G_{\square}}{G_{\square}'} = \left(1 - \frac{c_{N^{3-}}^{O^{2-}}}{2c_{\square O^{2-}}}\right)^{2/3} \quad (10)$$

shows that the scaling rate increases when the concentration of nitrogen ions in the zirconium oxide phase increases.

LITERATURE

1. Osthagen, K. and Kofstad, P.; J. Electrochem Soc. 109 (1962) 204.
2. Gulbransen, E. A. and Andrew, K. F.; Trans. AIME 209 (1957) 394.
3. Cubicciotti, D. J.; J. Am. Chem. Soc. 72 (1950) 4138.
4. Belle, J. and Mallett M. W.; J. Electrochem. Soc. 101 (1954) 339.
5. Mallett, M. W. and Albrecht, M. M.; J. Electrochem. Soc. (1955) 407.
6. Porte, H. A., Schnizlein, J. G., Vogel, R. C. and Fisher, D. F.; J. Electrochem. Soc. 107 (1960) 506.
7. Aronson, S.; J. Electrochem. Soc. 108 (1961) 312.
8. Flint, D. and Varley, J.H.D.; J. Phys. Chem. Solids 6 (1958) 213.
9. Flint, D. and Varley, J.H.D.; Nature 179 (1957) 145.
10. Kubaschewski, O. and Hopkins, B.E.; "Oxidation of Metals and Alloys", London, 1962.
11. Wagner, C.; Z. phys. Chem. B21 (1933) 25.
12. Wagner, C.; Atom. Movements, A.S.M. (1951) 153.
13. Engell, H.J., Hauffe, K. and Ilschner, B.; Z. Electrochem. 58 (1954) 478.
14. Kofstad, P., Hauffe, K. and Kjollesdal, H.; Acta Chem. Scand. 12 (1958) 239.
15. Cabrera, N. and Mott, N. F.; Repts. Prog. Phys. 12 (1949) 163.
16. Polling, J. J. and Charlesby, A.; Acta Met. 2 (1954) 667.
17. Belle, J., and Mallett, M. W.; J. Electrochem. Soc. 101 (1954) 339.
18. Akram, H. K., and Smeltzer, W. W.; Canadian Met. Quart. 1 (1962) 41.
19. Smeltzer, W. W., Hearing, R. R. and Kirkaldy, J.S.; Acta Met. 9 (1961) 880
20. Evans, U.R.; Trans. Electrochem. Soc. 46 (1924) 247.
21. Gulbransen, E. A.; Trans. Electrochem. Soc. 83 (1943) 301.

22. Glasstone, S., Laidler, K. J. and Eyring, H.; "The Theory of Rate Progress", McGraw-Hill, New York, 1941.
23. Kofstad, P.; Acta Chem. Scand. 12 (1958) 701.
24. Wagner, C. and Gruenwald, K.; Z. Phys. Chem. 40 (1938) 455.
25. Nauffe, K. and Rahmel, A.; Z. Phys. Chem. 199 (1952) 152.
26. Gulbransen, E. A. and Andrew, K. F.; J. Metals 1 (1949) 515.
27. Hussey, R. J. and Smeltzer, W. W.; J. Electrochem. Soc. 111 (1964) 564.
28. Jenkins, A. E., J. Inst. Met. 84 (1955) 1.
29. Vest, R. W., Tallan, N.M. and Tripp, W.C.; J. Am. Ceramic Soc. 47 (1964)635.
30. Charles, R. G., Barnatt, S. and Gulbransen, E.A.; J. Metals 9 (1958) 101.
31. Westerman, R. E.; J. Electrochem. Soc. 111 (1964) 140.
32. Pemsler, J. P.; J. Electrochem. Soc. 112 (1965) 477.
33. Hussey, R. J. and Smeltzer, W. W.; J. Electrochem. Soc. 111 (1964) 1221.
34. Debuigne, J. and Lehr, P.; Memories scientifiques Rev. Metallurg. 60 (1963) 911.
35. Kearns, J. J. and Chirigos, J. N.; U. S. Atomic Energy Report, WAPD-TM-306 (1962).
36. Pemsler, J. P.; J. Electrochem. Soc. 105 (1958) 315.
37. Mallett, M. W., Albrecht, W. M. and Wilson, P.R.; "The Diffusion of Oxygen in Alpha and Beta Zircaloy II and Zircaloy III at High Temperatures" B.M.I.-Report-1154 (1954).
38. Phalnikar, C. A. and Baldwin, W.M. Jr.; A.S.T.M. Proceedings 43 (1951) 1038.
39. Wallwork, G. R.; Thesis on Solid-Gas Reaction at High Temperatures, (1959) 36-74.
40. Aronson, S.; J. Electrochem. Soc. 108 (1961) 312.
41. Sarkisov, E. S., Chebatarov, N. T., Nevzorova, A. A. and Zverkov, A. T.; Soviet J. Atomic Energy 1 (1958) 1465.
42. Saur, G., Laue, H. J. and Borchers, H.; Metall. 15 (1961) 9.

43. Cox, B., J. Electrochem. Soc. 108 (1961) 24.
44. Dravnieks, A.; J. Am. Chem. Soc. 72 (1950) 3568.
45. Mallett, M. W., Belle, J. and Cleland, B. B.; J. Electrochem. Soc. 101 (1954) 1.
46. Loevenstein, H. and Gilbert, H. L., A.E.C.U. 3818 (Oct. 1958) 60.
47. Hayes, E. T. and Roberson, A. H.; Trans. Electrochem. Soc. 96 (1949) 142.
48. Ambartsumyan, R. S., Kiselev, A. A., Grebennikov, R. V., Myshkin, V. A., Tsuptun, L. J. and Nikulina, A. F.; Proceedings of the Second United Nations International Conference on the Peaceful Uses of Atomic Energy, Geneva, 5 (1958) 12.
49. Hall, M.N.A., Martin, S.L.H., and Rees, A.L.G.; Trans. Faraday Soc. 41 (1945) 310.
50. Martin, S.L.H., and Rees, A.L.G.; Trans. Faraday Soc. 50 (1954) 344.
51. Dravnieks, A.; J. Am. Chem. Soc. 72 (1950) 3761.
52. Hussey, R. J. and Smeltzer, W. W.; J. Electrochem. Soc. 112 (1965) 554.
53. Mallett, M. W., Albrecht, W.M. and Bennett, R.E.; J. Electrochem. Soc. 104 (1951) 349.
54. Cox, B.; J. Electrochem. Soc., 108 (1961) 24.
55. Pray, H.A. and Peoples, R. S.; U.S. Atomic Energy Commission, Report B.M.I.-T-55 (1951).
56. Wagner, C.; "Diffusion in Solids, Liquids, Gases" by W. Jost, Academic Press, New York, (1952) 71.
57. Hansen, M.; "Constitution of Binary Alloys". McGraw-Hill, New York (1958) 1079 and 996.
58. Jost, W.; "Diffusion in Solids, Liquids, Gases" Academic Press, New York (1960) 72.
59. Kidson, G.V.; J. Nuclear Materials 3, (1961) 21-29.
60. Evans, W.; Canadian Mining and Metallurgical Bulletin, 53 (1960) 897.
61. Cprek, E. R.; Trans. ASM, 55 (1962) 369.
62. Jenkins, A.E.; J. Inst. Met., 84 (1955) 1.

63. Smeltzer, W. W., Tollefson, E.L. and Cambron A.; Canadian J. Chem. 34 (1956) 1046.
64. Dalgaard, S.; Private communication.
65. Rieck, G. D. and Bruning H.A.; Nature; 190 (1961) 1181.
66. Dietzel, A. and Tober, H.; Chem. Abstr., 47 (1953) 9712.
67. Geller, R.F. and Yaworsky, P. J.; J. Research Natl. Bur. Standards, 35 (1945) 87-110.
68. Murray, M. W. and Allison, E.B.; Chem. Abstr. 48 (1954) 11891.
69. Heyes, E.E. and Kaufmann, A.R.; "Zirconium and Zirconium Alloys", ASM, Cleveland, (1958) 241-252.
70. Wallwork, G. R., Smeltzer, W. W. and Rosa, C. J.; Acta Met. 12(1964)409.
71. Samsonov, G.V.; "No. 2, Properties Index", Plenum Press Handbooks of High-Temperature Materials, New York, (1964) 138.
72. Gertsriken, S. D. and Dekhtyar, I.Ya.; "Solid State Diffusion in Metals and Alloys" AEC-tr-6313, (1960) 91.
73. Terco, R.M.; J. Metals 5 (1953) 344.
74. Gebhardt, E. and Seghezzi, H.D.; Z. Metallkunde, 49 (1958) 577.
75. Domagala, R. F. and McPerson, D.J.; J. Metals, 6 (1954) 239.
76. Elinson, S. V. and Petrov, K. I.; "Zirconium-Chemical and Physical Methods of Analysis", AEC-tr-5373, (1960) 22.
77. Hayes, E. T. and Roberson, A.H.; Trans. Electrochem. Soc., 96 (1949) 142.
78. Pemsler, J.P.; J. Nucl. Matl. 7 (1962) 16.
79. Davis, M., Montgomery, K.R. and Standring, K.; J. Inst. Metals 89 (1961) 172.
80. Gebhardt, E., Seghezzi, H.D. and Durrshnabel, W.; J. Nucl. Mat. 4(1961)255.
81. Pemsler, J.P.; J. Electrochem. Soc. 112 (1965) 477.
82. Domagala, R. F., McPherson, D. J., and Hansen, M.; J. Metals 8 (1956)98.
83. Hodgman, C.D., Weast, R.C., and Selby, S. M.; "Handbook of Chemistry and Physics", Cleveland (1960) 687.

84. Smithells, C. J.; "Metals Reference Book", London (1962) vol. 2, 696.
85. Van Bueren, H. G.; "Imperfections in Crystals", Amsterdam (1961) 417.
86. Seith, W.; "Diffusion in Metallen", Springer, Berlin, (1956).
87. Mallett, M. W. and Albrecht, W. M.; J. Electrochem. Soc. 102 (1955) 407.
88. Kendall, L. F.; AEC-Report, H.W.-39190 (1955).
89. Kofstad, P. and Osthagen, K.; J. Electrochem Soc. 109 (1962) 204.
90. Saur, G., Laue, H. J. and Borchers, H.; Metall, 15 (1961) 9.
91. Cox, B.; J. Electrochem Soc. 108 (1961) 24.
92. Lehr, P. and Debuigne, J.; Mem. Sci. Rev. Metal. LX (1963) 911.
93. O'Driscoll, W. C., Tyzack, C. and Raine, T.; Second U.N. Conference on the Peaceful Uses of Atomic Energy, Paper No. 1450 (1958).
94. Westerman, R. E.; J. Electrochem Soc. 111 (1964) 140.
95. Douglass, D. L.; Corrosion Science, 5 (1965) 347.
96. Carslaw, H.S. and Jaeger, J. C.; "Conduction of Heat in Solids", Oxford University Press, (1960) 291.